APPLICATIONS OF LIGHT–MATTER INTERACTION IN SEMICONDUCTOR STRUCTURES

ELENA CALLUS

JULY 2023

THESIS SUBMITTED FOR THE DEGREE OF
DOCTOR OF PHILOSOPHY

DEPARTMENT OF PHYSICS AND ASTRONOMY
UNIVERSITY OF SHEFFIELD

ABSTRACT

In this thesis, we study the applications of light–matter interactions in the context of quantum information processing. We consider interactions at the single- or few-photon level with semiconductor-based structures integrated within photonic setups. The work we present here, therefore, fits in well within the wider field of optical quantum information processing and technologies, whereby photons are utilised in the encoding, manipulation and transmission of information, as well as solid-state quantum optics, where the spin plays the role of the qubit. The work we present here is highly theoretical and we, therefore, keep in mind experimental challenges.

We first present the mathematical foundations of quantum mechanics, then move on to describe key concepts and formulations from the theory of quantum optics that we will use in our work. We describe in detail the important quantum feature of entanglement, which serves as a resource in various quantum technologies. This motivates us to study the generation of entanglement between spectrally dissimilar solid-state emitters using readily accessible optical states. The method we propose builds up the generated entanglement in a cumulative manner and is heralded by the detection of photons. We also study the effects of different sources of loss on the implementation of the scheme.

Next, we consider the use of the spin–photon interface to perform quantum error correction; specifically, syndrome extraction in quantum surface codes. Making use of quantum dots within micropillar cavities, we show how a photonic implementation of the surface code can make use of the resulting light–matter interaction in order to detect the presence of errors. We show that the scheme is robust to errors in the frequency detuning by using the confidence as a figure of merit. We also study the generation of entanglement between spectrally dissimilar spin systems and consider the efficiency and fidelity of such a scheme.

Finally, we study the light-matter interaction within a semiconductor-based device intended as a component within a wider quantum optical network. Using the input–output formalism, we obtain the single- and two-photon scattering matrices that allow us to describe the transport properties of the proposed setup. We also discuss the presence of the non-linearity in the interaction and the photon statistics of the transmitted field for a weak coherent state as the input.

ACKNOWLEDGEMENTS

I wish to start by thanking my supervisor, Pieter Kok, who has been a great mentor and patient supporter throughout these last few years. This work would not have been possible without him. He has taught me a great deal, more than he probably realises, with his unrelenting optimism and genuine enthusiasm for physics.

I am grateful to have had the opportunity to undertake my PhD in the Low Dimensional Structures and Devices group here in Sheffield. Just like an isolated two-level system could not be excited to a higher energy state without coupling to some electromagnetic field or by means of collision, so would I have maintained my state of ignorance that I started with were it not for meeting and interacting with so many fantastic people along the way! (The jury is still out on how short the lifetime of this "excited" state is and I claim nothing but a marginal improvement in my level of wisdom.) I would be remiss to not mention in particular Luke Wilson, Dominic Hallett and Mateusz Duda.

A special thank you goes to the people that I have worked with and with whom I have shared life during my PhD: Armanda Quintavalle, Maxine McCarthy, Marta Marchese and Alice Cullen. Thank you all for the wonderful friendships that have flourished as we've shared our time together in E13a, White Croft Works (the most bizarre over-representation!), ~~Five Guys~~ West Bar Tap, sunsets on Bole Hill grounds, lunches in Weston Park, Trani, Scotland and its rainforest, ... You have enriched these last few years! I also wish to express my gratitude to Domenico Pomarico, who has patiently listened to my complaining and offered encouragement along the way (*lì, là e a i tutti posti*). Your passion for physics and pragmatic approach helped to make the process of finishing much less arduous! I am also grateful to all the people I have met under various circumstances along the way and who have in some shape or form left a mark.

Finally, I wish to express my sincere appreciation to my dear family: Äiti, Papà and Irene. You have been unyielding in your support and encouragement throughout this project. Thank you for choosing to keep walking beside and lovingly tolerate me during my moments of frustration; you kept me sane.

DECLARATION

I, Elena Callus, declare that this thesis was written solely by me and presents my own work. The work presented here by others is appropriately referenced. Parts of this thesis are based upon published articles or manuscripts submitted for publication.

Publications

- **E. Callus** and P. Kok. *Cumulative generation of maximal entanglement between spectrally distinct qubits using squeezed light.* Phys. Rev. A **104** 052407 (2021).
- **E. Callus** and P. Kok. *Spin-augmented observables for efficient photonic quantum error correction.* arXiv: `2211.14123` (2022) – accepted for publication in Phys. Rev. A.
- D. Hallett, **E. Callus**, P. Kok, L. Wilson. *Statistics of photon transport in a waveguide-coupled nanocavity* – in preparation.

CONTENTS

1 Introduction **1**
1.1 History . . . 1
1.2 Current developments in quantum technologies . . . 2
1.3 Thesis outline . . . 4

2 Quantum mechanics **5**
2.1 Fundamentals in quantum mechanics . . . 5
2.2 Density matrices . . . 8
2.3 Dynamical pictures . . . 10
2.4 Quantisation of the electromagnetic field . . . 12
2.5 Quantum states of the electromagnetic field . . . 14
2.5.1 Fock states . . . 14
2.5.2 Coherent states . . . 15
2.6 Entanglement . . . 16
2.6.1 Entanglement as a resource . . . 16
2.6.2 Entanglement measures . . . 18
2.7 Quantum error correction . . . 19

3 Light–matter interaction **23**
3.1 Light–matter Hamiltonian . . . 23
3.2 Coupling to a waveguide . . . 25
3.2.1 Frequency basis . . . 26
3.2.2 Position basis . . . 26
3.2.3 Loss . . . 27
3.3 Wavefunction approach to scattering . . . 28
3.3.1 Waveguide-coupled two-level system . . . 28
3.3.2 Numerical approach . . . 30

3.4 Input–output formalism . . . 33
3.5 Scattering matrix . . . 35
3.6 Semiconductor quantum dots . . . 37
3.6.1 Energy levels . . . 37
3.6.2 Directional emission . . . 39

4 Cumulative generation of entanglement **41**
4.1 Background . . . 41
4.2 Setup . . . 42
4.3 Introducing Spectral Variation . . . 44
4.4 Protocol . . . 45
4.5 Losses . . . 49
4.5.1 Scattering losses . . . 49
4.5.2 Detector inefficiencies . . . 51
4.5.3 Measurement . . . 51
4.6 Practical implementation . . . 54
4.7 Summary . . . 55

5 Spin-augmented quantum information processing **57**
5.1 Background . . . 57
5.2 Surface codes . . . 58
5.3 Physical system . . . 59
5.4 Syndrome measurement procedure . . . 61
5.5 Inherent symmetry in the interaction . . . 64
5.6 Confidence . . . 64
5.7 Entanglement . . . 67
5.8 Summary . . . 72

6 Tuning the photonic output from a nanocavity device **73**
6.1 Background and motivation . . . 73
6.2 Physical system . . . 75
6.3 Single-photon scattering . . . 77
6.4 Two-photon scattering . . . 78
6.5 Second-order correlation function . . . 80
6.6 Summary . . . 84

7 Conclusion and future work **85**
7.1 Conclusion . . . 85
7.2 Future work . . . 86

A Concurrence trajectories **89**

B Two-photon scattering matrix **97**

CHAPTER

1

INTRODUCTION

1.1 History

The desire to understand the world around us has been present throughout human history, with the level of depth increasing over time. The turn of the 20th century was characterised by the development of several theories and hypotheses to explain phenomena that could not be reconciled using classical physics: quantum mechanics, the study of nature at atomic and subatomic scales, had emerged. Not only was quantum mechanics successful in explaining, e.g., the photoelectric effect [1] and (the lack of) the so-called ultraviolet catastrophe for black-body radiation [2], but it also predicted illogical and 'unnatural' behaviour. These included concepts such as quantum entanglement, whereby the state of a system is dependent on the state of another irrespective of spatial separation, and wave-particle duality, whereby matter may exhibit the properties of a wave whilst light behaves similar to discrete particles.

The combination of these revolutionary ideas with humankind's penchant for technology brought about the first quantum revolution. It is marked by ideas that can only be explained using the quantum theory framework, and includes the invention of the laser, the atomic clock and, perhaps most significantly, the transistor[1]. Today we find ourselves in the midst of the second quantum revolution [4], where we move from being passive witnesses of the quantum realm to actively controlling and manipulating individual quantum systems. This includes also the development of exotic engineered systems such as semiconductor quantum dots—which play a central role in the work of this thesis—superconducting circuits, and Majorana fermions. The aim behind this feat of quantum engineering is its ultimate use in communication, sensing, cryptography and information processing, with the application of

[1] The transistor is regarded by many as one of the most important inventions of the 20th century [3] with an estimated 13 sextillion (10^{21}) having been manufactured since its invention in 1947 up until 2018.

quantum phenomena to these fields allowing for better, faster and more accurate results. Amongst the most exciting prospects is the development of a quantum computer, first formally described by David Deutsch in 1985 [5]. This would have computing powers surpassing classical computing resources for certain classes of problems, solving otherwise intractable problems such as prime factorisation using Shor's algorithm [6], finding the (near to) exact solution of the electronic structures of higher order chemical compositions [7, 8] and the faithful preparation of Gibbs states of a quantum many-body system [9].

1.2 Current developments in quantum technologies

The development of quantum technologies holds exciting possibilities, as is evident from the vast amount of investment into various research projects, both on a governmental and private level. The underlying principle behind quantum information processing is the encoding of information onto qubits, the quantum counterpart of a bit, (or qu$d$its when considering d-dimensional systems), whilst processing them in a way that maintains their quantum properties and retains the fidelity of the encoded information. The conditions for successfully constructing a quantum computer have been well-defined. These were first established for the circuit model in 2000 and are known as the DiVincenzo's criteria [10], and include the requirement of scalability, a universal set of quantum gates and specific measurement capabilities. This was followed by a more formal operational definition of a quantum computer that is quantum computing model agnostic [11]. However, today there is still a clear lag in the physical realisation of these theoretical schemes. This is due to the difficulty in engineering systems that are sufficiently isolated from their environment so as to retain their quantum characteristics whilst still having control and manipulation capabilities.

There exist several architectures serving as qubit candidates that are being actively researched and developed. Some of the more promising ones include the photonic platform [12], with the information encoded in, say, the polarisation or spatial mode; the spin in semiconductor quantum dots [13] or nitrogen-vacancy centers in diamond [14]; superconducting electronic circuits [15]; and trapped ion qubits [16]. However, it is likely that the direction for future development will rely on the integration of different platforms. This is because none of the proposed schemes are inherently free of some form of drawback. For example, superconducting qubits require operation at cryogenic temperatures and have relatively short decoherence times, resulting in short-lived memories. Similarly, trapped ion setups are challenging to scale and have significantly low gate speeds. The photonic platform has proven to be one of the most promising for quantum information processing [17, 18]. Photons have relatively long coherence times which makes them ideal as flying qubits, transmitting information over long distances. Knill, Laflamme and Milburn proposed a scheme for quantum computation comprising of linear optical elements, single-photon sources and photon detectors [19]. Although the scheme is formally efficient, with the computation scaling polynomially in the input size, the constant overheads are very large and result in scalability difficulties. This is because the implementation of quantum gates is never deterministic, with the probability of success increased by repeating the series

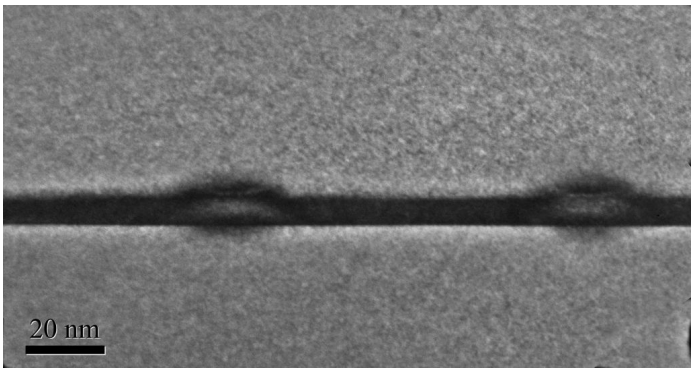

Figure 1.1: A dark field TEM image of InGaAs-capped InAs/GaAs quantum dots. Image courtesy of Edmund Clarke, EPSRC National Epitaxy Facility, University of Sheffield.

of operations.

However, optical quantum computing can be made more efficient and gates rendered deterministic by introducing non-linearities. This leads us to a drawback when relying solely on photons as information carriers: photons do not readily interact with each other and, therefore, require some mediator to generate non-linearities at the few-photon level. On the other hand, photons are capable of coupling strongly to atoms, molecules and other kinds of nanostructures, with the interactions showing interesting behaviour. This has motivated the research of light–matter interactions and the development of optical setups with integrated nanostructures. The interaction at the few-photon level with these solid-state emitters, commonly referred to in the literature as the spin–photon interface, has been adopted in numerous applications, ranging from transistors [20], photon-photon gates [21], generation of cluster states [22] and entanglement generation [23].

The work in this thesis is motivated by the development of quantum technologies and their physical realisation on some form of photonic platform. In fact, an overarching objective within the nanophotonics community is the integration of the aforementioned elements (i.e. photon sources, photonic gates, non-linear elements, detectors) into a single on-chip optical circuit [24–26]. This would offer the advantage of minimising coupling losses [27,28] whilst improving scalability due to the possibility of high component density [29]. The cornerstone of this project has been light–matter interactions at the few-photon level with solid-state emitters; specifically, we consider semiconductor quantum dots. The interest in the development of this kind of nanostructures has been rising, mostly due to its utility in generating [30, 31] and manipulating photonic states.

Quantum dots are structures with dimensions on the scale of just a few nanometers and may be produced using one of several methods. The most common way of fabricating is by self-assembly, whereby a layer of one type of semiconductor is placed on a substrate of another, resulting in a mismatch of the lattice-constants. In order to minimise the strain energy, one of the semiconductor layers will undergo a transition and self-assemble into small islands dispersed across the sample, as shown in Fig. 1.1. This tight spatial confinement of the electrons in all three dimensions leads to the discretisation of the allowed energy

levels, similar to the rudimentary model of a particle in a box. In fact, quantum dots are sometimes referred to as artificial atoms due to their discrete energy levels and bound electron transitions. Additionally, the spin of the charge carrier, be it either an electron or an electron hole, may be configured using magnetic and electric fields and, therefore, may also serve as a spin qubit. Given their solid state, quantum dots integrate well with various photonic structures [32, 33]. The strength of the light interaction can be enhanced by placing the emitter inside a cavity, such as a photonic crystal cavity [34] or a micropillar structure [35]. This occurs due to the Purcell effect [36]: the small mode volume of the photonic structure and the resulting increase in the local density of photonic states enhances the transition rate by Fermi's golden rule.

1.3 Thesis outline

In the previous sections, we have argued for the importance of quantum technologies with a special focus on photonic architectures. In this thesis, we are motivated to analyse some applications of the spin–photon interface in the context of quantum information processing. In particular, we take into account the interaction at the few-photon level with quantum dot-based structures. We study concepts that are purely quantum, such as entanglement generation and quantum error detection, and apply these to physical systems that are already being used in experimental settings.

This thesis is structured as follows. In Chapter 2, we introduce the key ideas of quantum mechanics and background theory on quantum information. This will serve as a foundation for the theoretical framework that future chapters build upon. In Chapter 3, we present a detailed view of some of the fundamental theory in quantum optics and the tools that we have used, whilst building on key concepts of quantum mechanics from the previous chapter. In particular, we introduce the basic form of the Hamiltonian describing light–matter interactions and show how this translates into the dynamics of a single photon interacting with some two-level system. We also give a detailed explanation of the input-output formalism and the scattering matrix used in quantum optical systems.

In Chapter 4, we present an entanglement generation scheme that overcomes the limitations posed by spectral inhomogeneity across fabricated quantum dots. The scheme makes use of a readily-available photonic source and allows for the deterministic entanglement of spin states, regardless of the spectral mismatch. We then look into how well the scheme performs given different sources of losses and degradation. Next, in Chapter 5, we demonstrate the possibility of using micropillar-based quantum dots for quantum error detection. Encoding the data into the polarisation of the photons, we can extract the syndrome by performing a quantum nondemolition measurement on the spin. We also analyse the effect of imperfections on the scheme. Finally, in Chapter 6, we seek to characterise a quantum dot-cavity device. We present the Hamiltonian for this setup and analyse the light–matter interaction at the single- and two-photon level. We also consider the photon statistics of the output and determine its use as a potential single-photon source. We conclude the thesis with a summary of the work done and the main results, as well as a discussion on potential future work and outlook in Chapter 7.

CHAPTER

2

QUANTUM MECHANICS

In this chapter, we start by introducing the postulates that underpin quantum mechanics and explain how these serve as the foundation to describe any system in terms of its state, physical observables and dynamics. We then delve into the density matrix formalism and dynamical representations of a given state, before moving to explain the quantisation of the electromagnetic field and the use of mode operators to mathematically represent different photonic states. Next, we give a detailed view of entanglement and motivate the use of a measure to properly characterise the degree of entanglement in different systems. Finally, we give an introduction to quantum error correction as a guide for the work presented later on in this thesis. This chapter is also meant to serve as a foundation for the quantum optics theory explained in Chapter 3.

2.1 Fundamentals in quantum mechanics

The need for a formal theory of quantum mechanics resulted from the observation of phenomena that could not be reconciled using, what would later be referred to as, classical physics. Examples that demonstrate the need for quantum physics include the Stern–Gerlach experiment [37], which shows that the intrinsic angular momentum of an electron is quantized, as well as photon antibunching, successfully first demonstrated by Kimble *et al.* [38] and proving that light requires a quantum treatment in order to be fully described. However, up until 1925, this new theory was still being defined within the confines of classical physics by using its mathematical structures. At this point, things started to rapidly evolve due to the groundbreaking contributions of prominent physicists[1] in the development

[1] Erwin Schrödinger, Werner Heisenberg, Max Born, Pascual Jordan, John von Neumann, Hermann Weyl, Paul Dirac.

of novel mathematical foundations. We now give a summary of the axioms that serve as the mathematical framework for quantum mechanics, broken down into the main constituents of any physical system: states, observables and dynamics.

The first postulate in quantum mechanics states that any quantum mechanical system at a time t can be fully described by its time-dependent wavefunction, $|\Psi(t)\rangle$. This wavefunction is a ray in the N-dimensional Hilbert space of the system, $\mathcal{H}$, which is a complex inner product space. Here we note that by using the term *ray*, rather than *vector*, we stipulate that all vectors equivalent up to some overall phase $\exp(\mathrm{i}\phi)$ describe the same state, where such an overall phase is not physically observable. Furthermore, the wavefunction represents the probability amplitude distribution of the quantum system and may be expressed using any basis $\{|\psi_i\rangle\}$ of the system's Hilbert space:

$$|\Psi(t)\rangle = \sum_i c_i(t)\,|\psi_i\rangle\,, \tag{2.1}$$

with $c_i(t) \in \mathbb{C}$ for all i. Here we consider that the wavefunction is properly normalised such that $\langle\Psi(t)\,|\Psi(t)\rangle = \sum_i |\,c_i(t)\,|^2 = 1$, where $|\,c_i(t)\,|^2$ is the probability of measuring the system in state $|\psi_i\rangle$.

The second postulate asserts that any observable of the system can be mathematically represented by a Hermitian operator, A,[2] acting on the state $|\Psi\rangle$ (we have dropped time dependence for notational convenience). The eigenvectors of the observable form a basis of $\mathcal{H}$ and, therefore, measuring the physical observable corresponding to A results in one of operator's eigenvalues. The probability of obtaining some measurement represented by the eigenvalue a is given by the Born rule in quantum mechanics. In the case of a discrete spectrum, the probability is given by

$$P(a) = |\,\langle\psi_a|\Psi\rangle\,|^2, \tag{2.2}$$

where $|\psi_a\rangle$ is the corresponding eigenvector.[3] For a continuous spectrum, where the probability amplitudes are expressed in terms of some density function, the probability of measuring some value between $(a, a + \mathrm{d}a)$ is given by

$$P(a, a + \mathrm{d}a) = |\,\langle\psi_a|\Psi\rangle\,|^2 \mathrm{d}a. \tag{2.3}$$

The act of measuring the system in $\mathcal{H}$ results in the collapse of the wavefunction: the state $|\Psi\rangle$ is projected onto the eigensubspace of the corresponding measurement outcome. Hence, when obtaining a measurement outcome a, we have

$$|\Psi\rangle \xrightarrow{\text{Measurement}} \frac{\Pi_a\,|\Psi\rangle}{\sqrt{\langle\Psi|\Pi_a|\Psi\rangle}}, \tag{2.4}$$

where $\Pi_a = |\psi_a\rangle\langle\psi_a|$ $(= \sum_i |\psi_a^{(i)}\rangle\langle\psi_a^{(i)}|$ in the case of a degenerate spectrum) satisfies the conditions of a projection operator. Given this collapse of the wavefunction resulting from

[2] It is common practice in quantum field theory to drop the use of "$\hat{}$", otherwise used to denote operators, as its implication is otherwise understood from the context. We also choose to drop its use in this thesis to ease the notation.

[3] Although, strictly speaking, the definition here is applicable to a non-degenerate discrete spectrum, this can be trivially generalised for the case of a degenerate spectrum.

the action of a measurement, a second immediate measurement of the same observable A would then necessarily result in the same outcome.

The third postulate relates to the evolution of the system with time. The dynamics of a *closed*, or perfectly isolated, quantum system can be obtained by applying a unitary transformation to the wavefunction, which evolves it from some initial time t_0 to some later time t:

$$|\psi(t_0)\rangle \to |\psi(t)\rangle = U(t, t_0)\,|\psi(t_0)\rangle\,, \tag{2.5}$$

where $U^\dagger U = \mathbb{1}$ by definition of a unitary operator.

We note here that having a transformation operator that is unitary is sufficient for the quantum mechanical system to be considered as closed. In fact, assuming a normalised wavefunction at some initial time t_0, we then obtain for any time t

$$\langle\psi(t)\,|\psi(t)\rangle = \langle\psi(t_0)\,|U^\dagger(t, t_0)\,U(t, t_0)\,|\psi(t_0)\rangle = \langle\psi(t_0)\,|\psi(t_0)\rangle = 1. \tag{2.6}$$

The wavefunction represents a complex-valued probability amplitude distribution. Taking the inner product of the (initially normalised) wavefunction is mathematically equivalent to finding the total probability of the quantum system occupying a state in the defined Hilbert space, and therefore having the inner product be constantly equal to unity means that the state can be fully described by the given Hilbert space at any given time. We will see further on that quantum systems may couple to the environment due to dissipation, necessitating the use of density matrices to properly characterise the system and its dynamics.

Any unitary operator may be written in the form of $\exp(\mathrm{i}A)$ where A is some Hermitian operator called the generator. Let us then consider the unitary transformation generated by the Hamiltonian of the system, H, such that

$$U(t + \Delta t, t) = \exp\left(-\mathrm{i}\frac{H\Delta t}{\hbar}\right), \tag{2.7}$$

where $\hbar$ is the reduced Planck constant, introduced to keep the generator dimensionless. The choice of our operator H here is analogous to the use of the Hamiltonian in classical mechanics, also representing the total energy of the system, to generate time evolution [39]. Applying this to our wavefunction in order to obtain $|\psi(t + \mathrm{d}t)\rangle$

$$\begin{aligned} |\psi(t + \mathrm{d}t)\rangle &= U(t + \mathrm{d}t, t)\,|\psi(t)\rangle \\ &= \left(\mathbb{1} - \mathrm{i}\frac{H\mathrm{d}t}{\hbar} + \ldots\right)|\psi(t)\rangle\,, \end{aligned} \tag{2.8}$$

where

$$|\psi(t + \mathrm{d}t)\rangle = |\psi(t)\rangle + \mathrm{d}t\frac{\mathrm{d}}{\mathrm{d}t}\,|\psi(t)\rangle + \ldots. \tag{2.9}$$

Taking the infinitesimal limit such that $\mathrm{d}t \to 0$, we can ignore higher order terms in $\mathrm{d}t$, giving us the Schrödinger equation:

$$\mathrm{i}\hbar\,\partial_t\,|\psi(t)\rangle = H\,|\psi(t)\rangle\,. \tag{2.10}$$

Given a set of initial conditions, one may use this equation to mathematically map out the trajectory of the system as it evolves over time.

2.2 Density matrices

At this stage we introduce the density matrix formalism [40]. The state of an isolated quantum system may be denoted in matrix form by taking the outer product of its wavefunction:

$$\rho = |\Psi\rangle\langle\Psi| = \sum_{i,j} c_i c_j^* |\psi_i\rangle\langle\psi_j| , \tag{2.11}$$

where the diagonal entry $\rho_{ii} = |c_i|^2$ is the probability of finding the system in state $|\psi_i\rangle$, and therefore referred to as the population of the state. For a normalised state, we have $\sum_i \rho_{ii} = 1$. The off-diagonal entries of the density matrix denote the interference between two orthogonal eigenstates and are a signature of the state's quantum superposition and coherence.

A quantum system may exist in a coherent superposition of different possible states. An attempt at measuring the state of the system (in the appropriate basis) results in a random outcome, the probability of which is determined by the probability amplitude distribution of the system. It therefore makes sense to assign an expectation value for a given observable, A. We define this as

$$\langle A\rangle = \langle\Psi|A|\Psi\rangle = \sum_{i,j} c_i^* c_j \langle\psi_i|A|\psi_j\rangle = \sum_{i,j} \rho_{ji}\langle\psi_i|A|\psi_j\rangle = \mathrm{Tr}\left[\rho A\right], \tag{2.12}$$

where we have used the notation for the density matrix elements given by $\rho_{ij} = \langle\psi_i|\rho|\psi_j\rangle$, the completeness of the eigenbasis such that $\sum_i |\psi_i\rangle\langle\psi_i| = \mathbb{1}$, and the definition of the trace given by $\mathrm{Tr}\left[A\right] = \sum_i \langle\psi_i|A|\psi_i\rangle$. Formally, the density matrix needs to satisfy the following properties:

$$\begin{aligned} &1.\quad \rho^\dagger = \rho \quad \text{(Hermiticity)},\\ &2.\quad \mathrm{Tr}\left[\rho\right] = 1 \quad \text{(normalisation)},\\ &3.\quad \langle\Psi|\rho|\Psi\rangle \geq 0 \text{ for all } |\Psi\rangle \quad \text{(positivity)}. \end{aligned} \tag{2.13}$$

The density matrix formalism therefore provides a convenient way to express the expectation value of an observable. At this stage we note the equivalence between an observable being Hermitian, as stipulated in the second postulate, and an expectation value that is real:

$$\langle A\rangle = \overline{\langle A\rangle} \iff \langle\Psi|A|\Psi\rangle = \overline{\langle\Psi|A|\Psi\rangle} = \langle\Psi|A^\dagger|\Psi\rangle \iff A = A^\dagger. \tag{2.14}$$

The usefulness of the density matrix description lies in its ability to also account for systems that are no longer in a *pure* state, i.e., they can not be expressed in the form of a vector of the system's Hilbert space as in Eq. (2.1). This is the case for systems that exist in some statistical mixture of different quantum states [41]. It is also a convenient way of describing open systems that have the same Hilbert space as a closed one but, due to the interaction with their environment, undergo different dynamics. This may happen in the event of some perturbation occurring to the system, coupling to the environment resulting in decoherence or making some measurement and obtaining only partial information about the full system. In such cases, we say the system exists in a mixed state.

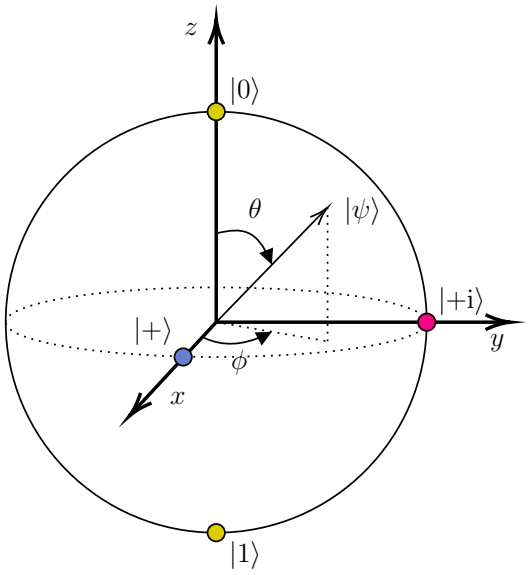

Figure 2.1: The Bloch sphere is a geometrical representation of all possible states of a qubit. The orthonormal basis vectors are $|0\rangle$ and $|1\rangle$. Points on the surface represent pure states, with $|+\rangle = (|0\rangle + |1\rangle)/\sqrt{2}$ and $|+\mathrm{i}\rangle = (|0\rangle + \mathrm{i}\,|1\rangle)/\sqrt{2}$, whilst mixed states are all located within the sphere.

Consider a system that is in an ensemble, or statistical mixture, of the pure states $\{|\Psi_i\rangle\}$, which are not necessarily orthogonal to each other. We make an important distinction here between a statistical ensemble and a quantum superposition: the latter is a system that coherently exists in multiple states at a given time, whilst the former is considered to be a statistical mixture only due to *lack of information on the observer's part* and there are no quantum interference effects between two eigenstates belonging to different pure states. The density matrix of such a mixed state then takes the form of

$$\rho = \sum_i p_i \,|\Psi_i\rangle \langle\Psi_i|\,. \tag{2.15}$$

We incorporate here classical probability in the form of p_i, which is the probability of the system occupying the state $|\Psi_i\rangle$ and where $\sum_i p_i = 1$. In order to distinguish between pure and mixed states, we may consider the purity of the density matrix. This is given by $\mathrm{Tr}\left[\rho^2\right] \leq 1$ and the inequality is saturated if and only if it describes a pure state. Furthermore, the expression for the expectation value defined in (2.12) also holds for mixed states.

The simplest nontrivial quantum system one may consider is a two-level system, ubiquitously referred to as a *qubit*. The Bloch sphere, shown in Fig. 2.1, is a geometric representation of all possible states of a qubit and provides a convenient intuition for the two types of density matrices. A qubit can be expressed as

$$|\psi\rangle = \cos\frac{\theta}{2}\,|0\rangle + e^{\mathrm{i}\phi}\sin\frac{\theta}{2}\,|1\rangle\,, \tag{2.16}$$

where $|0\rangle, |1\rangle$ are the orthonormal basis vectors of the qubit's two-dimensional Hilbert space, $\mathbb{C}^2$. Its density matrix can be expressed as a linear combination of the identity and Pauli matrices:

$$\rho = \frac{1}{2}\left(\mathbb{1} + r_x\sigma_x + r_y\sigma_y + r_z\sigma_z\right), \tag{2.17}$$

where the Pauli matrices are of the form

$$\sigma_x = \begin{pmatrix} 0 & 1 \\ 1 & 0 \end{pmatrix}, \quad \sigma_y = \begin{pmatrix} 0 & -\mathrm{i} \\ \mathrm{i} & 0 \end{pmatrix}, \quad \sigma_z = \begin{pmatrix} 1 & 0 \\ 0 & -1 \end{pmatrix}. \tag{2.18}$$

Defining $\mathbf{r} = (r_x, r_y, r_z)$, we can use the property that density matrices are positive semi-definite to conclude that $|\mathbf{r}|^2 \leq 1$. Furthermore, since pure states have unit purity, such that $\mathrm{Tr}\left[\rho^2\right] = \left(1 + |\mathbf{r}|^2\right)/2 = 1$, then we must conclude that pure states only occupy points on the surface of the sphere such that $|\mathbf{r}| = 1$. The interior would then correspond to only mixed states.

2.3 Dynamical pictures

So far we have assumed that the time dependence of our quantum system is captured and described by the state's wavefunction $|\Psi(t)\rangle$. The evolution of the system is then given by Schrödinger's equation and the operators associated with the system remain constant in time. This is known as the *Schrödinger picture*. Alternatively, one may choose to represent the system within the *Heisenberg picture*, whereby the time dependence is described by the operators and the states do not change in time. The two pictures are equivalent and give the same results, and the choice of one description over the other is usually a matter of convenience.

We start by considering the expectation value of an observable A as given by Eq. (2.12)

$$\begin{aligned} \langle A\rangle &= \mathrm{Tr}\left[|\Psi(t)\rangle\langle\Psi(t)| A_{\mathrm{S}}\right] \\ &= \mathrm{Tr}\left[U(t,t_0)|\Psi(t_0)\rangle\langle\Psi(t_0)| U^\dagger(t,t_0) A_{\mathrm{S}}\right] \\ &= \mathrm{Tr}\left[|\Psi(t_0)\rangle\langle\Psi(t_0)| U^\dagger(t,t_0) A_{\mathrm{S}} U(t,t_0)\right] \\ &= \mathrm{Tr}\left[|\Psi(t_0)\rangle\langle\Psi(t_0)| A_{\mathrm{H}}(t)\right], \end{aligned} \tag{2.19}$$

where we have used the cyclic property of the trace and the subscript 'S' and 'H' denotes operators in the Schrödinger and Heisenberg picture, respectively. We can therefore define the time-dependent operators in the Heisenberg picture by $A_{\mathrm{H}}(t) = U^\dagger(t,t_0) A_{\mathrm{S}} U(t,t_0)$, with the state of the system, $|\Psi_{\mathrm{H}}\rangle = |\Psi(t_0)\rangle$, being constant in time.

We now wish to understand the time evolution of the operator $A_{\mathrm{H}}(t)$, similarly to how we described the dynamics of the state using the Schrödinger equation in Eq. (2.10). Recall first that

$$U(t,t_0) = \exp\left(-\mathrm{i}\frac{Ht}{\hbar}\right) \quad \Longrightarrow \quad \frac{\mathrm{d}}{\mathrm{d}t}U(t,t_0) = -\mathrm{i}\frac{H}{\hbar}U(t,t_0). \tag{2.20}$$

Then by differentiating the operator with respect to time, we find

$$\begin{aligned}\frac{\mathrm{d}}{\mathrm{d}t}A_{\mathrm{H}}(t) &= \frac{\mathrm{d}}{\mathrm{d}t}U^{\dagger}(t,t_0)\,A_{\mathrm{S}}\,U(t,t_0)\\ &= \dot{U}^{\dagger}(t,t_0)\,A_{\mathrm{S}}\,U(t,t_0)+U^{\dagger}(t,t_0)\,\dot{A}_{\mathrm{S}}\,U(t,t_0)+U^{\dagger}(t,t_0)\,A_{\mathrm{S}}\,\dot{U}(t,t_0)\\ &= \frac{\mathrm{i}}{\hbar}HA_{\mathrm{H}}(t)+\partial_t A_{\mathrm{H}}(t)-\frac{\mathrm{i}}{\hbar}A_{\mathrm{H}}(t)\,H\\ &= -\frac{\mathrm{i}}{\hbar}\left[A_{\mathrm{H}}(t),H\right]+\partial_t A_{\mathrm{H}}(t),\end{aligned} \tag{2.21}$$

where we denote the commutator by $[A,B]=AB-BA$. This is known as the Heisenberg equation. Here, the partial derivative with respect to time takes into account only the *explicit* time-dependence of the operator in the Schrödinger picture. This applies in the case of, say, dependence on some external time-varying electric field. However generally this operator is independent of time.

In the study of physically interesting systems, we quickly find that relying on just one of the aforementioned representations is not the most convenient choice. It is therefore more useful to take a hybrid approach in the form of the interaction (or Dirac) picture, where the time dependence of the observables is captured by both the operators and the state vectors. This is commonly used when the system evolves due to some interaction. Here, the tractable part of the evolution is prescribed to the operators whilst any complications are confined to the dynamics of the state. This is done by taking the Hamiltonian of the system in the Schrödinger picture and splitting it up into a free, H_0, and interaction part, H_{int}, such that $H=H_0+H_{\mathrm{int}}$. Although the choice of partition is arbitrary, it is preferable to set H_0 such that it is easy to solve exactly and to have no explicit time-dependence, whilst attributing more complex perturbations to H_{int}. Moreover, it is typical to choose the free and interaction parts to be such that the interaction strength is much weaker than the energy associated with the free parts.

We may define the state vectors and operators in the interaction picture by keeping in mind the requirement of the invariance of the expectation values across the different representations:

$$\langle A(t)\rangle = \mathrm{Tr}\left[\rho(t)\,A(t)\right], \tag{2.22}$$

where ρ and A both describe the same picture. This then motivates the following definitions:

$$\begin{aligned}|\Psi_{\mathrm{I}}(t)\rangle &= U_0^{\dagger}(t,t_0)\,|\Psi_{\mathrm{S}}(t)\rangle\\ &= U_0^{\dagger}(t,t_0)\,U(t,t_0)\,|\Psi(t_0)\rangle,\end{aligned} \tag{2.23a}$$

$$A_{\mathrm{I}}(t) = U_0^{\dagger}(t,t_0)\,A_{\mathrm{S}}(t)\,U_0(t,t_0), \tag{2.23b}$$

where $U_0(t,t_0)=\exp\left(-\mathrm{i}H_0t/\hbar\right)$ and subscript 'I' denotes the interaction representation. Note the operator $A(t)$ normally does not have an explicit time-dependence, in which case we may denote it as simply A_{S}.

The Schrödinger equation in the interaction picture can then be expressed by means of the time derivative of the state, giving

$$\begin{aligned} \mathrm{i}\hbar\frac{\mathrm{d}}{\mathrm{d}t}\left|\Psi_{\mathrm{I}}\left(t\right)\right\rangle &= -U_0^{\dagger}\left(t,t_0\right)H_0\left|\Psi_{\mathrm{S}}\left(t\right)\right\rangle + U_0^{\dagger}\left(t,t_0\right)\mathrm{i}\hbar\frac{\mathrm{d}}{\mathrm{d}t}\left|\Psi_{\mathrm{S}}\left(t\right)\right\rangle \\ &= H_{\mathrm{int,I}}\left|\Psi_{\mathrm{I}}\left(t\right)\right\rangle, \end{aligned} \tag{2.24}$$

where we have defined the interaction part of the Hamiltonian in the interaction picture as

$$H_{\mathrm{int,I}}\left(t\right) = U_0^{\dagger}\left(t,t_0\right)H_{\mathrm{int}}U_0\left(t,t_0\right). \tag{2.25}$$

The free part of the Hamiltonian is similarly defined. However, given that H_0 commutes with itself, the operator in the interaction picture is left unchanged. It is then clear from Eq. (2.25) that the state does not evolve should H_{int} be set to zero and the interaction part of the Hamiltonian, and any complex perturbations attributed to it, is reflected in the evolution of the state, not the operators. Finally, we may express the time evolution of operators in the interaction picture by

$$\frac{\mathrm{d}}{\mathrm{d}t}A_{\mathrm{I}}\left(t\right) = -\frac{\mathrm{i}}{\hbar}\left[A_{\mathrm{I}}\left(t\right),H_0\right] + \partial_t A_{\mathrm{I}}\left(t\right). \tag{2.26}$$

2.4 Quantisation of the electromagnetic field

We now move on to consider the quantised electromagnetic field, composed of discrete and indivisible energy packets in the form of photons. Consequently, we can describe the field in terms of so-called ladder operators which are derived from the coefficients of the expansion of the field in terms of its basis functions. This technique is often referred to as second quantisation for historical reasons. However, in the context of quantum field theory, it is more apt to refer to canonical quantisation. There exist a few approaches to the quantisation of the electromagnetic field [42–44]. However, we choose to describe this in the context of a cavity [45].

Note that in this section we will adopt the convention of using the hat, or " $\hat{.}$ ", to distinguish operators from classical variables. We start off from the classical description of the electromagnetic field, whereby we can use Maxwell's equations to obtain the following wave equation for the electric field $\mathbf{E}(\mathbf{r},t)$ inside a cavity with perfectly conducting walls (and in the absence of free charges and currents)

$$\nabla^2\mathbf{E}(\mathbf{r},t) = \frac{1}{c^2}\frac{\partial^2\mathbf{E}(\mathbf{r},t)}{\partial t^2}, \tag{2.27}$$

where c is the speed of light. The magnetic field $\mathbf{B}(\mathbf{r},t)$ is related to the electric field by

$$\nabla\times\mathbf{E}(\mathbf{r},t) = -\frac{\partial\mathbf{B}(\mathbf{r},t)}{\partial t}. \tag{2.28}$$

The classical Hamiltonian of the field is given by [46]

$$H = \frac{1}{2}\int_V \mathrm{d}^3\mathbf{r}\left(\epsilon_0|\mathbf{E}(\mathbf{r},t)|^2 + \frac{1}{\mu_0}|\mathbf{B}(\mathbf{r},t)|^2\right), \tag{2.29}$$

where ϵ_0 and μ_0 are the free space permittivity and permeability, respectively, with $\epsilon_0\mu_0 = c^{-2}$, and the integral is taken over the volume, V, of the cavity.

Let us assume that our cavity supports only a single field mode with frequency ω and mode amplitude $q(t)$. The Hamiltonian can then be expressed in the more convenient form of [47]

$$H = \frac{1}{2}\left(\omega^2 q^2 + p^2\right), \tag{2.30}$$

where $p = \dot{q}$ is the canonical momentum of q and the expression is, therefore, formally equivalent to a harmonic oscillator.

Suppose we have a cavity that can support multiple modes, $j = 1, 2, 3, \ldots$, none of which interact with each other. We now proceed to quantise the electromagnetic field by transforming the canonical coordinates to operators, such that $q_j \to \hat{q}_j$ and $p_j \to \hat{p}_j = -\mathrm{i}\hbar\nabla$, and imposing the commutation relations

$$[\hat{q}_j, \hat{p}_k] = \mathrm{i}\hbar\delta_{jk}, \tag{2.31a}$$

$$[\hat{q}_j, \hat{q}_k] = [\hat{p}_j, \hat{p}_k] = 0, \tag{2.31b}$$

where δ_{jk} is the Kronecker delta. The first expression is due to the commutation relation between the canonical position and momentum operators in quantum mechanics, and is necessary to endow quantisation to the field.

In this procedure we have restricted ourselves to one spatial dimension, yet care should be taken in the three-dimensional case. Here, we need to remember that the fields need to be orthogonal to the propagation direction due to Gauss' law, $\nabla \cdot \mathbf{E} = 0$, assuming zero charges. Then, in generalising Eq. (2.31a) to the three-dimensional case we would need to modify the delta function on the right-hand side of the equation to ensure consistency with Gauss' law. We will not delve deeper in the treatment of this, however a more detailed account is given in, e.g., Ref. [48].

We next make a canonical transformation by defining the non-Hermitian operators $\hat{a}_j$ and $\hat{a}_j^\dagger$ as

$$\hat{a}_j = \frac{1}{\sqrt{2\hbar\omega_j}}\left(\omega_j\hat{q}_j + \mathrm{i}\hat{p}_j\right) \tag{2.32a}$$

$$\hat{a}_j^\dagger = \frac{1}{\sqrt{2\hbar\omega_j}}\left(\omega_j\hat{q}_j - \mathrm{i}\hat{p}_j\right), \tag{2.32b}$$

with $[\hat{a}_j, \hat{a}_k^\dagger] = \delta_{jk}$ and $[\hat{a}_j, \hat{a}_k] = [\hat{a}_j^\dagger, \hat{a}_k^\dagger] = 0$ by the commutation relations imposed on the original canonical operators.

This allows us to express the quantised Hamiltonian as

$$\hat{H} = \hbar\sum_j \omega_j\left(\hat{a}_j^\dagger\hat{a}_j + \frac{1}{2}\right). \tag{2.33}$$

where the eigenvalues, or energy levels, are given by $E(n_1, n_2, \ldots) = \hbar\sum_j \omega_j(n_j + \frac{1}{2})$, where $n_j = n_1, n_2, \ldots$ are non-negative integers. This is the Hamiltonian for the quantum harmonic oscillator with the fundamental frequency of the j^{th} mode given by ω_j. We can

therefore interpret the quantised electromagnetic field as being composed of an infinite sum of harmonic oscillators (assuming no sources) with the total energy being equal to the sum of the energies of the individual components, or modes. The operators $\hat{a}_j$ and $\hat{a}_j^\dagger$ are referred to as ladder operators and we will discuss their roles as mode operators in more detail in the next section.

2.5 Quantum states of the electromagnetic field

In the previous section we gave a quantised description of the electromagnetic field and its Hamiltonian in terms of the ladder, or mode, operators. We will now describe the quantum states pertaining to this field and resume the omission of the use of " ˆ " for notational convenience.

2.5.1 Fock states

We first introduce the operator $n = a^\dagger a$, which we refer to as the number operator and satisfies the eigenvalue problem given by

$$\hat{n}\,|n\rangle = n\,|n\rangle\,, \tag{2.34}$$

where $|n\rangle$ are eigenstates of $\hat{n}$, and consequently of $\hat{H}$ as given in Eq. (2.33), and n is an integer. These are referred to as Fock, or number, states. Without loss of generality, let us consider the Hamiltonian for a single mode and apply the ladder operator such that

$$\begin{aligned} Ha^\dagger\,|n\rangle &= \hbar\omega\left(a^\dagger a + \frac{1}{2}\right)a^\dagger\,|n\rangle \\ &= \hbar\omega\left[a^\dagger\left(a^\dagger a + \mathbb{1}\right) + \frac{a^\dagger}{2}\right]|n\rangle \\ &= (E_n + \hbar\omega)\,a^\dagger\,|n\rangle\,, \end{aligned} \tag{2.35}$$

where E_n is the energy of state $|n\rangle$. The action of $a^\dagger$ is therefore to increase the energy of the system by a quantum of energy, $\Delta E = \hbar\omega$; physically, this represents the addition of a single photon to the field. Similarly, we find that $Ha\,|n\rangle = (E_n - \hbar\omega)\,a\,|n\rangle$, with the energy decreasing by the same amount as a consequence of the application of a. The operators $a^\dagger$ and a are then aptly referred to as the *creation* and *annihilation* operators, respectively, and are analogous to the raising and lowering operators of the quantum harmonic oscillator ladder.

Using the number operator, we can probe a bit deeper the effect of the ladder operators on Fock states. We first operate on the state $|n\rangle$ with $a^\dagger$ and find its norm, obtaining the following

$$||\,a^\dagger\,|n\rangle\,||^2 = \langle n|aa^\dagger|n\rangle = \langle n|\left(a^\dagger a + 1\right)|n\rangle = n + 1. \tag{2.36}$$

From the normalisation condition, we can conclude that $a^\dagger\,|n\rangle = \sqrt{n+1}\,|n+1\rangle$ and, similarly, $a\,|n\rangle = \sqrt{n}\,|n-1\rangle$. Any Fock state can be expressed in terms of the creation operators

as

$$|n\rangle = \frac{\left(a^\dagger\right)^n}{\sqrt{n!}} |0\rangle \,. \tag{2.37}$$

Moreover, it is clear from these equations that the number of photons cannot be negative.

2.5.2 Coherent states

The coherent state is a state of the quantised electromagnetic field that serves as a convenient basis for various fields and whose behaviour very closely resembles that of a classical harmonic oscillator [49]. The description of light in classical optics considers states with very large, and highly uncertain, photon numbers. This has motivated the introduction and wide use of coherent states in quantum optics. It is also used as an idealised description of laser light due to its properties.

We define the coherent state $|\alpha\rangle$ to be the unique eigenstate of the annihilation operator a, such that $a\,|\alpha\rangle = \alpha\,|\alpha\rangle$. This can be expressed in terms of Fock states, with $|\alpha\rangle = \sum_n c_n\,|n\rangle$. Taking the inner product with $\langle n|$, we obtain

$$\langle n|a|\alpha\rangle = \langle n|\alpha|\alpha\rangle \quad \Longrightarrow \quad \sqrt{n+1}\,\langle n+1|\alpha\rangle = \alpha\,\langle n|\alpha\rangle \,, \tag{2.38}$$

giving us the recursion relation of $c_n = c_0\alpha^n/\sqrt{n!}$. Taking the state to be normalised, such that $\langle\alpha|\alpha\rangle = 1$, we obtain the expression for the coherent state given by

$$|\alpha\rangle = e^{-|\alpha|^2/2} \sum_n \frac{\alpha^n}{\sqrt{n!}} |n\rangle \,. \tag{2.39}$$

Here, α represents the amplitude of the state, which can be seen when taking the photon number expectation value given by $\langle n\rangle = \langle\alpha|a^\dagger a|\alpha\rangle = |\alpha|^2$. Furthermore, the standard deviation of the state is given by $\Delta n = |\alpha|$ and since this scales as the square root of the photon number, the statistics for high intensity fields with $\alpha \to \infty$ resemble that of a classical stable wave. Finally, we also consider the photon statistics of our coherent state. The probability of measuring n photons, $P\,(n)$, can be obtained by considering the inner product with $\langle n|$, which gives

$$\begin{aligned} \langle n|\alpha\rangle &= e^{-|\alpha|^2/2} \sum_m \frac{\alpha^m}{\sqrt{m!}} \langle n|m\rangle \\ &= e^{-|\alpha|^2/2} \frac{\alpha^n}{\sqrt{n!}}. \end{aligned} \tag{2.40}$$

We then find that

$$P\,(n) = |\,\langle n|\alpha\rangle\,|^2 = e^{-|\alpha|^2} \frac{|\alpha|^{2n}}{n!} = e^{-\bar{n}} \frac{\bar{n}^n}{n!}, \tag{2.41}$$

where $\bar{n}$ is the mean, or expectation value, of the number of photons. The coherent state therefore exhibits a Poissonian distribution.

We may also consider a photon wavepacket, i.e., an electromagnetic wave 'envelope' localised in space, with a single photon made up of a superposition of modes differing

in frequency, $b^\dagger |0\rangle = \int \mathrm{d}\omega\, f(\omega)\, a^\dagger(\omega)\, |0\rangle$. The wavefunction describing the probability amplitude density is normalised such that $\int \mathrm{d}\omega |f(\omega)|^2 = 1$. Using the Heisenberg equation of motion, we find that a single creation operator evolves with time as

$$a^\dagger(\omega, t) = a^\dagger(\omega)\, e^{\mathrm{i}\omega t}. \tag{2.42}$$

The time-evolution of the single photon wavepacket can be expressed by setting $f(\omega) \to f(\omega)\, e^{\mathrm{i}\omega t}$ and, therefore, a state that is coherent at some initial time would maintain this property as it evolves.

2.6 Entanglement

2.6.1 Entanglement as a resource

An essential element of the work in this thesis has been the generation of entanglement as a resource in quantum information processing. Consider a system composed of two sub-systems, described by the tensor product of the respective Hilbert spaces $\mathcal{H} = \mathcal{H}_1 \otimes \mathcal{H}_2$. Then any state of the composite system may be described as

$$|\Psi\rangle = \sum_{i,j} c_{ij}\, |i\rangle_1 \otimes |j\rangle_2 \,, \tag{2.43}$$

where $\{|i\rangle_1\}$ and $\{|j\rangle_2\}$ are some basis for $\mathcal{H}_1$ and $\mathcal{H}_2$, respectively. We call the state of the system separable if it can be expressed in the form $|\Psi\rangle = |\psi\rangle_1 \otimes |\phi\rangle_2$, i.e., it can be factorised as a product of state vectors of the individual sub-systems. However, if there does not exist any decomposition of the state in this product form, we say that the system is entangled and the state of one sub-system fundamentally depends on that of the other.

The presence of entanglement can be seen clearly by considering the density matrix formalism when describing the two sub-systems. Let us assume a two-qubit system that has been prepared in the state $|\Psi\rangle = (|01\rangle + |10\rangle)/\sqrt{2}$ and that Alice and Bob each hold one of the qubits. It is evident that the state of the qubits are correlated, since the state of Alice's qubit depends on that of Bob and vice versa. The density matrix for this state is then

$$\rho = \frac{1}{2}\left(|01\rangle\langle 01| + |01\rangle\langle 10| + |10\rangle\langle 01| + |10\rangle\langle 10|\right). \tag{2.44}$$

If we wish to now describe only Alice or Bob's systems, we may do so by considering the respective reduced density matrix. To do so, we take the partial trace with respect to the other sub-system and effectively trace it out. For Alice, we find

$$\rho_\mathrm{A} = \mathrm{Tr}_\mathrm{B}[\rho] = \sum_{i=0,1} \langle i|\rho|i\rangle = \frac{1}{2}\left(|1\rangle\langle 1| + |0\rangle\langle 0|\right), \tag{2.45}$$

and similarly for Bob,

$$\rho_\mathrm{B} = \mathrm{Tr}_\mathrm{A}[\rho] = \frac{1}{2}\left(|0\rangle\langle 0| + |1\rangle\langle 1|\right). \tag{2.46}$$

One might argue that this is similar to the classical correlation that would result, say, if Alice and Bob each had to choose a marble from a container holding one black and one white marble, which can be represented as the mixed state

$$\rho = \frac{1}{2}\left(|01\rangle\langle 01| + |10\rangle\langle 10|\right). \tag{2.47}$$

However, the difference becomes clear when we try to reconstruct the original density matrix from the reduced ones:

$$\rho_{\mathrm{A}} \otimes \rho_{\mathrm{B}} = \frac{1}{4}\left(|00\rangle\langle 00| + |01\rangle\langle 01| + |10\rangle\langle 10| + |11\rangle\langle 11|\right). \tag{2.48}$$

This is no longer equal to the original density matrix as given in Eq. (2.44), from which we can conclude that there is information about the composite system that cannot be obtained by considering just each sub-system on its own. We call this quantum correlation entanglement. Indeed, the action of tracing out one of the participants reduced the density matrix from a pure to a mixed state. In general, a pure state of a bipartite system is entangled if and only if the reduced density matrices are mixed. This signifies the loss of information and the introduction of classical uncertainty.

Another important aspect that distinguishes entanglement from classical correlations can be seen by rotating the basis of the states by

$$|0\rangle = \frac{|+\rangle + |-\rangle}{\sqrt{2}} \qquad \text{and} \qquad |1\rangle = \frac{|+\rangle - |-\rangle}{\sqrt{2}}. \tag{2.49}$$

We see that the original entangled state becomes $|\Psi\rangle = \left(|{+}{+}\rangle - |{-}{-}\rangle\right)/\sqrt{2}$ and therefore remains entangled. However, the mixed state exhibiting perfect classical correlations in Eq. (2.47) would transform to

$$\begin{aligned}\rho = \frac{1}{4}\big(&|{+}{+}\rangle\langle{+}{+}| + |{+}{-}\rangle\langle{+}{-}| + |{-}{+}\rangle\langle{-}{+}| + |{-}{-}\rangle\langle{-}{-}| \\ &- |{+}{+}\rangle\langle{-}{-}| - |{-}{-}\rangle\langle{+}{+}| - |{+}{-}\rangle\langle{-}{+}| - |{-}{+}\rangle\langle{+}{-}|\big),\end{aligned} \tag{2.50}$$

which exhibits zero correlations. We can therefore conclude that entanglement shows correlations *stronger* than correlations in purely classical systems.

One of the most prominent examples of entanglement as a resource is its application in quantum teleportation [50]. Suppose Alice holds a qubit prepared in some unknown state $|\psi\rangle_1 = \alpha\,|0\rangle_1 + \beta\,|1\rangle_1$ and wishes to transfer this state to a qubit held by Bob. By the no-cloning theorem [51], it is impossible to reproduce a copy of Alice's qubit faithfully without prior knowledge of the state. Instead, we have to make use of Bell states, which are maximally entangled and given by

$$|\Phi^{\pm}\rangle = \frac{|00\rangle \pm |11\rangle}{\sqrt{2}} \qquad \text{and} \qquad |\Psi^{\pm}\rangle = \frac{|01\rangle \pm |10\rangle}{\sqrt{2}}. \tag{2.51}$$

Alice and Bob will now share the Bell state $|\Phi^{+}\rangle$ between them (the choice of which Bell state is arbitrary) and the total system is given by

$$|\Psi\rangle_{123} = |\psi\rangle_1 \otimes |\Phi^{+}\rangle_{23} = \frac{1}{\sqrt{2}}\left(\alpha\,|000\rangle + \alpha\,|011\rangle + \beta\,|100\rangle + \beta\,|111\rangle\right), \tag{2.52}$$

where Alice holds the first 2 qubits and Bob holds the third. Let us express the state of qubits 1 and 2 in the Bell basis:

$$|\Psi\rangle_{123} = \frac{1}{2}\big[\,|\Phi^+\rangle\,(\alpha\,|0\rangle + \beta\,|1\rangle) + |\Phi^-\rangle\,(\alpha\,|0\rangle - \beta\,|1\rangle) \\ + |\Psi^+\rangle\,(\beta\,|0\rangle + \alpha\,|1\rangle) + |\Psi^-\rangle\,(-\beta\,|0\rangle + \alpha\,|1\rangle)\,\big]. \tag{2.53}$$

This means that Alice may transfer the state of qubit 1 up to some correction, without physical transmission of any matter, to qubit 3 held by Bob by performing a Bell measurement on her two qubits. Alice may then (classically) communicate her measurement outcome to Bob in order to determine the necessary corrections to faithfully obtain $|\psi\rangle$.

This protocol shows just how advantageous quantum entanglement can prove to be when combined with local operations and classical communication (LOCC). We note that we do not violate the no-cloning theorem at any stage: indeed, Alice's original qubit seizes to exist in the original state once it is transferred to Bob's qubit by means of measurement. We also do not violate the no-signalling principle, i.e., the transfer of information is always subluminal: although the projection of Bob's qubit is immediate as a result of the measurement of the entangled state, information about the measurement outcome needs to be conveyed by Alice to Bob in order to determine the exact state of the qubit, and this cannot exceed the speed of light.

2.6.2 Entanglement measures

Until now we have given examples of states that are maximally entangled, however not all states that are entangled are equally valuable resource-wise. For example, it is rather intuitive to see that the state $|\psi\rangle \propto |00\rangle + 0.1\,|11\rangle$ is not separable, and hence is entangled, but is not "as entangled" as $|\Phi^+\rangle$. In the context of quantum teleportation, say, the use of such a state would result in unfaithful transmission of the qubit state from Alice to Bob. Furthermore, determining whether or not a state is separable in some basis is not always trivial, especially when one considers a mixed state. It therefore makes sense to assign some measure to the amount of entanglement within a system.

There exist several entanglement measures, often applicable for bipartite systems, which necessarily satisfy the following conditions: the measure must be 1) a non-negative real function that is zero for a separable state and maximum for maximally entangled states, and 2) is invariant under LOCC. Some entanglement measures are tied to the operational task the entanglement is being used for, such as distillable entanglement and entanglement cost. Otherwise, one could characterise the amount of entanglement within a system by making use of more abstractly defined measures, which is what we will consider here.

In the previous section, we discussed how reduced density matrices of entangled pure states are mixed. This naturally leads us to the most commonly used entanglement measure, namely the von Neumann entanglement entropy [52] which is given by the expression

$$S\,(\rho_{\mathrm{A}}) = -\mathrm{Tr}\,[\rho_{\mathrm{A}} \log_2 \rho_{\mathrm{A}}] = -\sum_i \lambda_i \log_2 \lambda_i, \tag{2.54}$$

where ρ_{A} is the reduced density matrix of subsystem A and λ_i are its eigenvalues, and where $S\,(\rho_{\mathrm{A}}) = S\,(\rho_{\mathrm{B}})$. We can see that this concept and expression is parallel to the

use of entropy in thermodynamics, statistical mechanics and information theory. In the classical setting, entropy may be used as a measure of the lack of information associated with a system's macrostate given some probability distribution for the occupation of its various microstates. For a macrostate comprising of just one microstate, the uncertainty (and, hence, entropy) would be zero. On the other hand, the entropy of a macrostate is at its maximum when all possible microstates are occupied with an equal probability. In the quantum setting, the entropy would signify the uncertainty associated with the state of one subsystem resulting from the tracing out of the other. Furthermore, we can extend this measure to mixed states by defining [53]

$$S(\rho) = \min \sum_i p_i S(\rho_i), \tag{2.55}$$

where $\rho = \sum_i p_i \rho_i$ is the density matrix of the mixed state under consideration and the minimisation is done over all possible decompositions of ρ.

In this work, we will make use of concurrence [54, 55] as our measure of entanglement generated between the two spin states. The advantage of this measure is that it is well-defined for all systems comprising of a pair of qubits, including those that are in a mixed state. Given a state ρ describing the bipartite system, the concurrence is defined as

$$\mathcal{C}(\rho) = \max(0, \lambda_1 - \lambda_2 - \lambda_3 - \lambda_4), \tag{2.56}$$

where $\mathcal{C}(\rho) \in [0, 1]$ and $\lambda_1, \ldots, \lambda_4$ are the eigenvalues, in decreasing order, of

$$R = \sqrt{\sqrt{\rho}\,(\sigma_y \otimes \sigma_y)\,\rho^*\,(\sigma_y \otimes \sigma_y)\,\sqrt{\rho}}, \tag{2.57}$$

where σ_y is the Pauli Y matrix. The concurrence is bounded from below by zero with entangled states resulting in a strictly positive value that increases monotonically with the amount of entanglement, whilst separable states have concurrence values of zero.

For a pure two-qubit state $|\psi\rangle = \sum_{i,j} c_{ij} |i\rangle \otimes |j\rangle$, the concurrence simplifies to

$$\mathcal{C}(|\psi\rangle) = |\langle\psi|\sigma_y \otimes \sigma_y|\psi^*\rangle| = 2|c_{00}c_{11} - c_{01}c_{10}|, \tag{2.58}$$

where $|\psi^*\rangle = |\psi\rangle^*$ is the complex conjugate. This effectively gives a measure of how much the probability amplitudes of $|\psi\rangle$ differ from those of a fully separable state: it is clear from the expression that the concurrence is zero if and only if the state is separable, whilst all maximally entangled states, given by the four Bell states in Eq. (2.51), give a concurrence value of unity. When the state is mixed, $\mathcal{C}(\rho)$ gives the average concurrence of the pure state decomposition of ρ, minimised over all possible decompositions [55].

2.7 Quantum error correction

In Chapter 5, we investigate how quantum error correction may be performed using light–matter interfaces. Therefore, we will now give a brief description of the principles underpinning this type of error correction, first proposed by Peter Shor [56]. We first consider

the classical treatment, where error correction relies on the introduction of redundancy in the number of bits used to encode a single bit of information. A simple example is the three-bit repetition code, which maps $0 \to 000$ and $1 \to 111$. Should a single bit-flip error occur, e.g., $000 \to 100$, this can easily be detected by considering a majority vote, provided that the error probability is less than $1/2$. However, our rudimentary example would not be tolerant to two- or three-bit errors. Therefore, the type and complexity of the code needs to cater for the error probability of the computing hardware.

Moving from bits to qubits, however, is not trivial due to the quantum nature of the encoded information. Given that a qubit can be generally expressed as $|\psi\rangle = \cos\theta/2\,|0\rangle + e^{\mathrm{i}\phi}\sin\theta/2\,|1\rangle$ using the Bloch sphere representation, it is now subject to an infinite range of errors due to various physical processes. We restrict ourselves to coherent errors that simply rotate the state vector along the surface of the Bloch sphere. This can be mathematically described by means of a unitary operator $U(\delta\theta, \delta\phi)$ evolving the qubit as

$$U(\delta\theta, \delta\phi)\,|\psi\rangle = \cos\frac{\theta+\delta\theta}{2}\,|0\rangle + e^{\mathrm{i}(\phi+\delta\phi)}\sin\frac{\theta+\delta\theta}{2}\,|1\rangle\,. \tag{2.59}$$

This can be expressed using the Pauli basis, giving

$$\begin{aligned} U(\delta\theta, \delta\phi)\,|\psi\rangle &= c_{\mathbb{1}}\mathbb{1}\,|\psi\rangle + c_X X\,|\psi\rangle + c_Y Y\,|\psi\rangle + c_Z Z\,|\psi\rangle \\ &= c_{\mathbb{1}}\mathbb{1}\,|\psi\rangle + c_X X\,|\psi\rangle + c_{XZ} XZ\,|\psi\rangle + c_Z Z\,|\psi\rangle\,, \end{aligned} \tag{2.60}$$

where $c_{\mathbb{1}}, c_X, c_Y$ and c_Z are complex coefficients and the phase difference is absorbed by the coefficient c_{XZ}. Moreover, the Pauli matrices are given in Eq. (2.18) with $XZ = -\mathrm{i}Y$. Therefore, we see that we can digitise the error process and any coherent error may be decomposed into Pauli X-type and Pauli Z-type errors. The action of X on a qubit is a bit-flip ($X\,|0\rangle = |1\rangle$ and $X\,|1\rangle = |0\rangle$) whilst $Z\,|\psi\rangle = \alpha\,|0\rangle - \beta\,|1\rangle$ and the resulting error is, therefore, referred to as a phase-flip error.

We may now, analogously to the classical case, consider redundancy in the code by expanding the Hilbert space into which the information is encoded. Keeping to the three-bit example above, the single logical qubits are given by the physical three-qubit states: $|0_l\rangle = |000\rangle$ and $|1_l\rangle = |111\rangle$. However, given that the logical qubit is generally in some superposition, we may no longer simply perform a direct measurement of the physical qubits to detect error, as doing so would destroy some of the encoded information. Furthermore, by virtue of the no-cloning theorem, we may not create exact replicas of our physical qubits that would allow us to determine any errors. Instead, we can apply projective measurements that would protect the state. In our example, the state $\alpha\,|0_l\rangle + \beta\,|1_l\rangle = \alpha\,|000\rangle + \beta\,|111\rangle$ is preserved when a projective measurement of the form $Z\otimes Z\otimes\mathbb{1}$ and $\mathbb{1}\otimes Z\otimes Z$ is performed, and the corresponding eigenvalue is $+1$. In the presence of a bit-flip error, we see that the eigenvalue of either of the two measurements is changed (we simplify the notation by using

$A \otimes B = AB$):

$$\begin{aligned}
ZZ\mathbb{1}\,(\alpha\,|100\rangle + \beta\,|011\rangle) &= -\,(\alpha\,|100\rangle + \beta\,|011\rangle)\,,\\
\mathbb{1}ZZ\,(\alpha\,|100\rangle + \beta\,|011\rangle) &= +\,(\alpha\,|100\rangle + \beta\,|011\rangle)\,,\\
ZZ\mathbb{1}\,(\alpha\,|010\rangle + \beta\,|101\rangle) &= -\,(\alpha\,|010\rangle + \beta\,|101\rangle)\,,\\
\mathbb{1}ZZ\,(\alpha\,|010\rangle + \beta\,|101\rangle) &= -\,(\alpha\,|010\rangle + \beta\,|101\rangle)\,,\\
ZZ\mathbb{1}\,(\alpha\,|001\rangle + \beta\,|110\rangle) &= +\,(\alpha\,|001\rangle + \beta\,|110\rangle)\,,\\
\mathbb{1}ZZ\,(\alpha\,|001\rangle + \beta\,|110\rangle) &= -\,(\alpha\,|001\rangle + \beta\,|110\rangle)\,.
\end{aligned} \tag{2.61}$$

The string of eigenvalues resulting from the measurement process corresponds to the *syndrome of the error* and each error case has its own unique syndrome [57]. Given the extracted syndrome, we can therefore determine which qubit would need to be corrected by means of an X operation. In order to be able to detect phase-flip errors, we would need to increase the dimension of the Hilbert space further, with the procedure remaining the same. In fact, the code proposed by Shor makes use of nine physical qubits to ensure the detection of any arbitrary single-qubit error. The Steane code [58] is another model which similarly detects any error by encoding a logical qubit into seven physical qubits.

We can also define the above as a *stabiliser code*, where an operator S is said to be a stabiliser of some state $|\psi\rangle$ if $S\,|\psi\rangle = |\psi\rangle$. A given state may have a whole group of stabilisers, the size of which grows with the dimension of the state's Hilbert space. We define the stabiliser generator to be the group's minimal subset from which we can retrieve all other elements of the group by product operations. Therefore, $\{ZZ\mathbb{1}, \mathbb{1}ZZ\}$ is a generator[4] of our three-qubit bit-flip code and these elements suffice to define the subspace of the total Hilbert space where correct codes without single bit-flip errors exist. Removing an element from the generator would introduce a qubit degree of freedom and the stabilised subspace would now also include erroneous qubits. This shows just how powerful the stabiliser formalism is in quantum error correction [59].

[4] This need not be unique for a given stabiliser group.

CHAPTER

3

LIGHT–MATTER INTERACTION

In this chapter we provide a detailed description of the mathematical formulation of the theory of quantum optics that is used in the work of this thesis. We first give an account of the Hamiltonian that will be commonly used throughout, and adapt it for a continuum of electromagnetic field modes in order to properly describe a one-dimensional photonic waveguide. We then look at different mathematical approaches to describing the interaction between light and matter at the few-photon level, deriving the equations that will be used in future chapters. Finally, we give a description of the semiconductor quantum dot and how it may provide functionality as a spin-based qubit within a quantum optical setup.

3.1 Light–matter Hamiltonian

In this section, we will seek to formally describe the interaction between an applied electromagnetic field and matter in the quantum picture, following the treatment of the quantised field in Sec. 2.4. We start off by introducing the full system Hamiltonian [60],

$$H = H_{\text{field}} + H_{\text{matter}} + H_{\text{int}}. \tag{3.1}$$

The first two terms on the right-hand side make up the free Hamiltonian, H_0, and are relatively simple in form. The first is obtained as a result of the quantisation of the field, discussed in Sec. 2.4, whilst the second is given by $E_e \left|e\right\rangle \left\langle e\right| + E_g \left|g\right\rangle \left\langle g\right|$, where $E_e - E_g = \hbar\omega_0$. We can arbitrarily change the zero energy of both Hamiltonians without influencing the dynamics and, restricting ourselves for now to a cavity setup, we obtain

$$H_{\text{free}} = \hbar\omega_a a^\dagger a + \frac{\hbar\omega_0\sigma_z}{2}, \tag{3.2}$$

where ω_a is the resonance frequency of the cavity mode and $\sigma_z = 2\sigma_+\sigma_- - \mathbb{1}$.

The interaction Hamiltonian, H_{int}, introduces complexities when it comes to the study of the interaction dynamics. Therefore, we make certain assumptions and approximations to the Hamiltonian in order for the interaction to be tractable. We introduce these simplifications in what follows. The interaction between an atom and applied electric field can be described semiclassically[1] by

$$H_{\text{int}} = -\mathbf{d}.\mathbf{E}, \tag{3.3}$$

where $\mathbf{d}$ is the dipole moment operator of the atom, and the electric field has frequency ω_L and is given by $\mathbf{E}(t) = \mathbf{E}_0 e^{-\mathrm{i}\omega_L t} + \mathbf{E}_0^* e^{\mathrm{i}\omega_L t}$. The above expression is based on the *dipole approximation*, where we assume that the external field can be considered constant across the system due to the wavelength of the field being much larger than the system under consideration. This is an apt assumption when considering that optical wavelengths range in the few hundreds of nanometers, whilst the spatial dimension tends to be in the range of a few Ångströms for atoms [43] and a few nanometers for quantum dots [61].

The transition dipole moment is the electric dipole moment that results from the transition between two states; in this case, the transition of the electron between two energy levels. The diagonal entries of the operator are zero (transitions that preserve the state of the electron are not allowed) and we can therefore express the operator solely in terms of its off-diagonal elements: $\mathbf{d} = \mathbf{d}_{e,g} |e\rangle \langle g| + \mathbf{d}_{e,g}^* |g\rangle \langle e|$. We then obtain

$$H_{\text{int}} = -\hbar \left(\Omega e^{-\mathrm{i}\omega_L t} + \tilde{\Omega} e^{\mathrm{i}\omega_L t} \right) \sigma_+ - \hbar \left(\Omega^* e^{\mathrm{i}\omega_L t} + \tilde{\Omega}^* e^{-\mathrm{i}\omega_L t} \right) \sigma_-, \tag{3.4}$$

where $\Omega = \mathbf{d}_{e,g}.\mathbf{E}_0/\hbar$ is the so-called Rabi frequency and $\tilde{\Omega} = \mathbf{d}_{e,g}.\mathbf{E}_0^*/\hbar$ is referred to as the counter-rotating frequency. The operators σ_+ and σ_- are the raising and lowering operators of the two-level system, respectively, and are defined as

$$\sigma_+ = |e\rangle \langle g|, \qquad \text{and} \qquad \sigma_- = |g\rangle \langle e|. \tag{3.5}$$

Next, we change the Hamiltonian into the interaction representation with respect to the free Hamiltonian of the atom; here, the unitary operator is $U = \exp(\mathrm{i}\omega_0 t |e\rangle \langle e|)$. This gives us

$$\begin{aligned} H_{\text{int},I} &= U H_{\text{int},S} U^\dagger \\ &= -\hbar \left(\Omega e^{-\mathrm{i}(\omega_L - \omega_0)t} + \tilde{\Omega} e^{\mathrm{i}(\omega_L + \omega_0)t} \right) \sigma_+ - \hbar \left(\Omega^* e^{\mathrm{i}(\omega_L - \omega_0)t} + \tilde{\Omega}^* e^{-\mathrm{i}(\omega_L + \omega_0)t} \right) \sigma_-, \end{aligned} \tag{3.6}$$

where subscripts I and S indicate the interaction and Schrödinger representations, respectively. We assume that the field is near resonance to the atomic transition such that $\omega_L - \omega_0 \ll \omega_L + \omega_0$. Therefore, the exponential factors multiplying the counter-rotating frequencies rapidly oscillate with respect to time and average out to zero over substantial time scales. At this stage we can make the *rotating-wave approximation* and assume that we can eliminate these terms. Transforming the modified Hamiltonian back to the Schrödinger picture, we obtain

$$H_{\text{RWA},S} = U^\dagger H_{\text{RWA},I} U = -\hbar\Omega e^{-\mathrm{i}\omega_L t} \sigma_+ - \hbar\Omega^* e^{\mathrm{i}\omega_L t} \sigma_-. \tag{3.7}$$

[1] Semiclassical theory describes one part of a system classically, whilst treating the other part as quantum.

We can obtain the Hamiltonian for the *Jaynes–Cummings model* [62] by considering a fully quantum mechanical representation of our setup and taking the field to be quantised. Replacing the amplitude terms in Eq. (3.7) by mode operators, the interaction part of the Hamiltonian changes to

$$H_{\text{int}} = \hbar g a \sigma_+ + \hbar g^* a^\dagger \sigma_-, \tag{3.8}$$

where a is the mode operator of the field. The coupling constant of the light–matter interaction, g, describes how strongly the applied field and matter couple to each other and is given by

$$g = \sqrt{\frac{2\pi}{\hbar\omega}} \Omega \mathbf{d}_{e,g}.\mathbf{e}, \tag{3.9}$$

where $\mathbf{d}_{e,g}$ is the dipole moment and $\mathbf{e}$ is the unit polarisation vector of the field. Although we have assumed a single mode interacting with the dipole, we see that the above can be easily generalised to a multi-mode field, resulting in

$$H_{\text{int}} = \hbar \sum_j \left(g_j a_j \sigma_+ + g_j^* a_j^\dagger \sigma_- \right). \tag{3.10}$$

One point to observe at this stage is the fact that this simplification has resulted in an expression that preserves the number of excitations: an annihilation (creation) operator is coupled only to an excitation (de-excitation) operator. There exist regimes, however, where the rotating-wave approximation is no longer valid, such as the ultra-strong coupling regime where the separation of relevant timescales is greatly reduced [63].

3.2 Coupling to a waveguide

In our analysis of the light–matter Hamiltonian in Sec. 3.1, we consider a cavity setup. Although the generalisation from a single cavity mode to multiple ones is trivial, we will also need to work with two-level systems coupled to a continuum of modes in the form of fields propagating within optical waveguides. We will formally define the Hamiltonian for such cases in this section.

We start by considering the quantised electromagnetic field in Sec. 2.4. Here, we have ignored the wavevector dependence of the field mode operators for notational convenience. However, this is a consequence of the position dependence of the electromagnetic field and the mode operator being a function of the conjugate variable, i.e., the wavevector k. We make the transformation from a discrete sum to a continuous one [64, 65], and the Hamiltonian then becomes

$$H = \hbar \int \mathrm{d}k\, \omega(k)\, a^\dagger(k)\, a(k) + \frac{\hbar\omega_0 \sigma_z}{2} + \hbar \int \mathrm{d}k \left[\tilde{V}(k)\, a(k)\, \sigma_+ + \text{H.c.} \right], \tag{3.11}$$

where H.c. is the Hermitian conjugate and the integration is performed over the whole reciprocal space.

3.2.1 Frequency basis

We may wish to work in the frequency basis and, therefore, need to consider the dispersion relation of our optical setup. We may assume that the bandwidth of the propagating field under study is narrow enough that we may apply a linear dispersion relation around some wavenumber k_0 such that $\omega_k = v_g\,(k - k_0) + \omega_{k_0}$, where $v_g = \partial_k \omega|_{k=k_0}$ is the group velocity at k_0 and assuming that the waveguide supports only right-moving fields. The Hamiltonian becomes

$$\begin{aligned} H &= \hbar \int \mathrm{d}k\, \left[v_g\,(k - k_0) + \omega_{k_0}\right] a^\dagger\,(k)\, a\,(k) + \frac{\hbar\omega_0\sigma_z}{2} + \hbar \int \mathrm{d}k\, \left[\tilde{V}\,(k)\, a\,(k)\, \sigma_+ + \mathrm{H.c.}\right] \\ &\to \hbar \int \mathrm{d}k\, v_g\,(k - k_0)\, a^\dagger\,(k)\, a\,(k) + \frac{\hbar\Omega\sigma_z}{2} + \hbar \int \mathrm{d}k\, \left[\tilde{V}\,(k)\, a\,(k)\, \sigma_+ + \mathrm{H.c.}\right], \end{aligned} \tag{3.12}$$

where we define $\Omega \equiv \omega_0 - \omega_{k_0}$. In the second line, we have shifted the zero energy of the free part by $\hbar\omega_{k_0}$. This is done by changing into the interaction picture such that we work in a frame rotating with with frequency ω_{k_0}, by applying the transformation $H \to U^\dagger H U + \mathrm{i}\hbar\partial_t U^\dagger U$ with $U = \exp\left[-\mathrm{i}\omega_{k_0} t\left(\sigma_z/2 + \int \mathrm{d}k\, a^\dagger\,(k)\, a\,(k)\right)\right]$.

Finally, we perform a change of variables and defining the mode operators as $a\,(\omega) = a\,(k + k_0)\,/\sqrt{v_g}$ and setting $\omega \equiv v_g k$, we obtain

$$H = \hbar \int \mathrm{d}\omega\, \omega\, a^\dagger\,(\omega)\, a\,(\omega) + \frac{\hbar\Omega\sigma_z}{2} + \hbar \int \mathrm{d}\omega\, \left[V a\,(\omega)\, \sigma_+ + \mathrm{H.c.}\right], \tag{3.13}$$

where we assume that the coupling strength $V \equiv \tilde{V}\,(k)\,/\sqrt{v_g}$ is constant over the photonic bandwidth. The treatment of left-moving fields follows similarly.

3.2.2 Position basis

We may also choose to express the system's Hamiltonian in real space, following a procedure similar to one set out in Ref. [66, 67]. We start by defining the Fourier transforms

$$a\,(k) = \frac{1}{\sqrt{2\pi}} \int_{-\infty}^{+\infty} \mathrm{d}x\, a\,(x)\, e^{-\mathrm{i}kx} \qquad \text{and} \qquad a^\dagger\,(k) = \frac{1}{\sqrt{2\pi}} \int_{-\infty}^{+\infty} \mathrm{d}x\, a^\dagger\,(x)\, e^{\mathrm{i}kx}, \tag{3.14}$$

where $a\,(x)$ ($a^\dagger\,(x)$) annihilates (creates) a photon at position x moving towards the right. Although the operators used here are obtained by defining a Fourier transform of the reciprocal space operators, we note here recent work on the formulation of a local quantised field description by taking into account positive and negative frequency solutions to Maxwell's equations [68–70] which motivates strongly the use of such operators.

The field Hamiltonian given by the first term in Eq. (3.12) then transforms to

$$\begin{aligned} H_{\text{field}} &= \frac{\hbar}{2\pi} \int \mathrm{d}k\, \mathrm{d}x\, \mathrm{d}x'\, v_g k\, a^\dagger\,(x)\, a\left(x'\right) e^{-\mathrm{i}(x - x')k} \\ &= \hbar \int \mathrm{d}x\, \mathrm{d}x'\, a^\dagger\,(x)\, a\left(x'\right) \left(-\mathrm{i}v_g \partial_x\right) \delta\left(x - x'\right) \\ &= \hbar \int \mathrm{d}x\, a^\dagger\,(x)\, \left(-\mathrm{i}v_g \partial_x\right) a\,(x)\,. \end{aligned} \tag{3.15}$$

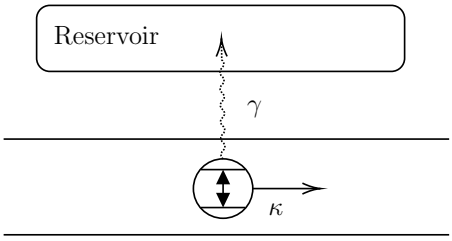

Figure 3.1: Modelling interaction losses by means of a reservoir coupled to the two-level system with a coupling rate γ. The coupling rate of the two-level system to the waveguide-supported modes is given by $\kappa = 2\pi g^2$.

The interaction part of the Hamiltonian evolves in the same manner (assuming once again that the coupling strength is independent of frequency), giving

$$H_{\text{int}} = \hbar \int \mathrm{d}x \, \sqrt{2\pi} V \, \delta(x) \left[a(x) \, \sigma_+ + \text{H.c.} \right]. \tag{3.16}$$

3.2.3 Loss

Unless a physical system is perfectly isolated from its environment, it will likely undergo losses during its interaction. One way of modelling for the loss is by modelling the loss-inducing environment as a reservoir, given by the mode operator r and supporting modes of all frequencies, as shown in Fig. 3.1. The two-level system would couple to the reservoir with some rate γ that depends on the rate of loss due to the interaction. In the frequency basis, the Hamiltonian of the system given by (3.13) then changes by $H \to H + H_{\text{res}}$ [71], where

$$H_{\text{res}} = \hbar \int \mathrm{d}\omega \, \omega r^\dagger(\omega) \, r(\omega) + \hbar \int \mathrm{d}\omega \left[\sqrt{\frac{\gamma}{2\pi}} r(\omega) \, \sigma_+ + \text{H.c} \right]. \tag{3.17}$$

Alternatively, one may employ the so-called quantum jump method, first used in describing open quantum systems [72, 73]. Here, losses are described by the addition of non-Hermitian terms to the atomic part of the free Hamiltonian:

$$H_{\text{atom}} = \frac{\hbar \omega_0 \sigma_z}{2} \to \frac{\hbar}{2} \left(\omega_0 - \frac{\mathrm{i}\gamma}{2} \right) \sigma_z. \tag{3.18}$$

The system now evolves according to this newly defined pseudo-Hamiltonian where, at each time step, a discontinuous change, or jump, takes place with some probability.

The two approaches are invariant in the dynamics that may be derived from them. The first offers a more intuitive representation for the occurrence of loss, whilst the second does not require the expansion of the Hilbert space as all possible lossy modes are effectively traced out.

3.3 Wavefunction approach to scattering

We may explore the evolution of a photonic state as it interacts with the two-level system by means of coherent, or elastic, scattering. We use the two terms here interchangeably. However, they apply to slightly different contexts: elastic scattering refers to the conservation of kinetic energy of the scattering particle, whilst coherence relates to the preservation of a strict relationship between the phases of the initial and final states. We work under the assumption that both conditions are satisfied.

3.3.1 Waveguide-coupled two-level system

In this section we will show how the evolution of a single photon can be described with respect to time, as has been detailed in Refs [74, 75]. We first remind the reader that the Hamiltonian for the system is rendered excitation number preserving by the application of the rotating wave approximation. This means that we can safely work in the single-excitation manifold, without needing to consider states of higher order excitations as these would not result from the dynamics described by the Hamiltonian. The time-dependent wavefunction, assuming zero loss, can then be expressed as a linear combination of all waveguide modes and the excited state of the two-level system:

$$|\Psi(t)\rangle = \int \mathrm{d}k\, \alpha(k,t)\, a^\dagger(k)\,|0\rangle \otimes |g\rangle + \beta(t)\,|0\rangle \otimes \sigma_+\,|g\rangle\,, \tag{3.19}$$

where $|0\rangle$ is the vacuum state, with zero photons within the waveguide, and $|g\rangle$ is the ground state of the two-level system. The wavefunction is normalised such that $\int \mathrm{d}k\,|\alpha(k,t)|^2 + |\beta(t)|^2 = 1$ at all times t. The evolution of this state is described by the Schrödinger equation, $\mathrm{i}\hbar\partial_t|\Psi(t)\rangle = H|\Psi(t)\rangle$. We choose to use a Hamiltonian derived from Eq. (3.11), where we now set the zero energy at the ground state of the two-level system and transform to a frame rotating with the transition frequency ω_0:

$$H = \hbar\int \mathrm{d}k\,[\omega(k)-\omega_0]\,a^\dagger(k)\,a(k) + \hbar\int \mathrm{d}k\,\left[\tilde{V}(k)\,a(k)\,\sigma_+ + \mathrm{H.c.}\right]. \tag{3.20}$$

We obtain a set of coupled differential equations by considering the projection of the resulting equation onto the orthogonal states $a^\dagger(k)\,|0\rangle\otimes|g\rangle$ and $|0\rangle\otimes\sigma_+|g\rangle$:

$$\partial_t\alpha(k,t) = \mathrm{i}\,[\omega(k)-\omega_0]\,\alpha(k,t) - \mathrm{i}\tilde{V}^*\beta(t) \tag{3.21a}$$

$$\begin{aligned}\partial_t\beta(t) &= \mathrm{i}\int \mathrm{d}k\,\tilde{V}\,\alpha(k,t)\\ &= \mathrm{i}\int \mathrm{d}k\,\tilde{V}\,\alpha(k,t_0)\,e^{-\mathrm{i}[\omega(k)-\omega_0](t-t_0)} - \int \mathrm{d}k\,\mathrm{d}t'\,|\tilde{V}|^2\beta\left(t'\right)e^{-\mathrm{i}[\omega(k)-\omega_0](t-t')},\end{aligned} \tag{3.21b}$$

where the last line of the second equation is obtained by formally integrating the first equation with respect to time from some initial time t_0 to t and making a substitution. We next apply the Wigner–Weisskopf approximation used in the theory for spontaneous emission [76], by which we may assume that the function $\beta(t)$ varies slowly compared to

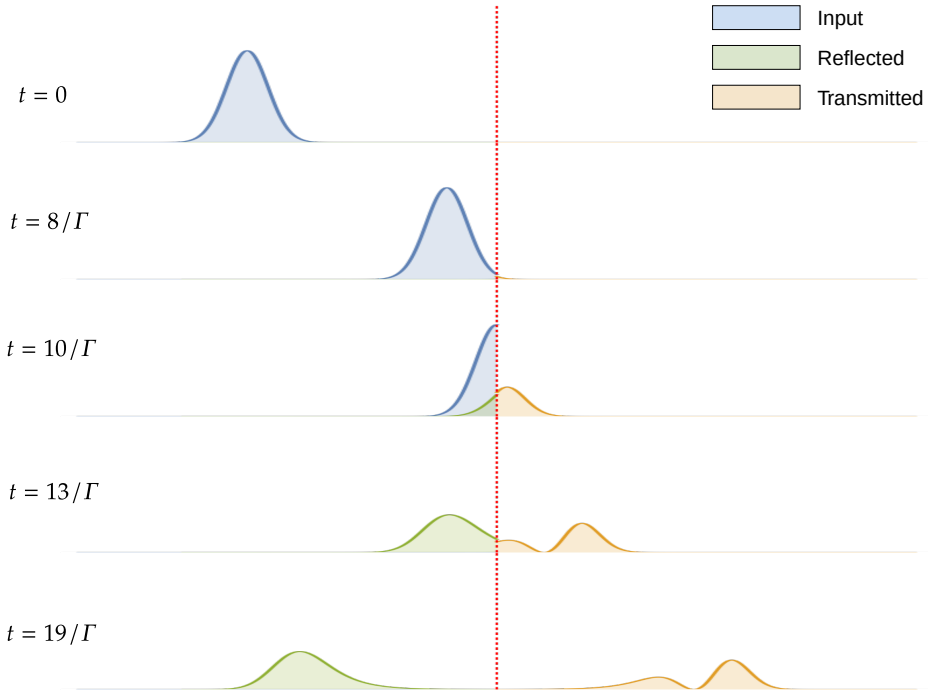

Figure 3.2: The temporal pulse profile of a single photon propagating towards the right and scattering off a two-level emitter, the position of which is indicated by the vertical red line. The incoming photon is assumed to have a Gaussian waveshape with linewidth $\sigma = v_g\Gamma$. We show the pulse shapes of the input (blue), reflected (green) and transmitted (orange) photons at different times t in units of emitter lifetime, Γ^{-1}.

the exponential term. This implies that the second term in the last line essentially has no memory of the past, or is Markovian, and can be expressed in a simpler form:

$$\int_{-\infty}^{+\infty} \mathrm{d}k \int_{-\infty}^{t} \mathrm{d}t' \, |\tilde{V}|^2 \beta\left(t'\right) e^{-\mathrm{i}[\omega(k)-\omega_0](t-t')} \xrightarrow[\text{approximation}]{\text{Wigner–Weisskopf}} \frac{\Gamma}{2}\beta\left(t\right), \tag{3.22}$$

Here, Γ is the total spontaneous emission decay rate, which under the assumption of a narrow bandwidth photonic state is related to the coupling strength by $\tilde{V} \approx \tilde{V}\left(k_0\right) = \sqrt{\Gamma v_g / \left(4\pi\right)}$.

Next, we define our wavefunction at initial time, t_0, where we assume that the two-level system is in the ground state, i.e., $\beta\left(t_0\right) = 0$ and an input photon of the Gaussian form:

$$\alpha\left(k, t_0\right) = \frac{1}{\left(\pi\sigma'^2\right)^{1/4}} \exp\left[-\frac{\left(k-k_0\right)^2}{2\sigma'^2} - \mathrm{i}x_0\left(k-k_0\right)\right], \tag{3.23}$$

where the pulse is centered around $k_0 = \omega_0/v_g$ and x_0 is the peak's position at initial time t_0. The linewidth at full width-half maximum is taken to be $\sigma = v_g\Gamma$, where Γ is the linewidth of the two-level emitter, and $\sigma' = \sigma/\left(2\sqrt{\ln 2}\right)$. We can therefore obtain an analytical expression for $\alpha\left(k, t\right)$ (see Ref. [74]) and find the probability for detecting a

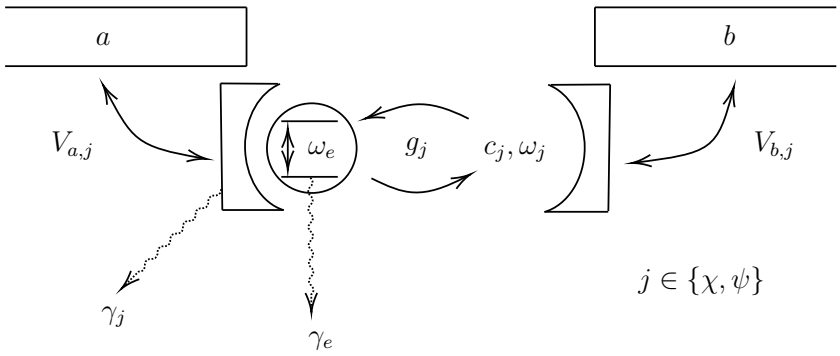

Figure 3.3: A schematic of the model consisting of a two-level system in a photonic crystal cavity. The cavity supports two orthogonal modes, c_j, with mode resonance frequency ω_j and coupling to the two-level system with coupling strength g_j, where $j = \chi, \psi$. The cavity further couples to two semi-infinite waveguides, denoted by a and b, with coupling strength $V_{a,j}$ and $V_{b,j}$, respectively. Losses from non-resonant decay and from the cavity to non-guided modes are characterised by γ_e and γ_j, respectively.

photon at position x at any time t by applying the photon number operator to the state:

$$P(x,t) = \langle \Psi(t) | a^\dagger(x)\, a(x) | \Psi(t) \rangle = \frac{1}{2\pi} \left| \int \mathrm{d}k\, \alpha(k,t)\, e^{\mathrm{i}kx} \right|^2 . \tag{3.24}$$

We reproduce the results of the waveguide excitation density in Fig. 3.2, showing clearly how the finite temporal length and, hence, non-zero bandwidth of the wavepacket results in simultaneous transmission and reflection of the photon. Furthermore, the scattering event leads to a modification in the spatial shape of the photon scattering in either direction.

3.3.2 Numerical approach

In the previous section, we have described a setup that allows us to obtain analytical solutions to describe the scattering interaction. However, if we wish to study a more general case, we might need to make use of a numerical approach to obtain the desired results, as outlined in [75]. In this section, we will consider a setup that does not allow an easily tractable analytical solution and discuss the numerical implementation of its solution. This work has been done with Mateusz Duda, who has performed the calculations and the numerical simulations.

We consider a Hamiltonian of the form

$$\begin{aligned} H = {} & \hbar \int \mathrm{d}\omega\, \omega \left[a^\dagger(\omega)\, a(\omega) + b^\dagger(\omega)\, b(\omega) \right] + \frac{\hbar\omega_0 \sigma_z}{2} + \hbar \sum_j \omega_j c_j^\dagger c_j \\ & + \hbar \sum_j \left\{ g_j c_j \sigma_+ + \int \mathrm{d}\omega \left[V_{a,j} a(\omega) + V_{b,j} b(\omega) \right] c_j^\dagger \right\} + \mathrm{H.c.}, \end{aligned} \tag{3.25}$$

which may describe a two-level system, with transition frequency ω_0, coupled to a two-mode cavity, denoted by modes c_j and resonant frequency ω_j with $j = 1, 2$, with coupling strength g_j. Furthermore, each cavity mode couples to an infinite waveguide supporting both right- and left-moving modes, given by a and b respectively, with some coupling strength V.[2] In Fig. 3.3, we give a schematic diagram of the setup.

The first line of the equation gives the free part of the Hamiltonian, whilst the interaction part is described in the second line. It becomes quickly clear that attempting to solve this analytically is non trivial due to the indirect coupling between the fields in the waveguide and the two-level system. Instead, we may obtain the system of differential equations by using $\mathrm{i}\hbar\partial_t |\Psi(t)\rangle = H |\Psi(t)\rangle$ where, once again, we may assume that the wavefunction will be a state in the single-excitation manifold at all times t and is given by

$$\begin{aligned} |\Psi(t)\rangle = &\int \mathrm{d}\omega \left[\alpha_a(\omega, t)\, a^\dagger(\omega) + \alpha_b(\omega, t)\, b^\dagger(\omega)\right] |0\rangle \\ &+ \sum_j \beta_j(t)\, c_j^\dagger |0\rangle + \gamma(t)\, \sigma_+ |0\rangle . \end{aligned} \tag{3.26}$$

The form is similar to that given by Eq. (3.19), with the waveguide modes represented in frequency space instead of reciprocal space. However, we also need to account for the excitation probability amplitudes for the two cavity modes, represented by $\beta_j(t)$. We obtain the following set of coupled differential equations by projecting onto the orthogonal basis states, $\left\{a^\dagger(\omega)|0\rangle, b^\dagger(\omega)|0\rangle, c_j^\dagger|0\rangle, \sigma_+|0\rangle\right\}$:

$$\mathrm{i}\partial_t \alpha_a(\omega, t) = \omega\alpha_a(\omega, t) + \sum_j V_{a,j}^* \beta_j(t), \tag{3.27a}$$

$$\mathrm{i}\partial_t \alpha_b(\omega, t) = \omega\alpha_b(\omega, t) + \sum_j V_{b,j}^* \beta_j(t), \tag{3.27b}$$

$$\mathrm{i}\partial_t \beta_j(t) = \int \mathrm{d}\omega \left[V_{a,j}\alpha_a(\omega, t) + V_{b,j}\alpha_b(\omega, t)\right] + \omega_j\beta_j(t) + g_j^*\gamma(t), \tag{3.27c}$$

$$\mathrm{i}\partial_t \gamma(t) = \frac{\omega_0\gamma(t)}{2} + \sum_j g_j\beta_j(t). \tag{3.27d}$$

At this stage, we may discretise the set of equations in both time and frequency, with $\partial_t \to \Delta t$ and $\mathrm{d}\omega \to \Delta\omega$. This allows us to express the problem as a system of linear equations in matrix form and is easily solved. We show the dynamics of the system as a function of time in units of the emitter lifetime τ in Fig. 3.4, assuming an initial photon propagating towards the right and all other modes occupying their respective ground states. We also include the effect of dissipation, both from losses mediated by the two-level emitter as well as cavity losses to the environment, by applying the quantum jump formalism to the Hamiltonian, as outlined in Sec. 3.2.3. From the figure, we can see how we can effectively map out the interaction in terms of the probability of the photon occupying one of the

[2] We will not delve deeper into the form of the Hamiltonian here, as it is outside the scope of this section. It will be properly discussed in Chapter 6.

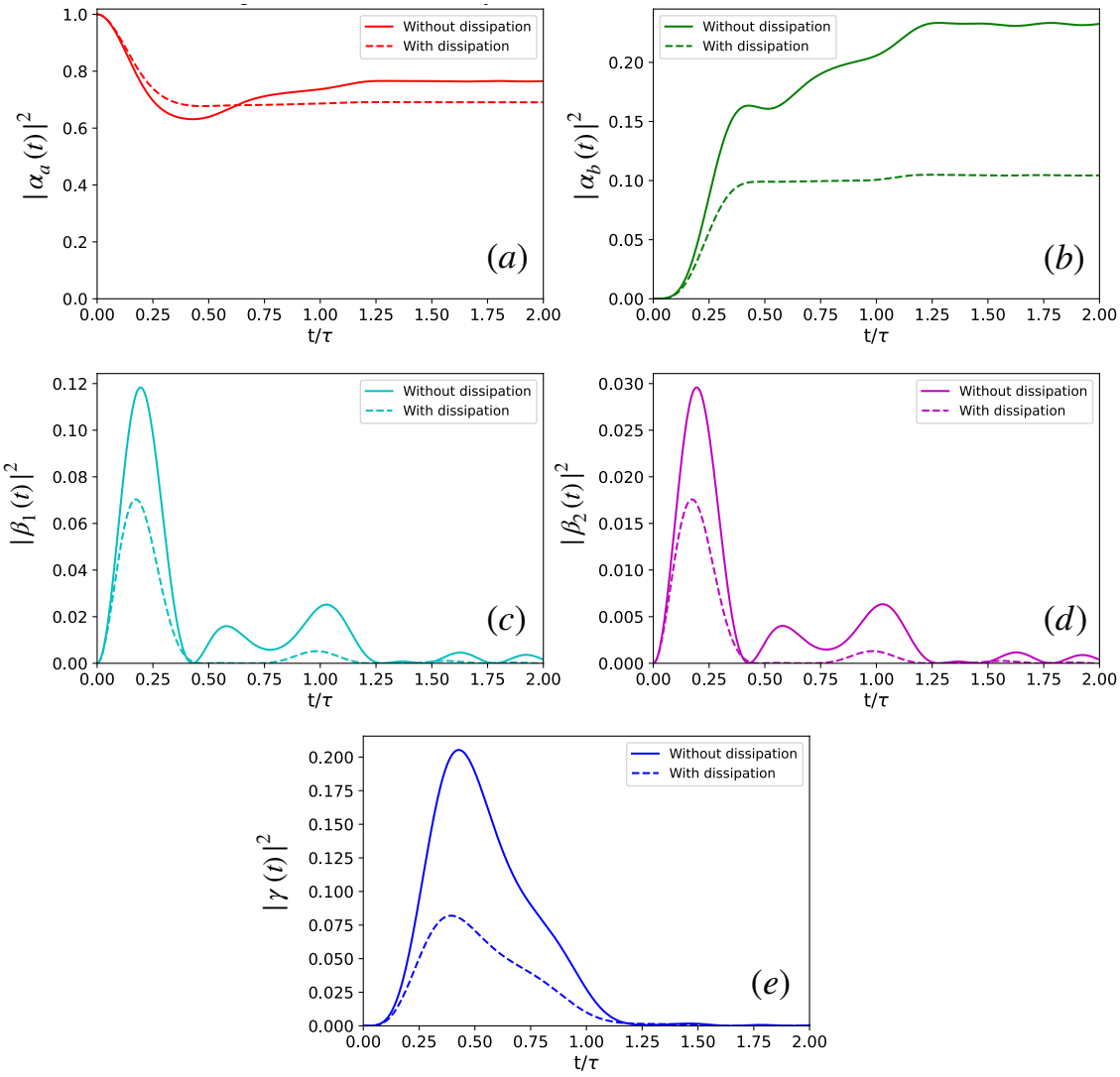

Figure 3.4: The occupation probability of a single excitation as a function of time in units of emitter lifetime τ: we show left- (a) and right-moving modes (b) in the waveguide, cavity modes 1 (c) and 2 (d), and occupation of the excited state of the emitter (e). We assume $\omega_0 = \omega_1 = \omega_2$, $g_1 = g_2/2 = 0.1\omega_0$ and $V_{1,i} = V_{2,i}/2 = \sqrt{\omega_0}$ for $i = a, b$. The dissipation rates for losses are given by $\gamma_0 = \gamma_j/3 = 0.1\omega_0$ for $j = 1, 2$. Figures generated in [77].

modes and the excitation of the two-level system. The photon couples first to the two cavity modes which then results in an oscillatory behaviour as the excitation oscillates between the cavity, two-level system and waveguides. The system reaches a steady state after some time, as the photon fully exits the cavity and is transmitted into either waveguide with some probability.

To conclude, we note two things: first is that generalising this analysis to two or more photons quickly increases the computational complexity, especially due to the induced non-linear effects in the form of four-wave mixing [78]. Second, we can see from the figure that,

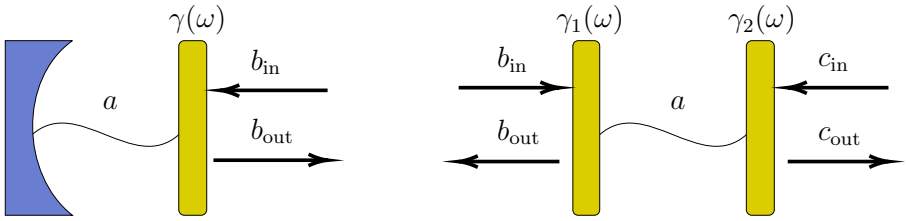

(a) One-sided optical cavity. (b) Two-sided optical cavity.

Figure 3.5: (a) A one-sided optical cavity supporting mode a and coupled to a bosonic bath of a continuum of modes $b(\omega)$ with rate $\gamma(\omega)$. (b) A two-sided optical cavity coupling to two bosonic baths, $b(\omega)$ and $c(\omega)$, with respective rate $\gamma_1(\omega)$ and $\gamma_2(\omega)$ by means of partially reflecting sides.

after some time, the system reaches a steady state that depends on the system parameters. These observations motivate our use of a different formalism to describe the interaction in the asymptotic time limit and will be the subject of future sections.

3.4 Input–output formalism

In this section we will describe the input–output formalism widely used in quantum optics. It was first introduced by Gardiner and Collett [79] as a way to formally describe the response of a finite system coupled to some driving field, without providing an exact formulation of the dynamics occurring within the system. It may therefore be used to model, say, a coherent optical field interacting with a cavity.

We follow the approach set out by Gardiner and Collett, as well as Walls and Milburn [80], by starting off with a single-sided cavity comprised of a fully reflective side and a partially transmissive one, as shown in Fig. 3.5. The cavity supports a single mode a that couples with some rate $\gamma(\omega)$ to a bosonic bath, i.e., a continuum of harmonic oscillators, denoted by $b(\omega)$. The system Hamiltonian is given by

$$\begin{aligned} H &= H_{\text{cavity}} + H_{\text{bath}} + H_{\text{int}} \\ &= \hbar\omega_0 a^\dagger a + \hbar \int \mathrm{d}\omega\, \omega\, b^\dagger(\omega)\, b(\omega) + \mathrm{i}\hbar \int \mathrm{d}\omega \sqrt{\frac{\gamma(\omega)}{2\pi}} \left[b(\omega)\, a^\dagger - b^\dagger(\omega)\, a \right], \end{aligned} \tag{3.28}$$

where we assume that the detuning between the resonant frequency of the cavity, ω_0, and the frequencies within the bandwidth of occupied bosonic modes is sufficiently small for the rotating-wave approximation to be valid and to allow us to extend the limits of integration over the infinite range of frequencies.

Next, we define the Heisenberg equations of motion for our mode operators, given by $\partial_t \bullet = -\mathrm{i}\,[\bullet, H]/\hbar$:

$$\partial_t b(\omega) = -\mathrm{i}\omega b(\omega) - \sqrt{\frac{\gamma(\omega)}{2\pi}} a, \tag{3.29a}$$

$$\partial_t a = -\mathrm{i}\omega_0 a + \int \mathrm{d}\omega\, \omega \sqrt{\frac{\gamma(\omega)}{2\pi}} b(\omega). \tag{3.29b}$$

Formally integrating Eq. (3.29a) from some initial time t_0 to t, we obtain

$$b(\omega) = e^{-\mathrm{i}\omega(t-t_0)} b_0(\omega) - \sqrt{\frac{\gamma(\omega)}{2\pi}} \int_{t_0}^{t} \mathrm{d}t'\, e^{-\mathrm{i}\omega(t-t')} a, \tag{3.30}$$

where $b_0(\omega) \equiv b(\omega, t = t_0)$ is the mode operator at initial time t_0.[3] Substituting the above equation into Eq. (3.29b), we get

$$\partial_t a = -\mathrm{i}\omega_0 a - \frac{\gamma}{2} a + \sqrt{\frac{\gamma}{2\pi}} \int \mathrm{d}\omega\, e^{-\mathrm{i}\omega(t-t_0)} b_0(\omega), \tag{3.31}$$

where we have applied the *first Markov approximation* such that the coupling rate may be considered to be independent of frequency. Once again, this is justified if we consider the bandwidth of populated bosonic modes to be sufficiently narrow in relation to the cavity linewidth. The first two terms of the above equation are representative of a harmonic oscillator with characteristic frequency ω_0 undergoing damping with rate γ. The last term of the equation is used to define the *input operator*, which drives the oscillatory cavity mode:

$$b_{\mathrm{in}}(t) = \frac{1}{\sqrt{2\pi}} \int \mathrm{d}\omega\, e^{-\mathrm{i}\omega(t-t_0)} b_0(\omega) \tag{3.32}$$

with $\left[b_{\mathrm{in}}(t), b_{\mathrm{in}}^{\dagger}(t')\right] = \delta(t-t')$. Similarly, we may choose to integrate from t to some final time t_1 to obtain a similar definition for the *output operator*, from which we then obtain

$$b_{\mathrm{out}}(t) = b_{\mathrm{in}}(t) + \sqrt{\gamma} a(t). \tag{3.33}$$

This may be interpreted as a boundary condition relating the different modes. The definition of the input and output operators also induces the following causality relations:

$$\left[a(t), b_{\mathrm{in}}(t')\right] = 0 \text{ for } t' > t \qquad \text{and} \qquad \left[a(t), b_{\mathrm{out}}(t')\right] = 0 \text{ for } t' < t. \tag{3.34}$$

These stem from the fact that the cavity mode $a(t)$ will not depend on the input operator $b_{\mathrm{in}}(t')$ if enacted at an earlier time, $t < t'$, and similarly for the output case.

The derived expressions may be generalised to a two-sided cavity coupling to two separate bosonic baths, $b(\omega)$ and $c(\omega)$, as shown in Fig. 3.5. The relation between the input and output operators is then obtained from

$$\partial_t a = -\mathrm{i}\omega_0 a - \left(\frac{\gamma_1}{2} + \frac{\gamma_2}{2}\right) a + \sqrt{\gamma_1} b_{\mathrm{in}} + \sqrt{\gamma_2} c_{\mathrm{in}}. \tag{3.35}$$

Finally, we note that this formalism generalises to any system that couples linearly in the bosonic mode operators and requires only a substitution of $H_{\mathrm{cavity}} \to H_{\mathrm{system}}$.

[3] Although the operators are in the Heisenberg picture, we will not notate the time-dependence explicitly for notational convenience, except when the time argument is no longer t.

3.5 Scattering matrix

In this section we will describe the scattering matrix, also commonly referred to as the S-matrix, which is ubiquitous in the work of this thesis. It is used to describe scattering phenomena, occurring on relatively short timescales, in quantum mechanics and quantum field theory by relating initial and final states of the physical system. It is also widely employed in the context of photonic-based quantum information processing: the interaction between a photonic 'flying' qubit and a stationary qubit physically realised by a two-level system is of the scattering form.

We follow the approach presented in Ref. [81], where Fan *et al.* extend the input–output formalism, discussed in Sec. 3.4 to derive the S-matrix for the scattering of one and two photons off a two-level system within an optical waveguide. We start from the Hamiltonian in the frequency basis, given by Eq. (3.13)

$$H = \underbrace{\hbar \int \mathrm{d}\omega\, \omega a^{\dagger}(\omega)\, a(\omega)}_{H_0} + \underbrace{\frac{\hbar\Omega\sigma_z}{2} + \hbar \int \mathrm{d}\omega\, \left[V a(\omega)\, \sigma_+ + \mathrm{H.c.}\right]}_{H_{\mathrm{int}}}, \tag{3.36}$$

with the operator split into the free and interaction parts as shown. We work in the interaction representation and define the initial and final states to be free states occurring long before, or after, the interaction. The elements of the scattering matrix S are the probability amplitudes relating these two states and are therefore given by the inner product of the final state with the initial state evolved in the interaction picture:

$$S_{\mathrm{final,initial}} = \langle \Psi_{\mathrm{final}} | S | \Psi_{\mathrm{initial}} \rangle\,, \tag{3.37}$$

where S is given by the evolution operator in the long time limit

$$S = \lim_{\substack{t_0 \to -\infty \\ t_1 \to +\infty}} U_{\mathrm{int}}(t_1, t_0) = \lim_{\substack{t_0 \to -\infty \\ t_1 \to +\infty}} e^{\mathrm{i}H_0 t_1/\hbar} e^{-\mathrm{i}H(t_1 - t_0)/\hbar} e^{-\mathrm{i}H_0 t_0/\hbar}. \tag{3.38}$$

The initial and final states may be expressed in terms of appropriately defined input and output operators:[4]

$$\begin{aligned} a_{\mathrm{in},S}(\omega) &= e^{\mathrm{i}Ht_0/\hbar} e^{-\mathrm{i}H_0 t_0/\hbar} a(\omega)\, e^{\mathrm{i}H_0 t_0/\hbar} e^{-\mathrm{i}Ht_0/\hbar} \\ \text{and} \qquad a_{\mathrm{out},S}(\omega) &= e^{\mathrm{i}Ht_1/\hbar} e^{-\mathrm{i}H_0 t_1/\hbar} a(\omega)\, e^{\mathrm{i}H_0 t_1/\hbar} e^{-\mathrm{i}Ht_1/\hbar}, \end{aligned} \tag{3.39}$$

where the limits of $t_{0,1} \to \mp\infty$ still apply and are dropped for notational convenience, and $a^{\dagger}_{\mathrm{in}}(\omega)\,|0\rangle \equiv |\,\omega^{+}\rangle$ and $a^{\dagger}_{\mathrm{out}}(\omega)\,|0\rangle \equiv |\,\omega^{-}\rangle$ are scattering eigenstates.

Fan *et al.* show that these operators coincide with the field operators $a_{\mathrm{in}}(t)$ and $a_{\mathrm{out}}(t)$ obtained by means of the input–output formalism discussed in Sec. 3.4. The relationship between the two operators is given by

$$a_{\mathrm{in}}(t) = \frac{1}{\sqrt{2\pi}} \int \mathrm{d}\omega\, a_{\mathrm{in},S}(\omega)\, e^{-\mathrm{i}\omega t} \qquad \text{and} \qquad a_{\mathrm{out}}(t) = \frac{1}{\sqrt{2\pi}} \int \mathrm{d}\omega\, a_{\mathrm{out},S}(\omega)\, e^{-\mathrm{i}\omega t}. \tag{3.40}$$

[4] These operators are related to the so-called Møller wave operators, $\Omega_{\pm}$, that define the relation between scattered and free states.

Therefore, the two types of input and output operators are simply Fourier transforms of each other in the limit of $t_{0,1} \to \mp\infty$ and we therefore choose to drop the subscript S. This connection is key in deriving the analytical form of the S-matrix elements. The problem then reduces to solving

$$\langle \omega_1^- | \, \omega_0^+ \rangle = \langle 0 | a_{\text{out}}(\omega_1) \, | \, \omega_0^+ \rangle = \frac{1}{\sqrt{2\pi}} \int \mathrm{d}t \; \langle 0 | a_{\text{out}}(t) \, | \, \omega_0^+ \rangle \, e^{\mathrm{i}\omega_1 t}. \tag{3.41}$$

This can be done by considering the input–output equation and Heisenberg equations of motion for the system operators, given by

$$a_{\text{out}} = a_{\text{in}} - \mathrm{i}\sqrt{\frac{2}{\tau}}\sigma_-, \tag{3.42a}$$

$$\frac{\mathrm{d}}{\mathrm{d}t}N = -\mathrm{i}\sqrt{\frac{2}{\tau}}\left(\sigma_+ a_{\text{in}} - \text{H.c.}\right) - \frac{2}{\tau}N, \tag{3.42b}$$

$$\frac{\mathrm{d}}{\mathrm{d}t}\sigma_- = \mathrm{i}\sqrt{\frac{2}{\tau}}\sigma_z a_{\text{in}} - \frac{1}{\tau}\sigma_- - \mathrm{i}\Omega\sigma_-, \tag{3.42c}$$

where τ is the lifetime of the two-level system, with $\tau = (\pi v_g V^2)^{-1}$ and $N = \sigma_+\sigma_-$ projects onto the emitter's excited state. We apply the above equations to $\langle 0| \bullet \, | \, \omega_0^+ \rangle$ and solve the resulting system of equations by means of Fourier transforms and using the commutation relation $[a_{\text{in}}(\omega), a_{\text{in}}^\dagger(\omega')] = \delta(\omega - \omega')$. The S-matrix for the single-photon scattering event is then defined to be

$$\langle \omega_1^- | \, \omega_0^+ \rangle = \frac{(\omega_0 - \Omega) - \mathrm{i}/\tau}{(\omega_0 - \Omega) + \mathrm{i}/\tau}\delta(\omega_1 - \omega_0) \equiv t(\omega_0)\,\delta(\omega_1 - \omega_0), \tag{3.43}$$

where the Dirac delta function ensures conservation of energy and $t(\omega_0)$ is the transmission coefficient.

The procedure can be generalised to a waveguide supporting both right- and left-moving photons, in which case the transmission and reflection coefficients are given by

$$t(\omega_0) = \frac{\omega_0 - \Omega}{(\omega_0 - \Omega) + 2\mathrm{i}/\tau} \qquad \text{and} \qquad r(\omega_0) = \frac{-2\mathrm{i}/\tau}{(\omega_0 - \Omega) + 2\mathrm{i}/\tau}, \tag{3.44}$$

where we have effectively made the substitution $\tau \to \tau/2$ due to the coupling of the emitter in both the forwards and backwards direction.

We will now go briefly over the two-photon scattering case. Following a similar procedure as defined above, the S-matrix elements are found using

$$\langle \omega_3\, \omega_4^- | \, \omega_1\, \omega_2^+ \rangle = \int \mathrm{d}\omega \; \langle 0 | a_{\text{out}}(\omega_3) \, | \, \omega^+ \rangle \, \langle \omega^+ | a_{\text{out}}(\omega_4)\, a_{\text{in}}^\dagger(\omega_1)\, a_{\text{in}}^\dagger(\omega_2) \, | 0 \rangle, \tag{3.45}$$

where we use the identity operator $\int \mathrm{d}\omega \; |\omega^+\rangle \langle \omega^+| = \mathbb{1}$. This simplifies by means of Fourier transforms and may be expressed in terms of the transmission coefficient in Eq. (3.43), giving

$$\begin{aligned} \langle \omega_3\, \omega_4^- | \, \omega_1\, \omega_2^+ \rangle = {} & t(\omega_3)\, t(\omega_4) \left[\delta(\omega_3 - \omega_1)\,\delta(\omega_4 - \omega_2) + \delta(\omega_3 - \omega_2)\,\delta(\omega_4 - \omega_1)\right] \\ & + \frac{\mathrm{i}}{\pi}\sqrt{\frac{2}{\tau}} s_{\omega_3} s_{\omega_4} \left(s_{\omega_1} + s_{\omega_2}\right) \delta(\omega_1 + \omega_2 - \omega_3 - \omega_4), \end{aligned} \tag{3.46}$$

where

$$s(\omega) = \frac{\sqrt{2/\tau}}{(\omega - \Omega) + \mathrm{i}/\tau}. \tag{3.47}$$

We see that this expression has a linear contribution, given by the first two terms on the right-hand side and a non-linear term, where the energies of the individual photons is not necessarily conserved, describing the four-wave mixing that results from the interaction with the two-level system.

3.6 Semiconductor quantum dots

Throughout this work, we assume that the matter qubit is implemented by means of a semiconductor quantum dot. In this section we aim to give a sufficient description of these nanostructures as it pertains to the work in this thesis. We will therefore first discuss their energy level structure before moving on to describe the directional emission of these emitters when coupled to photonic waveguides.

3.6.1 Energy levels

A quantum dot is strongly confined in all three dimensions, with the dimensions being in the order of a few nanometers. This results in the discretisation of its energy levels, similar to what is observed in an atom, and is therefore also commonly referred to as an artificial atom. We only consider the energy levels adjacent to the band gap, which is the gap that exists between the valence and conduction bands and in which no electron states may exist. Here, an optical transition would excite an electron to the s-shell in the conduction band and leave a heavy hole in the valence band, whilst we neglect higher energy states due to their relative isolation. This allows us to model the quantum dot as a two-level system.[5]

The lowest energy level can be occupied by up to two electrons or holes. The optical excitation of the quantum dot may induce a transition of an electron to a higher energy level, leaving behind a hole. Given the polarity in their respective charges, the two particles are attracted to each other by the Coulomb force and form an *exciton*, X^0 [82]. Given that the exciton is neutral in charge, it is not easy to detect directly. However its decay is signalled by the emission of a photon as the electron relaxes back to the valence band. Another quasiparticle of interest is the charged exciton, or *trion*. This is comprised of three particles that depend on the charge of the trion: a negatively charged trion X^- is made up of two electrons and a hole and relaxes radiatively to an electron e^-, whilst a positively charged trion X^+ has two holes and one electron and transitions to a hole h^+.[6] In Fig. 3.6, we show level diagrams of the different quasiparticles.

A quantum dot can serve as a qubit given that it can be initialised to a given state and measured post-interaction, and the information is encoded in the spin degree of freedom. However all excitons we have mentioned are degenerate in their spin unless under the

[5] In reality, the quantum dot may also be used as a three- or four-level system, however these are not relevant to the work we present here.

[6] There also exists the biexciton, X^2, however we do not consider this in our work.

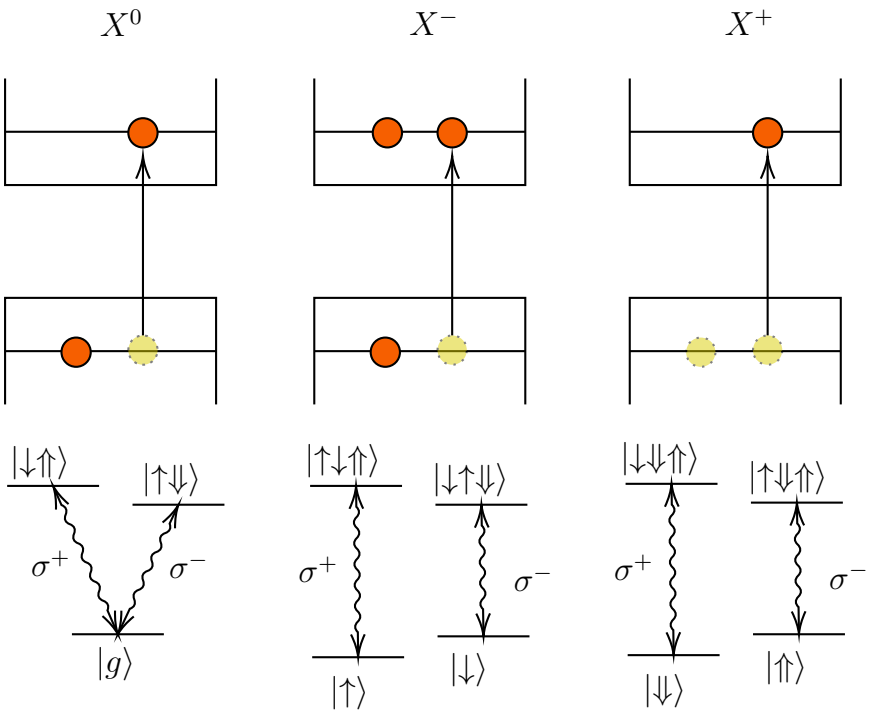

Figure 3.6: Level diagrams showing the optical transitions for an exciton, X^0, and negatively- and positively-charged trions, X^- and X^+, respectively, with magnetic field $\mathbf{B} \neq 0$. The transitions show electrons (orange) and holes (yellow) present in the three different quasiparticles and how they couple to left- (σ^+) and right-circularly polarised (σ^-) photons.

influence of some external magnetic field that induces Zeeman splitting [83, 84]. Upon the lifting of this degeneracy by means of a field applied in the so-called Faraday geometry, the optical transitions become circularly polarised, where the polarisations of the two possible transitions are mutually orthogonal and depend on the spin state.

3.6.2 Directional emission

In our theoretical formulations we have considered an emitter that couples solely in the forward direction; this is also a requisite in quantum optical networks if we wish deterministic directional transmission of the photonic qubits post-interaction. However, a quantum dot placed within an optical waveguide will not necessarily show directional emission as it may couple to all of the waveguide-supported modes. This has led to the development of chiral quantum optics [85], where light-matter interaction and propagation direction are mutually dependent, with the types of nanostructures under study going beyond what we consider in this thesis.

In our work, we will be referring to so-called *c-points* within photonic waveguides. These arise from the transversal confinement of the electric field which results in the circular polarisation of the field at certain locations [86]. These locations carry spin angular momentum, with the rotational handedness depending on the propagation direction of the field mode [87]. Suppose we place a quantum dot with a circularly polarised transition dipole moment at such a point and optically excite one of the spin states. Upon the radiative emission of a photon we would observe spin-momentum locking as the photon couples solely to the direction that preserves its spin angular momentum. The direction of emission can be changed by choosing to excite the orthogonal spin state. As a final remark, we note that although the term 'chiral' is used, this is a slight abuse of terminology. Although chirality implies handedness,[7] the symmetry of the waveguide geometry and the structure of the quantum dot is preserved. (This may also hold for other setups used in this field of quantum optics.) However, the term is used given that it helps convey the idea of unidirectional emission that would otherwise, under typical circumstances, be omnidirectional.

[7] The object cannot be superimposed on its mirror image.

CHAPTER

4

CUMULATIVE GENERATION OF ENTANGLEMENT

In this chapter, we will be studying the creation of entanglement between spectrally different quantum solid-state emitters by means of the light-matter interaction that arises from the scattering of photons off these emitters. Specifically, we will be considering squeezed light, chosen due to the relative ease with which it can be sourced using current technology, and repeated photon scattering in order to build up the amount of entanglement between the two quantum emitters. Next, we will consider the effect of scattering losses as well as detector inefficiencies on the entanglement generation protocol. Finally, we will briefly address the limitations of experimental implementation. Work in this chapter is based on Callus and Kok [88].

4.1 Background

Entanglement is a linchpin of quantum computing and information processing [89, 90]. The entanglement of multipartite systems is a necessary requirement for efficient quantum computing, without which it would not be sufficient to gain computational advantage over classical computing methods [91,92]. The phenomenon is also an important resource in the development of quantum technologies in fields such as metrology, imaging and cryptography, with examples that include secure quantum key distribution [93], quantum teleportation [50] and entanglement-assisted classical communication, allowing for an improvement in the classical capacity of noisy quantum channels [94].

There exist many different proposals for the physical implementation of quantum computers. These include superconducting circuits [95–97], trapped ion systems [98, 99] and photonic architectures [19, 100, 101]. Here, we will consider the qubit encoded in the spin state of an electron in a solid-state emitter [30]. This can be physically realised, for example, by using a charged semiconductor quantum dot with the excess electron (or hole)

transitioning to a negative (positive) trion upon excitation [102, 103]. Furthermore, the generation of entanglement is key in ensuring the scalability of quantum information processors. This has been well-addressed theoretically in the case of solid-state emitters, and various schemes relating to entanglement generation have been established [104–114]. These protocols utilise single- or few-photon interactions, require a relatively simple optical setup with few components, and are based on either controllable emitter interactions or interference effects resulting in the erasure of "which-path" information.

The success of these schemes depends on the optical interference effects that result in the coherent erasure of which-path information, and therefore it is assumed that emitters need to be spectrally identical. However, one drawback of the solid-state emitter is that its intricate mesoscopic environment results in spectral inhomogeneity across and within fabricated samples [30, 115]. Furthermore, methods to tune the emitter frequencies, such as diameter tuning [116], strain tuning [117] and utilising Raman transitions tuned into resonance [118], add further technical complexity to the setup and may be used only in the case of sufficiently close emitter pairings. These factors make scaling of the entanglement generation process very expensive in terms of resources.

Taking these practical limitations into consideration, Hurst *et al.* [119] show how the variation in central energies and linewidths between emitter pairings is not as detrimental to the entanglement generation process as previously thought. Indeed, near perfect entanglement is deterministically possible for certain emitter combinations by optimising the input optical state and tuning the photonic frequency. However, there are two disadvantages to this proposal. First, it calls for the use of two-mode Fock states, $|n, m\rangle$, which are difficult to source with current state of the art. Second, only certain areas of the parameter space may be near-perfectly entangled for a given Fock state, with some combinations necessitating the use of increasingly difficult to produce higher-order Fock states. In this work, we try to overcome these difficulties by considering instead squeezed light and by showing how we can deterministically generate perfect entanglement regardless of the chosen combination of emitters. Moreover, unlike the proposal by Hurst *et al.*, our scheme always makes use of the same type of optical input state and fully entangles the two spin states, independent of the spectral properties of the chosen emitters. Finally, other schemes consider a single interaction event, which do not cater for spectral variations, and therefore the novelty in our work lies in the cumulative process of repeated scattering events to build up perfect entanglement.

4.2 Setup

The setup consists of two emitters embedded in a Mach–Zehnder interferometer, one fixed in each arm, as shown in Fig. 4.1. Each emitter is of the L-type configuration, with only one of the two low-lying spin states, $|\uparrow\rangle$ and $|\downarrow\rangle$, coupling to an excited state $|e\rangle$, and where the transition is circularly polarized. The positioning of the emitters occurs at so-called

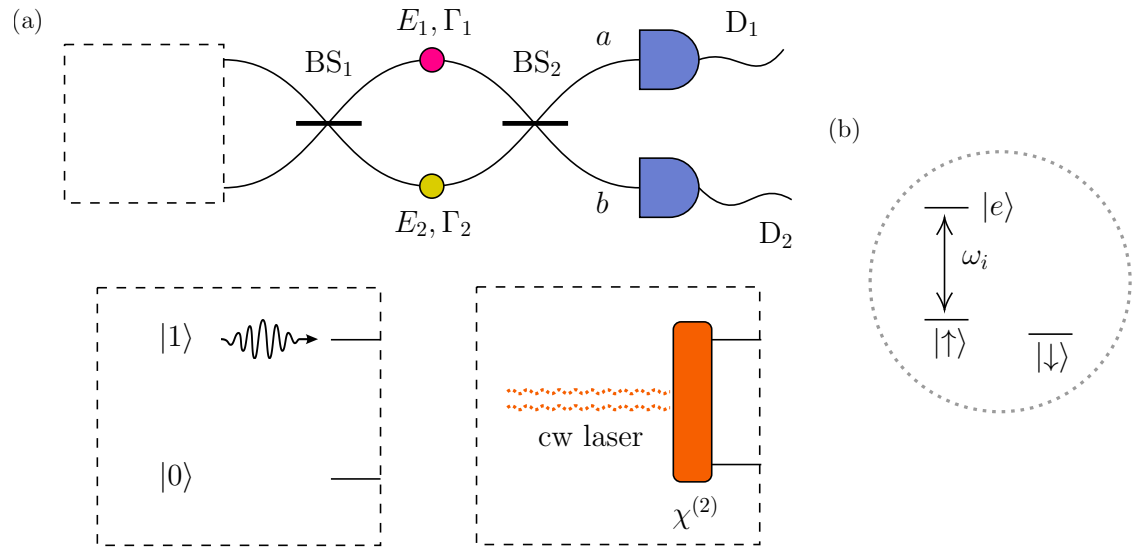

Figure 4.1: (a) A schematic representation of the setup: some photonic input state (dotted box) enters the Mach-Zehnder interferometer, after which the photons scatter off the two solid-state emitters characterised by energies and line-widths E_i and Γ_i, where $i = 1, 2$, followed by photon measurement at output modes a and b using detectors D_1 and D_2; below, on the left we show the input state $a^\dagger |0\rangle$ for the ideal case, i.e., using identical emitters, and on the right, our scheme makes use of biphoton pairs generated by a $\chi^{(2)}$ nonlinear crystal driven with a continuous-wave laser. (b) The emitters have an L-type configuration for their level structure, with the state $|\uparrow\rangle$ coupled to the excited state $|e\rangle$ with transition energy $E_i = \hbar\omega_i$, with $i = 1, 2$.

c-points[1] [85, 87]. These are points where the photon emission from circularly polarized dipoles is highly directional, resulting from the lateral confinement of the electromagnetic field within the waveguide, and leads to photons scattering off the emitters solely in the forward direction.

Let us first consider the ideal case with two identical emitters, as discussed in, e.g., Ref. [120]. The spins of both emitters are initialised in the state $|+\rangle = (|\uparrow\rangle + |\downarrow\rangle)/\sqrt{2}$ and the input state is comprised of a single monochromatic photon into the interferometer arm given by mode a, and a vacuum state input for mode b. The state of the total system is then described by

$$|\Psi\rangle = \frac{1}{2}(|\uparrow\rangle + |\downarrow\rangle) \otimes (|\uparrow\rangle + |\downarrow\rangle) \otimes a^\dagger |0\rangle . \tag{4.1}$$

Next, the optical state passes through the first beam splitter, resulting in a transformation given by $a \to (a + b)/\sqrt{2}$ and $b \to (a - b)/\sqrt{2}$. This is then followed by interactions with either emitter, characterised by the transmission coefficient as discussed in Sec. 3.5. We assume that the photon is on resonance with the emitters and therefore the interaction imparts a π-phase shift on the spin-photon state. The total system after the scattering

[1] We note here that although the name and concept elicits the notion of chirality, the waveguide geometry is perfectly symmetric and the material is non-chiral.

process is

$$|\Psi\rangle = \frac{1}{2\sqrt{2}}\left[(-|\uparrow\rangle + |\downarrow\rangle) \otimes (|\uparrow\rangle + |\downarrow\rangle) \otimes a^\dagger + (|\uparrow\rangle + |\downarrow\rangle) \otimes (-|\uparrow\rangle + |\downarrow\rangle) \otimes b^\dagger\right]|0\rangle\,. \quad (4.2)$$

The optical state is transformed again by the second beam splitter, resulting in the state

$$\begin{aligned}|\Psi\rangle &= \frac{1}{2}\left[(-|\uparrow\uparrow\rangle + |\downarrow\downarrow\rangle) \otimes a^\dagger + (-|\uparrow\downarrow\rangle + |\downarrow\uparrow\rangle) \otimes b^\dagger\right]|0\rangle \\ &= \frac{1}{\sqrt{2}}\left(-|\Phi^-\rangle \otimes a^\dagger - |\Psi^-\rangle \otimes b^\dagger\right)|0\rangle\,,\end{aligned} \quad (4.3)$$

where we adopt the use of $|i\rangle \otimes |j\rangle = |ij\rangle$ for notational convenience. It is then evident that by performing a projective measurement by means of photon detectors at either output arm of the interferometer, the state of the spins collapses with equal probability onto either $|\Phi^-\rangle$ or $|\Psi^-\rangle$, which are two of the four Bell states and maximally entangled. The generation of entanglement here occurs by means of which-path information erasure at the second beam splitter, as one cannot obtain information about which emitter the photon has interacted with at the detection stage. Furthermore, the success of this scheme is contingent on the π phase shift. Therefore, we have described a protocol where, in the case of no dissipation losses and perfect photon scattering in the forward direction, one can create a maximally entangled bipartite state in a deterministic way.

4.3 Introducing Spectral Variation

We now introduce the (highly likely) possibility of spectral variation between the two emitters, both in terms of central energy as well as line-width. The phase-shift imparted by the interaction of a photon with frequency ω with a two-level system can be obtained from the single-photon S-matrix and, in the case of perfectly unidirectional scattering, is given by the following transmission coefficient [81, 121]:

$$t(\omega) = \frac{\hbar\omega - E - \mathrm{i}\hbar(\Gamma - \gamma)/2}{\hbar\omega - E + \mathrm{i}\hbar(\Gamma + \gamma)/2}, \quad (4.4)$$

where E is the emitter central energy, and Γ and γ represent the coupling of the emitter to the waveguide and the non-guided (or dissipation channel) modes, respectively. We assume for now that the emitter is perfectly coupled to the guided mode, such that there are no photon losses and $\gamma = 0$. In this case, the transmission coefficient describes a pure phase shift with $|t(\omega)| = 1$, and is equal to π only when $\hbar\omega = E$.

Given that it is impossible to tune the input photon frequency such that the detuning $\hbar\omega - E_i$ is equal to zero for both emitters simultaneously, the phase shift imparted at the scattering stage will deviate from π. As a result, there could be residual which-path information left as the photon interferes with itself at the second beam splitter, and the process no longer necessarily entangles the spin states in a deterministic manner.

4.4 Protocol

We now turn to the proposed setup, where the two-mode squeezed vacuum serves as the input into the interferometer. This type of state is routinely produced by means of spontaneous parametric down-conversion (SPDC), whereby a crystal with a $\chi^{(2)}$ non-linearity is pumped using a continuous-wave laser [122, 123]. Although most of the pump photons pass through the crystal unaltered, every now and then the non-linearity causes a single photon to be annihilated and so-called signal and idler photons are created in its stead. By conservation of energy, the frequency of the pump photon, ω_p, needs to be equal to the sum of that of the signal and idler photons, ω_s and ω_i. We will consider the degenerate SPDC process, that is, where the signal and idler photons are of the same frequency.

The output of the SPDC process, i.e., the two-mode squeezed state, is given by [124]

$$|\xi\rangle = \frac{1}{\cosh r} \sum_{n=0}^{\infty} (-\mathrm{e}^{\mathrm{i}\phi} \tanh r)^n \frac{(a^\dagger b^\dagger)^n}{n!} |0\rangle \,, \tag{4.5}$$

where a, b are the two input mode operators, and $\xi = r\mathrm{e}^{\mathrm{i}\phi}$ depends on the crystal properties and the laser power. We may ignore the vacuum contribution as this does not affect or alter the state of the system in any way. Furthermore, we will be working under the assumption that the pump power is low such that r is small and we may neglect higher order photon pair contributions given by $n \geq 2$. In fact, for typical experimental values, the ratio of generated multi-pair states to single bi-photons is of the order of 10^{-8} per Watt of pump power [125]. Therefore, this limits the power with which the crystal may be pumped before one would need to account for changes to the proposed scheme.

As was done in the ideal case, both spins are initialised in the $|+\rangle$ state. Once a photon pair is created, it is transformed by the first beam splitter as

$$a^\dagger b^\dagger |0\rangle \to \frac{1}{2} \left[(a^\dagger)^2 - (b^\dagger)^2 \right] |0\rangle \,, \tag{4.6}$$

where we observe the Hong-Ou-Mandel effect [126] as a result of the degeneracy between the two photonic frequencies. We will therefore need to consider the interaction between a two-level emitter and two photons.

The post-scattering two-photon wavefunction in the general case is given by [71]

$$\begin{aligned} \tilde{\beta}(\omega_1, \omega_2) = &\frac{t(\omega_1) t(\omega_2)}{2} \left[\beta(\omega_1, \omega_2) + \beta(\omega_2, \omega_1) \right] \\ &+ \frac{\sqrt{\Gamma}}{\pi} S(\omega_1, \omega_2) \int \mathrm{d}k \left\{ \left[s(k) + s(\omega_1 + \omega_2 - k) \right] \beta(k, \omega_1 + \omega_2 - k) \right\} , \end{aligned} \tag{4.7}$$

where $\beta(\omega_1, \omega_2)$ is the initial wavefunction and the second line describes the nonlinear contribution of the light–matter interaction. We require the optical state to be quasi-monochromatic, which can be achieved either by using a monochromatic laser pump or by frequency filtering post-SPDC. In the case of quasi-monochromatic photons, the nonlinear part of the interaction tends towards zero and the process becomes linear, with the total phase shift imparted on the photons being equal to the sum of the individual accumulated

phase shifts. Moreover, it may be more desirable to avoid the use of broader linewidth photons as their shorter temporal length is more likely to excite the two-level system and cause unwanted spontaneous emission [127].

Taking the two photons to be monochromatic with frequency ω, the resulting state of the joint optical and spin system post emitter interaction is

$$\begin{aligned}|\Psi\rangle = &\frac{1}{4}\left[t_1^2(\omega)\,|\uparrow\uparrow\rangle + t_1^2(\omega)\,|\uparrow\downarrow\rangle + |\downarrow\uparrow\rangle + |\downarrow\downarrow\rangle\right] \otimes \left(a^\dagger\right)^2 |0\rangle \\ &+ \frac{1}{4}\left[t_2^2(\omega)\,|\uparrow\uparrow\rangle + |\uparrow\downarrow\rangle + t_2^2(\omega)\,|\downarrow\uparrow\rangle + |\downarrow\downarrow\rangle\right] \otimes \left(b^\dagger\right)^2 |0\rangle\,,\end{aligned} \tag{4.8}$$

where $t_i(\omega)$ is the transmission coefficient due to emitter i, where $i = 1, 2$. This state evolves at the second beam splitter to

$$\begin{aligned}|\Psi\rangle = &\frac{1}{8}\left[(t_1^2(\omega) - t_2^2(\omega))\,|\uparrow\uparrow\rangle + (t_1^2(\omega) - 1)\,|\uparrow\downarrow\rangle + (1 - t_2^2(\omega))\,|\downarrow\uparrow\rangle + 0\,|\downarrow\downarrow\rangle\right] \\ &\otimes \left[\left(a^\dagger\right)^2 + \left(b^\dagger\right)^2\right]|0\rangle \\ &+ \frac{1}{4}\left[(t_1^2(\omega) + t_2^2(\omega))\,|\uparrow\uparrow\rangle + (t_1^2(\omega) + 1)\,|\uparrow\downarrow\rangle + (1 + t_2^2(\omega))\,|\downarrow\uparrow\rangle + 2\,|\downarrow\downarrow\rangle\right] \otimes a^\dagger b^\dagger\,|0\rangle\,.\end{aligned} \tag{4.9}$$

The final step of a single round of entanglement accumulation involves the detection of photons in order to project the spins onto a more entangled state. The measurement process is expressed mathematically by means of projective operators acting on the state, defined by

$$\Pi_{n_a,n_b} = \frac{1}{n_a! n_b!}\left(a^\dagger\right)^{n_a}\left(b^\dagger\right)^{n_b}|0\rangle\langle 0|\,a^{n_a} b^{n_b}, \tag{4.10}$$

where n_a and n_b are the number of photons detected in detectors a and b, respectively. The post-measurement state for the outcome (n_a, n_b) is then obtained as

$$|\Psi\rangle \xrightarrow{\text{Measurement}} |\psi_{n_a,n_b}\rangle = \frac{\text{Tr}_{\text{field}}\left[\Pi_{n_a,n_b}|\Psi\rangle\right]}{\sqrt{\langle\Psi|\Pi_{n_a,n_b}|\Psi\rangle}}, \tag{4.11}$$

where we take the partial trace over the optical modes and where the probability of obtaining the measurement outcome is given by

$$P(n_a, n_b) = \langle\Psi|\Pi_{n_a,n_b}|\Psi\rangle\,. \tag{4.12}$$

We note at this stage that in the case of zero photon losses and perfectly efficient detectors the only possible photon measurement outcomes are: (i) a coincidence detection (where $n_a = n_b = 1$), and (ii) both photons arriving at one of the detectors (either n_a or n_b equal to two). This means that we would not need to employ detectors that are capable of resolving in the number of photons in order to project the spins onto a pure state. We will see that this is no longer the case when imperfections are introduced.

A photon measurement heralds one of the following states:

$$|\psi_{2,0}\rangle = |\psi_{0,2}\rangle = \frac{(t_1^2(\omega) - t_2^2(\omega))\,|\uparrow\uparrow\rangle + (t_1^2(\omega) - 1)\,|\uparrow\downarrow\rangle + (1 - t_2^2(\omega))\,|\downarrow\uparrow\rangle + 0\,|\downarrow\downarrow\rangle}{\sqrt{\left[|t_1^2(\omega) - t_2^2(\omega)|^2 + |t_1^2(\omega) - 1|^2 + |1 - t_2^2(\omega)|^2\right]}} \tag{4.13a}$$

$$\text{or} \qquad |\psi_{1,1}\rangle = \frac{(t_1^2(\omega)+t_2^2(\omega))\,|\uparrow\uparrow\rangle + (t_1^2(\omega)+1)\,|\uparrow\downarrow\rangle + (1+t_2^2(\omega))\,|\downarrow\uparrow\rangle + 2\,|\downarrow\downarrow\rangle}{\sqrt{\left[|t_1^2(\omega)+t_2^2(\omega)|^2 + |t_1^2(\omega)+1|^2 + |1+t_2^2(\omega)|^2 + 4\right]}}\,. \tag{4.13b}$$

Let us now consider what happens to our system when we repeat the optical probing process without re-initialising the spin state, each time performing a photon measurement at the end of a cycle. Let $N = m + n$ be the total number of photon measurements performed, where m is the number of coincidence detection events and n is the number of occurrences where both photons arrive at the same detector. The state of the total system after $(N+1)$ scattering events and immediately before the subsequent measurement is expressed as

$$\begin{aligned}|\psi_{m,n}\rangle = \frac{1}{4c_{m,n}}\Big[&(t_1^2(\omega)+t_2^2(\omega))^m(t_1^2(\omega)-t_2^2(\omega))^{n+1}\,|\uparrow\uparrow\rangle + (1+t_1^2(\omega))^m(t_1^2(\omega)-1)^{n+1}\,|\uparrow\downarrow\rangle \\ &+ (1+t_2^2(\omega))^m(1-t_2^2(\omega))^{n+1}\,|\downarrow\uparrow\rangle\Big] \otimes \left[\left(a^\dagger\right)^2 + \left(b^\dagger\right)^2\right]|0\rangle \\ + \frac{1}{2c_{m,n}}\Big[&(t_1^2(\omega)+t_2^2(\omega))^{m+1}(t_1^2(\omega)-t_2^2(\omega))^n\,|\uparrow\uparrow\rangle + (1+t_1^2(\omega))^{m+1}(t_1^2(\omega)-1)^n\,|\uparrow\downarrow\rangle \\ &+ (1+t_2^2(\omega))^{m+1}(1-t_2^2(\omega))^n\,|\downarrow\uparrow\rangle + 2^{m+1}0^n\,|\downarrow\downarrow\rangle\Big] \otimes a^\dagger b^\dagger\,|0\rangle\,,\end{aligned} \tag{4.14}$$

where $c_{m,n}$ is the normalization constant given by

$$\begin{aligned}c_{m,n} = \Big[&\left|(t_1^2(\omega)+t_2^2(\omega))^m(t_1^2(\omega)-t_2^2(\omega))^n\right|^2 + \left|(1+t_1^2(\omega))^m(t_1^2(\omega)-1)^n\right|^2 \\ &+ \left|(1+t_2^2(\omega))^m(1-t_2^2(\omega))^n\right|^2 + |2^m 0^n|^2\Big]^{1/2}.\end{aligned} \tag{4.15}$$

We set the photonic frequency ω such that $t_1^2(\omega) = t_2^2(\omega) \equiv t^2(\omega)$, satisfied by either

$$\hbar\omega = \frac{1}{2}\left[E_1 + E_2 \pm \sqrt{(E_1-E_2)^2 - \hbar^2\Gamma_1\Gamma_2}\right] \tag{4.16a}$$

or

$$\hbar\omega = \frac{E_2\Gamma_1 - E_1\Gamma_2}{\Gamma_1 - \Gamma_2}. \tag{4.16b}$$

This simplifies Eq. (4.14) to

$$\begin{aligned}|\psi_{m,n}\rangle = \frac{1}{4c_{m,n}}\Big[&(1+t^2(\omega))^m(t^2(\omega)-1)^{n+1}\,|\uparrow\downarrow\rangle + (1+t^2(\omega))^m(1-t^2(\omega))^{n+1}\,|\downarrow\uparrow\rangle\Big] \\ &\otimes \left[\left(a^\dagger\right)^2 + \left(b^\dagger\right)^2\right]|0\rangle \\ + \frac{1}{2c_{m,n}}\Big[&(t^2(\omega)+t^2(\omega))^{m+1}0^n\,|\uparrow\uparrow\rangle + (1+t^2(\omega))^{m+1}(t^2(\omega)-1)^n\,|\uparrow\downarrow\rangle \\ &+ (1+t^2(\omega))^{m+1}(1-t^2(\omega))^n\,|\downarrow\uparrow\rangle + 2^{m+1}0^n\,|\downarrow\downarrow\rangle\Big] \otimes a^\dagger b^\dagger\,|0\rangle\,.\end{aligned} \tag{4.17}$$

We show in Fig. 4.2 typical concurrence trajectories for combinations of spectrally different emitters as we repeatedly send through photon pairs and track the resulting photon

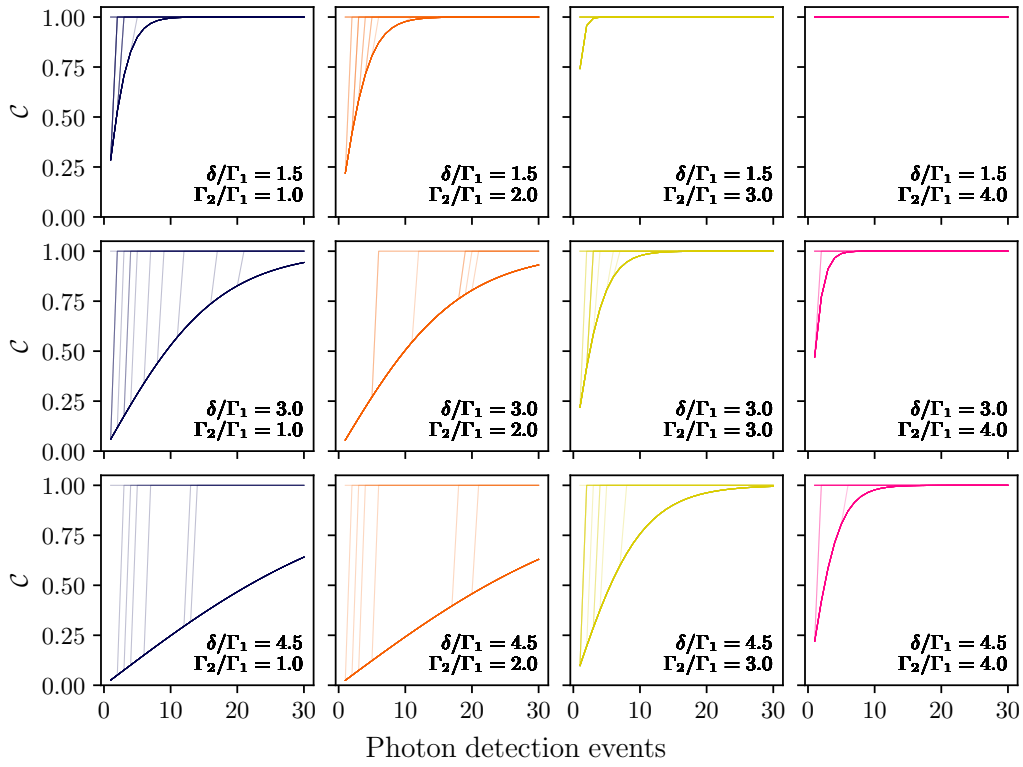

Figure 4.2: Typical concurrence trajectories given a sequence of photon detection events (horizontal axis) for different emitter pairings, in the case of zero losses ($\gamma = 0$). Γ_1 and Γ_2 are the emitter linewidths, and the energy detuning between emitter combinations is given by $\delta = E_2 - E_1$.

detection signature. By using this iterative method, the concurrence reaches unity, thereby signalling perfect entanglement, within $O\left(10^1\right)$ steps. Moreover, the protocol is successful regardless of the measurement outcomes, eliminating the need to reject samples on the basis of certain detection signatures. Irrespective of the value of N, if both photons arrive at the same detector during a measurement stage, the spins are projected onto a maximally entangled Bell state $|\Psi^-\rangle = (|\uparrow\downarrow\rangle - |\downarrow\uparrow\rangle)/\sqrt{2}$ (up to some global phase). This can be seen in the figure when the concurrence trajectory suddenly jumps to unity. Furthermore, continuing the probing process would not destroy any of the generated entanglement, but may possibly toggle the system between two Bell states: after n single-detector clicks, the state is given by $|\Psi^\pm\rangle = (|\uparrow\downarrow\rangle + (-1)^n |\downarrow\uparrow\rangle)/\sqrt{2}$. Otherwise, a series of coincidence measurements ($m \geq 1, n = 0$) would herald the approach towards the maximally entangled state $\exp(\mathrm{i}\phi)\,|\uparrow\uparrow\rangle + |\downarrow\downarrow\rangle$ as the contribution to the other two states goes to zero. Here, the relative phase ϕ may be obtained by considering the number of iterations required to reach the state in the case of only coincident detection events ($n = 0$): after M iterations we have that $\exp(\mathrm{i}\phi) = t^{2M}(\omega)$. Therefore, the protocol does not destroy any of the previously generated entanglement.

Interestingly, in certain cases it may be preferable to pair emitters with larger differences

in linewidth as a way to increase the rate with which entanglement is built up in the case of $n = 0$. The reason is that an increase in the linewidth results in a larger range of frequencies over which the scattering phase shift is substantial, and therefore increasing the linewidth of just one emitter for a given energy detuning improves on the interaction strength. This results in a greater reduction in the probability amplitudes of $|\uparrow\downarrow\rangle$ and $|\downarrow\uparrow\rangle$, and generates the entangled state $\exp(\mathrm{i}\phi)|\uparrow\uparrow\rangle + |\downarrow\downarrow\rangle$ faster. Although this dissimilarity is not sufficient for all regimes of δ/Γ_1 and Γ_2/Γ_1, the parameter space over which entanglement can be efficiently generated is much larger than when limited to perfectly identical emitters.

4.5 Losses

Until now we have assumed an ideal setup without factoring in any losses. Realistically, an experimental implementation of this protocol would be susceptible to such imperfections, which end up negatively impacting the entanglement process. We will now consider the two main sources of loss: scattering losses and detector inefficiencies.

4.5.1 Scattering losses

We introduce first the β-factor, given by $\beta = \Gamma/(\Gamma + \gamma)$ and defined to be the coupling of the emitter to the guided modes as a fraction of the total coupling of the emitter. In our treatment of the light–matter interaction until now, we have assumed that the emitter scatters all of the field perfectly to the waveguide mode in the forward direction, i.e., $\beta = 1$. Current best experimental values show β-factors that exceed 98% [128–130], with perfect coupling still proving to be elusive.

One way of overcoming this imperfection is by considering photon number resolving detectors and rejecting cases where photon losses have occurred. The detector would only be required to discriminate between a single photon and two or more photons. Given that such detectors are still in development [131–133], we will assume non-number resolving detectors. The trajectories are generated in the same manner as when $\beta = 1$. However we will have to make use of density matrices as the qubits will project onto a mixed state after the first photon measurement is made.

Given that $\gamma \neq 0$, the transmission coefficient defined in Eq. (4.4) no longer has an absolute value of unity, and therefore a photon coupling to the guided mode undergoes a phase shift as well as a change in its probability amplitude. The coefficient associated with the photon that is lost to the environment is given by [71]

$$t_e(\omega) = \frac{-\mathrm{i}\hbar\sqrt{\Gamma\gamma}}{\hbar\omega - E + \mathrm{i}\hbar(\Gamma + \gamma)/2}. \tag{4.18}$$

For a given emitter pairing, we will choose a frequency ω that satisfies any of the conditions in Eq. (4.16). However $t_1^2(\omega) = t_2^2(\omega)$ no longer necessarily holds since γ is no longer equal to zero. Furthermore, the trajectories resulting from the possible frequencies for a given emitter combination may behave very differently due to the potential variation in the resulting scattering amplitudes.

In order to obtain the general expression for the evolution of the two qubits, we start with the tensor product of an arbitrary density matrix ρ_{emitters} and a photon-pair input:

$$\rho_1 = \rho_{\text{emitters}} \otimes \left[a^\dagger b^\dagger \left|0\right\rangle \left\langle 0\right| a\, b\right], \tag{4.19}$$

with the qubits initialised in the state

$$\rho_{\text{emitters}} = \frac{1}{4}\left[(\left|\uparrow\right\rangle + \left|\downarrow\right\rangle) \otimes (\left|\uparrow\right\rangle + \left|\downarrow\right\rangle)\right]\left[\text{h.c.}\right], \tag{4.20}$$

where h.c. is the Hermitian conjugate.

The state evolves at the first beam splitter to

$$\rho_2 = \rho_{\text{emitters}} \otimes \frac{1}{4}\left[\left(a^\dagger\right)^2 - \left(b^\dagger\right)^2\right]\left|0\right\rangle\left\langle 0\right|\left[a^2 - b^2\right], \tag{4.21}$$

and post-scattering to

$$\begin{aligned}\rho_3 = \frac{1}{4}\sum_{i,j=1,2,3}\Big\{&\rho(M_i, M_j)\otimes\left[M_i\left|0\right\rangle\left\langle 0\right| M_j\right] + \rho(N_i, N_j)\otimes\left[N_i\left|0\right\rangle\left\langle 0\right| N_j\right]\\ &- \rho(M_i, N_j)\otimes\left[M_i\left|0\right\rangle\left\langle 0\right| N_j\right] + \rho(N_i, M_j)\otimes\left[N_i\left|0\right\rangle\left\langle 0\right| M_j\right]\Big\},\end{aligned} \tag{4.22}$$

where

$$\mathbf{M} = \begin{bmatrix}a^2 & a\, r_1 & r_1^2\end{bmatrix}^{\mathrm{T}} \qquad \text{and} \qquad \mathbf{N} = \begin{bmatrix}b^2 & b\, r_2 & r_2^2\end{bmatrix}^{\mathrm{T}}. \tag{4.23}$$

Here r_i is the photon annihilation operator associated with the scattering loss around emitter i. Furthermore, $\rho(m, n)$ is the density matrix of the qubits associated with the scattered optical state $m^\dagger\left|0\right\rangle\left\langle 0\right| n$ and is obtained using the following field-dependent transformations:

$$\begin{bmatrix}\left|\uparrow\uparrow\right\rangle\\ \left|\uparrow\downarrow\right\rangle\\ \left|\downarrow\uparrow\right\rangle\\ \left|\downarrow\downarrow\right\rangle\end{bmatrix}\otimes\left(a^\dagger\right)^2 \to \begin{bmatrix}t_1^2\left|\uparrow\uparrow\right\rangle\\ t_1^2\left|\uparrow\downarrow\right\rangle\\ \left|\downarrow\uparrow\right\rangle\\ \left|\downarrow\downarrow\right\rangle\end{bmatrix}\otimes\left(a^\dagger\right)^2 + \begin{bmatrix}2t_1t_{e,1}\left|\uparrow\uparrow\right\rangle\\ 2t_1t_{e,1}\left|\uparrow\downarrow\right\rangle\\ 0\\ 0\end{bmatrix}\otimes a^\dagger r_1^\dagger + \begin{bmatrix}t_{e,1}^2\left|\uparrow\uparrow\right\rangle\\ t_{e,1}^2\left|\uparrow\downarrow\right\rangle\\ 0\\ 0\end{bmatrix}\otimes\left(r_1^\dagger\right)^2,$$

$$\text{and}\quad \begin{bmatrix}\left|\uparrow\uparrow\right\rangle\\ \left|\uparrow\downarrow\right\rangle\\ \left|\downarrow\uparrow\right\rangle\\ \left|\downarrow\downarrow\right\rangle\end{bmatrix}\otimes\left(b^\dagger\right)^2 \to \begin{bmatrix}t_2^2\left|\uparrow\uparrow\right\rangle\\ \left|\uparrow\downarrow\right\rangle\\ t_2^2\left|\downarrow\uparrow\right\rangle\\ \left|\downarrow\downarrow\right\rangle\end{bmatrix}\otimes\left(b^\dagger\right)^2 + \begin{bmatrix}2t_2t_{e,2}\left|\uparrow\uparrow\right\rangle\\ 0\\ 2t_2t_{e,2}\left|\downarrow\uparrow\right\rangle\\ 0\end{bmatrix}\otimes b^\dagger r_2^\dagger + \begin{bmatrix}t_{e,1}^2\left|\uparrow\uparrow\right\rangle\\ 0\\ t_{e,2}^2\left|\downarrow\uparrow\right\rangle\\ 0\end{bmatrix}\otimes\left(r_2^\dagger\right)^2, \tag{4.24}$$

where once again we suppress the notation $t_{e,i}\left(\omega\right) \to t_{e,i}$ for the probability amplitude associated with a photon lost at emitter i.

The field then passes through the second beam splitter, leaving the state of the emitters unchanged whilst transforming the optical state:

$$\begin{aligned}\rho_4 = \frac{1}{4}\sum_{i,j}\Big\{&\rho(M_{i,1}, M_{j,1})\otimes\left[M_{i,2}\left|0\right\rangle\left\langle 0\right| M_{j,2}\right] + \rho(N_{i,1}, N_{j,1})\otimes\left[N_{i,2}\left|0\right\rangle\left\langle 0\right| N_{j,2}\right]\\ &- \rho(M_{i,1}, N_{j,1})\otimes\left[M_{i,2}\left|0\right\rangle\left\langle 0\right| N_{j,2}\right] + \rho(N_{i,1}, M_{j,1})\otimes\left[N_{i,2}\left|0\right\rangle\left\langle 0\right| M_{j,2}\right]\Big\},\end{aligned} \tag{4.25}$$

where $\mathbf{M}$ and $\mathbf{N}$ now become

$$\mathbf{M} = \begin{bmatrix} a^2 & \frac{1}{2}(a^2+2ab+b^2) \\ ar_1 & \frac{1}{\sqrt{2}}(a+b)r_1 \\ r_1^2 & r_1^2 \end{bmatrix} \quad \text{and} \quad \mathbf{N} = \begin{bmatrix} b^2 & \frac{1}{2}(a^2-2ab+b^2) \\ br_2 & \frac{1}{\sqrt{2}}(a-b)r_2 \\ r_2^2 & r_2^2 \end{bmatrix}. \tag{4.26}$$

We have therefore described the transformation of the total system, for an arbitrary state of two qubits, during one round of probing and before performing a photon measurement.

4.5.2 Detector inefficiencies

The development of ideal photon detectors is an active area of research, with perfect efficiency still proving to be elusive. Superconducting nanowire single-photon detectors are the current leaders amongst this family of instruments, having been used for detection efficiencies of $> 95\%$ [134–137]. We will therefore factor this as a source of imperfection in our protocol.

This inefficiency can be modelled by assuming a beam splitter with a transmission coefficient η placed before the detector [80], described by the following transformations:

$$a \to \sqrt{\eta}\, a + \sqrt{1-\eta}\, r_3 \qquad \text{and} \qquad b \to \sqrt{\eta}\, b + \sqrt{1-\eta}\, r_4. \tag{4.27}$$

Here r_3 and r_4 are the mode operators of the loss channels before the detectors at either output arm of the interferometer, and are distinct from the interaction-based loss channels at the emitters, r_1 and r_2. The state given by Eq. (4.25) then remains unchanged, such that $\rho_5 = \rho_4$, except for $\mathbf{M}$ and $\mathbf{N}$ that transform to

$$\mathbf{M} = \begin{bmatrix} a^2 & \frac{1}{2}\big[(\sqrt{\eta}\, a + \sqrt{1-\eta}\, r_3)^2 + (\sqrt{\eta}\, b + \sqrt{1-\eta}\, r_4)^2 \\ & +2(\sqrt{\eta}\, a + \sqrt{1-\eta}\, r_3)(\sqrt{\eta}\, b + \sqrt{1-\eta}\, r_4)\big] \\ ar_1 & \frac{1}{\sqrt{2}}(\sqrt{\eta}\, a + \sqrt{\eta}\, b + \sqrt{1-\eta}\, r_3 + \sqrt{1-\eta}\, r_4)r_1 \\ r_1^2 & r_1^2 \end{bmatrix}$$

$$\text{and} \qquad \mathbf{N} = \begin{bmatrix} b^2 & \frac{1}{2}\big[(\sqrt{\eta}\, a + \sqrt{1-\eta}\, r_3)^2 + (\sqrt{\eta}\, b + \sqrt{1-\eta}\, r_4)^2 \\ & -2(\sqrt{\eta}\, a + \sqrt{1-\eta}\, r_3)(\sqrt{\eta}\, b + \sqrt{1-\eta}\, r_4)\big] \\ br_2 & \frac{1}{\sqrt{2}}(\sqrt{\eta}\, a - \sqrt{\eta}\, b + \sqrt{1-\eta}\, r_3 - \sqrt{1-\eta}\, r_4)r_2 \\ r_2^2 & r_2^2 \end{bmatrix}. \tag{4.28}$$

4.5.3 Measurement

The last step at each iteration is the measurement process. However, in the presence of losses and absence of photon-number resolution, this step will project the emitter state onto a mixed one. This is because the observer does not gain any information on whether or not a loss has occurred and, if so, at what stage.

A single click by the detector at output arm a is possible either in the event of a concurrent arrival of both photons, or a single photon arriving while the other is lost at some point. In order to obtain the corresponding projective operator for this detection

signature, we need to modify Eq. (4.10) to

$$\Pi_{1,0} = \frac{1}{2} \sum_{i,j=a,r_1,r_2,r_3,r_4} i^\dagger j^\dagger \left|0\right\rangle \left\langle 0\right| i\, j. \tag{4.29}$$

The corresponding reduced density matrix of the qubits post-measurement is then

$$\begin{aligned}\rho_{(1,0)} &= \frac{1}{P(1,0)} \mathrm{Tr}_{\text{field}} \left[\Pi_{1,0}\, \rho_5\, \Pi_{1,0}\right] \\ &= \frac{1}{P(1,0)} \Bigg\{ \frac{\eta^2}{16} \left[\rho\left(a^2, a^2\right) + \rho\left(b^2, b^2\right) - \rho\left(a^2, b^2\right) - \rho\left(b^2, a^2\right)\right] \\ &\qquad + \frac{\eta(1-\eta)}{2} \left[\rho\left(a^2, a^2\right) + \rho\left(b^2, b^2\right)\right] + \frac{\eta}{8} \left[\rho(a\, r_1, a\, r_1) + \rho(b\, r_2, b\, r_2)\right] \Bigg\},\end{aligned} \tag{4.30}$$

where $\rho\,(m, m)$ is the state of the emitters associated with the scattered optical state $m^\dagger \left|0\right\rangle \left\langle 0\right| m$, as given in Eq. (4.22), and the probability of obtaining this measurement outcome is

$$P\,(1,0) = \mathrm{Tr}\left[\Pi_{1,0}\, \rho_5\, \Pi_{1,0}\right]. \tag{4.31}$$

Here, we see clearly how the sources of imperfection herald a density matrix of the mixed form, that is, decomposed into a sum of pure state density matrices with probability distribution that depends on the rate of losses.

The measurement outcome corresponding to a single click at the detector at output arm b is similarly defined, with the projective operator instead modified to

$$\Pi_{0,1} = \frac{1}{2} \sum_{i,j=b,r_1,r_2,r_3,r_4} i^\dagger j^\dagger \left|0\right\rangle \left\langle 0\right| i\, j, \tag{4.32}$$

and the resulting qubit state and associated probability defined as in Eqs (4.30) and (4.31), respectively.

In the event of a coincidence measurement, where each detector measures a photon, we maintain a pure state as we can rule out the possibility of loss, and the post-measurement state is similar to the one defined in the ideal case:

$$\begin{aligned}\rho_{(1,1)} &= \frac{1}{P(1,1)} \mathrm{Tr}_{\text{field}} \left[\Pi(ab) \rho_4 \Pi(ab)\right] \\ &= \frac{\eta^2}{4P(1,1)} \left[\rho(a^2, a^2) + \rho(b^2, b^2) + \rho(a^2, b^2) + \rho(b^2, a^2)\right],\end{aligned} \tag{4.33}$$

with

$$P(1,1) = \mathrm{Tr}\left[\Pi(ab) \rho_4 \Pi(ab)\right]. \tag{4.34}$$

Finally, we also account for the loss of both photons at some stage of the probing process, characterised by the projective operator

$$\Pi_{0,0} = \frac{1}{2} \sum_{i,j=1,2,3,4} r_i^\dagger r_j^\dagger \left|0\right\rangle \left\langle 0\right| r_i\, r_j, \tag{4.35}$$

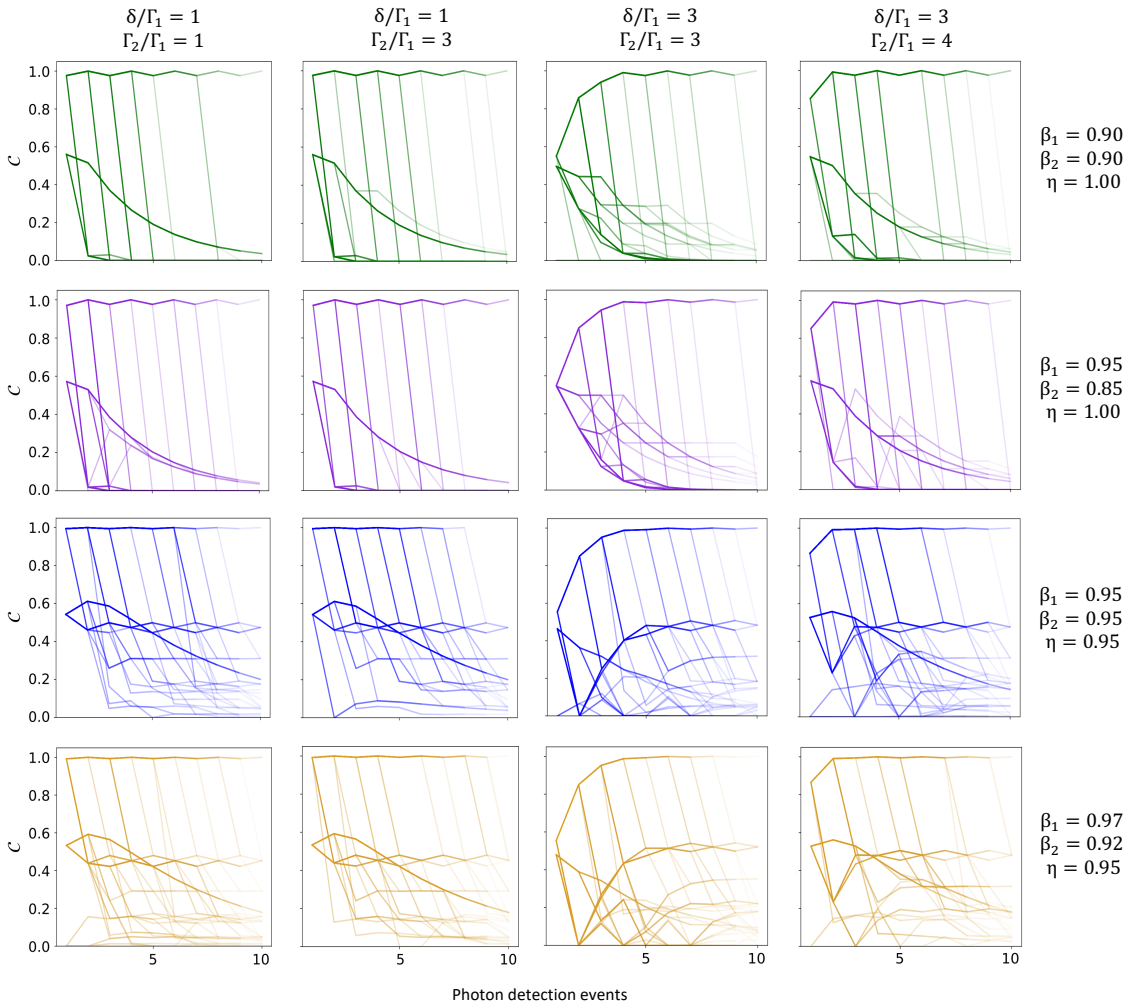

Figure 4.3: Typical concurrence trajectories for various β-factors and detector efficiencies, η. Γ_1 and Γ_2 are the emitter line widths and the central energy detuning between the two is given by $\delta = E_2 - E_1$. We factor in both successful detection events as well as zero-photon outcomes.

with the resultant density matrix and probability obtained as outlined before.

The process is then repeated from Eq. (4.19), where we replace ρ_{emitters} with the obtained density matrix, in an attempt to understand how well entanglement can be generated by accumulation in this manner. We show some results for such trajectories in Fig. 4.3, where we also include the possibility of zero-photon detection outcomes. For emitter combinations that are entangled rapidly in the lossless case and $\beta \sim 0.9$, concurrence of > 0.99 is possible within a few repetitions of the probing cycle; for the configurations shown in the figure, the likelihood of such near perfect entanglement is 10 – 50%. Furthermore, there is no qualitative difference when accounting for small variations between the β-factors of the two emitters.

In order to maximise the amount of concurrence attained, we perform a bit flip in the

computational basis on both qubits after every measurement event:

$$\rho \xrightarrow{\text{bit flip}} \sigma_x \otimes \sigma_x \, \rho \, \sigma_x \otimes \sigma_x, \tag{4.36}$$

where $\sigma_x = |\uparrow\rangle\langle\downarrow| + |\downarrow\rangle\langle\uparrow|$ is the Pauli X matrix. The reason behind this stems from the fact that $\gamma \neq 0$. This leads to scattering events that result in an accumulation of probability amplitudes on $|\uparrow\uparrow\rangle$ and $|\downarrow\downarrow\rangle$, and $|\uparrow\downarrow\rangle$ and $|\downarrow\uparrow\rangle$ that is skewed. This unevenness is detrimental to the amount of entanglement, and can be partially addressed by introducing the bit flip operations that balance out the contributions to the qubit states.

4.6 Practical implementation

We now turn to practical considerations and challenges when it comes to the physical implementation of the protocol. We have already addressed the deterioration of the entanglement process as a result of photon loss and detector inefficiencies. One also needs to consider possible deviation of the optical frequency away from the optimum. In Fig. 4.4 we show how a shift in the frequency affects the maximum amount of concurrence that may be attained in the lossless case, averaging over many trajectories. For a non-optimal frequency, the scattering events at either emitter would no longer be identical, as the condition in Eq. (4.16) is no longer satisfied, which in turn influences the coherent interference that occurs at the second beam splitter and the resulting erasure of which-path information. This affects the buildup of concurrence in a negative way, with the degree of impact depending on the choice of emitter combination. Furthermore, we see an asymmetry in the resulting plots that stems from the fact that the rate of change of the phase shift is not symmetric about frequencies away from resonance.

Another practical limitation that needs to be kept in consideration is the finite coherence time of solid-state emitters, affected by processes such as the spin-orbit and nuclear-spin interactions [138–140]. Current experimental values for the lifetime in semiconductor quantum dots range between >100 ns and several microseconds [141–143], whilst for nitrogen-vacancy centres in diamond, this value may reach the millisecond range [144–146] and can be enhanced to more than half a second by means of decoupling pulsing [147]. Increasing the pump power of the SPDC source is one way of overcoming this limitation as this would increase the generation rate of biphotons. However this will also increase the likelihood of higher order pairs, and we would need to account for scattering and measurement of larger photon number states. We account for the possibility of $|2,2\rangle$ state production and show its effect on the entanglement generation scheme, whilst assuming photon-number resolving detectors, in Fig. 4.5. By assuming such resolution, we observe that such multi-photon pairs do not impact the scheme in a disruptive way. In fact, the concurrence trajectories here are bounded from below by the lowest possible trajectory when assuming solely $|1,1\rangle$ probing states whilst exhibiting the possibility of enhancement of the scheme in terms of speed.

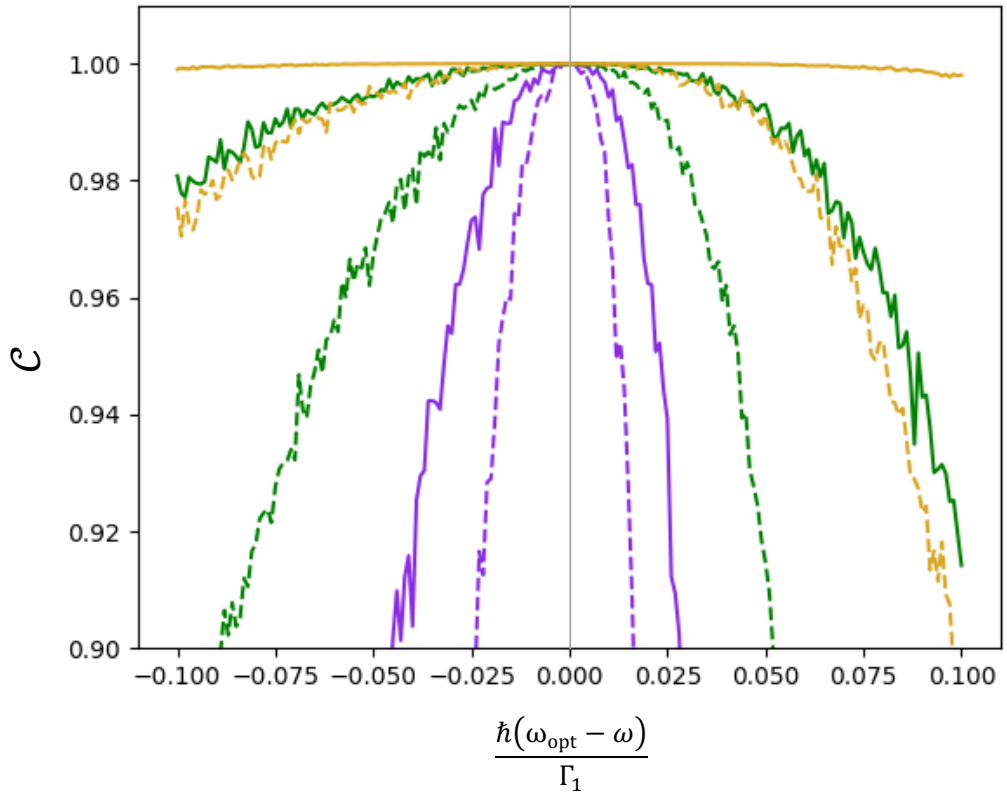

Figure 4.4: The maximum possible concurrence during a single trajectory, averaged over 300 trajectories, as a function of the difference between the optimal and actual input frequency, $\omega_{opt} - \omega$. Here, Γ_2/Γ_1 is set to 1 (purple), 3 (green) and 5 (yellow), and δ/Γ_1 is set to 3 (solid) and 5 (dotted).

4.7 Summary

In conclusion, we have introduced a protocol that allows us to entangle two solid-state emitters up to near-perfect concurrence, by considering a cumulative process that overcomes the limitations posed by the inhomogeneity resulting from the fabrication process. This eases the very restrictive requirement of spectrally identical emitters. Our scheme makes use of a relatively simple optical setup and experimentally accessible photonic states. It is also advantageous in that it does not require us to discard any samples on the basis of certain measurement outcomes, and therefore entanglement is generated in a deterministic way. Furthermore, it provides more flexibility when it comes to combining different emitters, with larger energy detunings and linewidth ratios offering the possibility of faster generation of concurrence.

Secondly, we accounted for photon losses at the scattering stage as well as detector inefficiencies, both of which degrade the scheme up to some extent. Nonetheless, near perfect entanglement is still possible for certain regions of the parameter space within a few number of detection events. Our results are promising, especially when considering the development in the field of photon-number resolving detectors, which would allow for

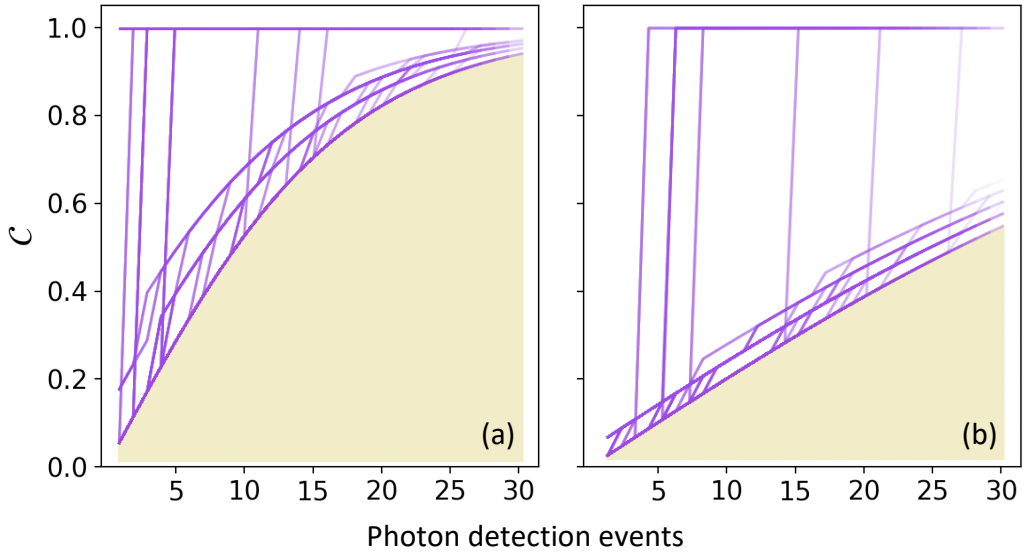

Figure 4.5: Typical concurrence trajectories for the lossless case ($\gamma = 0$) when probing with $|1,1\rangle$ and $|2,2\rangle$ states, with the latter being generated $\sim 15\%$ of the time. Here, Γ_2/Γ_1 is equal to 1, whilst δ/Γ_1 is equal to 3 (a) and 5 (b), and we assume the use of photon-number resolving detectors. The shaded region represents the area under the curve in Fig. 4.2, showing that the generation of higher order photon pairs is not detrimental to our scheme.

the discarding of samples in the event of photon loss. We do note however that this would naturally lead to a lower success probability, the rate of which would depend on the amount of scattering loss.

Finally, we have also considered practical limitations to our scheme, including the finite coherence time of solid-state emitters and multiphoton pairs. The generation of higher order pairs as a result of an increase in the SPDC pump power, which would otherwise reduce the time to reach perfect entanglement, might actually enhance our protocol when paired with photon-number resolution.

CHAPTER

5

SPIN-AUGMENTED QUANTUM INFORMATION PROCESSING

In this chapter, we will be considering the spin-photon interface in the form of a micropillar cavity coupled to a quantum dot. The interaction occurs selectively due to cavity quantum electrodynamics and resulting selection rules for optical transitions. By using this property, we are able to augment the performance of protocols that utilise linear optics alone. We will consider how, in the context of quantum error correction, this setup can be used for photonic syndrome extraction by means of quantum non-demolition measurement, and show the confidence in the read-out as a function of detuning errors. Furthermore, we will also study the generation of entanglement between spin systems with dissimilar characteristic energies. Work in this chapter is based on Callus and Kok [148].

5.1 Background

The spin–photon interface has proved to be highly suitable when it comes to applications in quantum information technologies [149,150]. The photon, with its relatively long coherence time, acts as a flying qubit between stationary nodes, physically implemented by means of solid-state emitters, transmitting information over large distances. The photon also readily interacts with the solid-state emitters, which therefore has the potential to overcome the restriction caused by weak photon–photon interactions [101]. This area of research has attracted a lot of interest, and different architectures falling under this category have been studied with various applications in mind. Some examples include the development of photonic quantum gates [100, 151] and application of optical non-linearities [21, 152], as well as the entanglement of remote spin states [153–155], photon polarisation [156] and spin–photon states [157].

The physical system that we shall be considering in this work exhibits the property of circular birefringence, whereby the plane of polarisation for a linearly polarised photon is

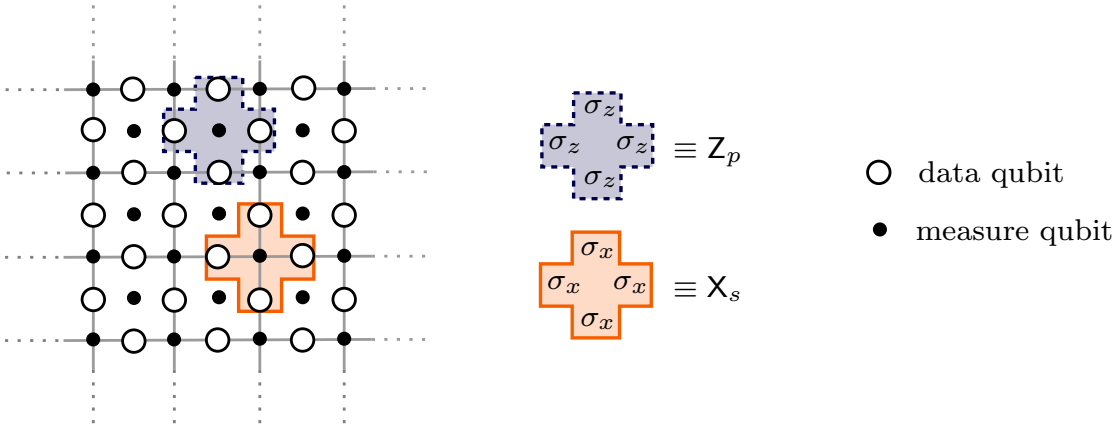

Figure 5.1: A schematic of the two-dimensional surface code made up of data (hollow circles) and measure (filled circles) qubits. An example of plaquette, Z_p, and star, X_s, operators are shown in blue (dotted outline) and orange (solid outline), respectively.

rotated by some amount. This phenomenon has been used in schemes for, e.g., quantum teleportation [158], quantum non-demolition measurements [159] and entanglement beam splitters [160]. This property has also been adopted in the design of a complete and deterministic Bell-state analyzer [158, 161], where information about the qubit parity is obtained using the spin–photon system whilst a linear optical setup measures the symmetry of the state. This overcomes the inherent limitation posed by the use of linear optics alone [162]: here, the setup based on the use of various beam splitters can correctly identify only two of the four Bell states. In our work, we show that we can employ a similar spin–photon interface to perform projective stabiliser measurements used in quantum error detection.

5.2 Surface codes

We will be considering the application of the spin–photon interface in the carrying out of efficient photonic syndrome, or stabilizer, measurements on the surface code. The surface code is a family of stabilizer codes implemented on a two-dimensional lattice of physical qubits. It is designed for the implementation of quantum computing in a fault-tolerant way by means of quantum error detection and correction [56, 163]. The first proposal for this type of code was in the form of the toric code [164, 165], with its boundary conditions allowing it to be mapped onto a torus, and later generalised to different planar codes with variations in the boundary conditions [166–168].

In Fig. 5.1, we show a schematic of the surface code: it is comprised of data and measure qubits in a structured arrangement. The single logical qubit is encoded into the multiple (physical) data qubits, with error correction making use of the redundancy resulting from the encoding of information in an expanded Hilbert space. The surface code is stabilized by the complete set of so-called star, X_s, and plaquette, Z_p, operators; given a surface

code with state $|\Psi\rangle$, we have that $\mathsf{X}_s |\Psi\rangle = \mathsf{Z}_p |\Psi\rangle = |\Psi\rangle$ for all s and p. Here, a star s is a set of data qubits adjacent to a vertex on the lattice, whilst a plaquette p is a set of qubits adjacent to a face, as represented in the figure. The star and plaquette operators, or stabilizers, are defined as

$$\mathsf{X}_s = \prod_{j \in \mathrm{star}(s)} \sigma_{x,j} \qquad \text{and} \qquad \mathsf{Z}_p = \prod_{j \in \mathrm{plaq}(p)} \sigma_{z,j}, \tag{5.1}$$

where $\sigma_{x,j} = |0\rangle_j \langle 1| + |1\rangle_j \langle 0|$ and $\sigma_{z,j} = |0\rangle_j \langle 0| - |1\rangle_j \langle 1|$ are the Pauli X and Pauli Z matrices, respectively, acting on physical qubit j.

Given that the eigenstates of σ_z are denoted by $|0\rangle$ and $|1\rangle$, the $+1$ and -1-eigenspaces of Z_p are generated by the following sets of eigenstates:

$$\begin{aligned} +1: &\quad \left\{ \otimes_{j \in \mathrm{plaq}(p)} |i_j\rangle : \sum_j i_j \bmod 2 = 0 \right\} = \{|0000\rangle, |0011\rangle, \ldots, |1111\rangle\}, \\ -1: &\quad \left\{ \otimes_{j \in \mathrm{plaq}(p)} |i_j\rangle : \sum_j i_j \bmod 2 = 1 \right\} = \{|0001\rangle, |0010\rangle, \ldots, |1110\rangle\}, \end{aligned} \tag{5.2}$$

respectively. The eigenspaces of X_s are similarly defined, albeit with $|0\rangle \to |+\rangle$ and $|1\rangle \to |-\rangle$, where $|\pm\rangle = (|0\rangle \pm |1\rangle)/\sqrt{2}$. We therefore see that an eigenvalue of $+1$ (-1) corresponds to an even (odd) parity state.

Since the surface code is stabilized by the stabilizer, the state of each star and plaquette must therefore be in some superposition of the $+1$-eigenstates (whilst also entangled with the rest of the data qubits to some extent). However, in the case of errors, be it either a bit-flip or a phase-flip on some physical qubit(s), some measurement operators will return an eigenvalue of -1, and the surface code is no longer stabilized by all the operators. Therefore, the presence and location of errors may be obtained from the eigenvalues of the operators in a process referred to as the extraction of the syndrome. The conventional method for syndrome extraction involves the operation of CNOT gates to each data qubit, with the measure qubit being the target. Our proposal overcomes this requirement, as we introduce the spin–photon interaction in its stead, which can be integrated in an otherwise purely photonic implementation of the surface code.

5.3 Physical system

We now present the physical system that will serve as the spin–photon interface. The setup is shown in Fig. 5.2 and is comprised of a single-sided micropillar cavity with two distributed Bragg reflectors at either end, with one side being fully reflective and the other being partially transmissive. The micropillar holds a charged quantum dot, where the excess electron or hole spin couples selectively to the cavity mode. This selective coupling is a consequence of cavity QED and the optical selection rules that arise from the Pauli exclusion principle, rendering the interaction between a photon and the two-level system dependent on both the photonic polarisation and the spin state [169], as mentioned in

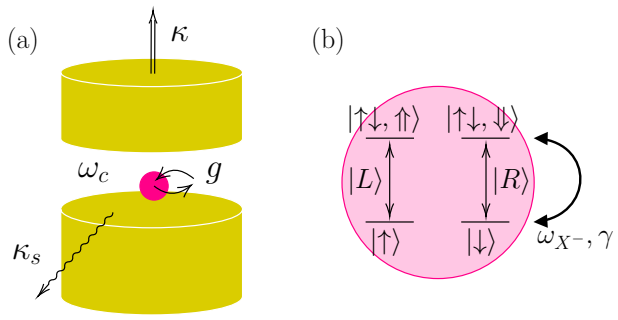

Figure 5.2: (a) A single-sided micropillar cavity with mode frequency ω_c coupled to a quantum dot with coupling strength g. The cavity mode within the micropillar couples to the output mode and leakage modes with rates κ and κ_s, respectively. (b) The energy level structure of the quantum dot showing photon polarisation- and spin-dependent selection rules. The trion transition frequency and its decay rate are given by ω_{X^-} and γ, respectively.

Sec. 3.6.1. Considering a negatively charged quantum dot with a single excess electron, the spin state $|\uparrow\rangle$ ($|\downarrow\rangle$) transitions to the negative trion state X^-, given by $|\uparrow\downarrow, \Uparrow\rangle$ ($|\uparrow\downarrow, \Downarrow\rangle$), when optically excited by a left-handed (right-handed) circularly polarised photon $|L\rangle$ ($|R\rangle$). Here, $|\uparrow\downarrow, \Uparrow\rangle$ denotes a state with two electrons in a singlet in the conduction band and the heavy-hole spin state $|\Uparrow\rangle$ in the valence band that results from the dipole transition, and similarly for $|\uparrow\downarrow, \Downarrow\rangle$.

Let us consider first the case when a photon enters the single-sided cavity, interacts with the quantum dot and then couples back to the output mode outside the cavity. Here, the cavity may be referred to as a 'hot' cavity due to the occurrence of an optical transition. The reflection coefficient arising from this interaction may be obtained by employing the input–output formalism as described in Sec. 3.4 and is given by [158, 170]

$$r_h(\omega) = \frac{\left[\mathrm{i}\left(\omega_{X^-} - \omega\right) + \frac{\gamma}{2}\right]\left[\mathrm{i}\left(\omega_c - \omega\right) - \frac{\kappa}{2} + \frac{\kappa_s}{2}\right] + g^2}{\left[\mathrm{i}\left(\omega_{X^-} - \omega\right) + \frac{\gamma}{2}\right]\left[\mathrm{i}\left(\omega_c - \omega\right) + \frac{\kappa}{2} + \frac{\kappa_s}{2}\right] + g^2}, \tag{5.3}$$

where ω, ω_{X^-} and ω_c are the photon, the trion transition and the cavity mode frequencies, respectively; γ is the decay rate of the trion dipole; κ and κ_s are the cavity coupling rates to the output mode and leakage modes, respectively; and g is the coupling strength between the quantum dot and the cavity field.

In the event of a 'cold' cavity, i.e., when a photon exits back to the output mode without having coupled to the quantum dot, the only contribution to the reflection coefficient comes from the empty cavity interaction. This occurs when the selection rules prohibit the optical transition. We can characterise this by setting $g = 0$ in Eq. (5.3) and obtaining [158, 170]

$$r_0(\omega) = \frac{\mathrm{i}\left(\omega_c - \omega\right) - \frac{\kappa}{2} + \frac{\kappa_s}{2}}{\mathrm{i}\left(\omega_c - \omega\right) + \frac{\kappa}{2} + \frac{\kappa_s}{2}}. \tag{5.4}$$

We will consider the resonant interaction case, where $\omega_c = \omega_{X^-}$, and allow for the relative detuning of the photonic frequency ω, with the detuning given by $\delta = \omega_c - \omega =$

$\omega_{X^-} - \omega$. We will also consider cavity losses, given by κ_s, to be small enough such that we can assume $|r_0(\omega)| \simeq 1$ for all values of δ. Moreover, we assume the system to be in the strong-coupling regime, with $g > (\kappa + \kappa_s)/4$ and $g >> \kappa, \gamma$, resulting in $|r_h(\omega)| \simeq 1$ for all δ except around $\pm g$ [171], which we may ignore since we will be working near resonance with $|\delta| << g$. The frequency detuning δ is adjusted such that the difference in the phase shifts imparted by the hot and the cold cavities is of $\pm\pi/2$, i.e., by defining $\phi_i(\omega) = \arg[r_i(\omega)]$ for $i = h, 0$, we obtain $\tilde{\phi}(\omega) \equiv \phi_h(\omega) - \phi_0(\omega) = \pm\pi/2$. The transformation matrix for this spin–photon interaction in the basis $\{|L\uparrow\rangle, |L\downarrow\rangle, |R\uparrow\rangle, |R\downarrow\rangle\}$, with $|ij\rangle \equiv |i\rangle \otimes |j\rangle$, is therefore

$$U = \begin{bmatrix} r_h(\omega) & 0 & 0 & 0 \\ 0 & r_0(\omega) & 0 & 0 \\ 0 & 0 & r_0(\omega) & 0 \\ 0 & 0 & 0 & r_h(\omega) \end{bmatrix} \xrightarrow{\tilde{\phi}=\pm\pi/2} e^{i\phi_0} \begin{bmatrix} \pm i & 0 & 0 & 0 \\ 0 & 1 & 0 & 0 \\ 0 & 0 & 1 & 0 \\ 0 & 0 & 0 & \pm i \end{bmatrix} = U_{\tilde{\phi}=\pm\pi/2}. \tag{5.5}$$

Hereafter we choose to drop the frequency dependence for ease of notation.

Theoretical modelling shows that this non-linear phase shift can be experimentally achieved up to π [172–174]. Experimentally, these phase shifts are now being observed, with results improving over time from only a few micro-degrees fifteen years ago up to $\sim \pi$ in the last couple of years [175–180], demonstrating the viability of using photonic quantum dot interactions for quantum information processing.

5.4 Syndrome measurement procedure

We now introduce the syndrome measurement procedure, shown schematically in Fig. 5.3. The photons serve as the data qubits with the computational basis states encoded in the polarisation: $|0\rangle \to |L\rangle$ and $|1\rangle \to |R\rangle$; the spin state of the quantum dot acts as the measure qubit and is initialised to $|+\rangle_S = (|\uparrow\rangle + |\downarrow\rangle)/\sqrt{2}$, where we use subscript S to denote the spin subsystem. We let the four photons belonging to a star or plaquette set interact with the spin system sequentially in time. In the case of a star measurement X_s, we also apply a Hadamard transformation, H, pre- and post-interaction defined by

$$H = \frac{1}{\sqrt{2}} \begin{bmatrix} 1 & 1 \\ 1 & -1 \end{bmatrix}. \tag{5.6}$$

The application of this gate effectively rotates the σ_x eigenstates around the Bloch sphere such that $|+\rangle \leftrightarrow |0\rangle$ and $|-\rangle \leftrightarrow |1\rangle$, and is necessary for the spin–photon interaction to occur in such a way as to impart information about the syndrome onto the spin state as given in Eq. (5.5).

The evolution of a photonic star or plaquette eigenstate and the spin state can then be

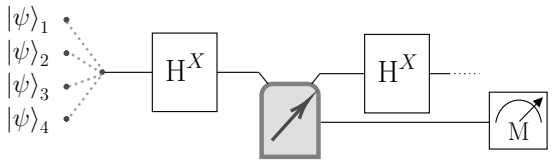

Figure 5.3: Schematic of the syndrome extraction setup using a single quantum dot. The optical states $|\psi\rangle_1, \ldots, |\psi\rangle_4$ interact with the spin state successively in time, and Hadamard gates, H^X, are applied pre- and post-interaction solely in the case of a star measurement, X_s. A spin read-out, M, in the X-basis is performed in order to retrieve the syndrome.

expressed as

$$\begin{aligned}\left[\otimes_{\substack{j\in\mathrm{star}(s)\\ \text{or plaq}(p)}} |i_j\rangle\right] \otimes |+\rangle_S &\to \frac{1}{\sqrt{2}}\left[\bigotimes_j \exp\left(\mathrm{i}\phi_{j,\uparrow}\right)|i_j\rangle\right]\otimes|\uparrow\rangle + \frac{1}{\sqrt{2}}\left[\bigotimes_j \exp\left(\mathrm{i}\phi_{j,\downarrow}\right)|i_j\rangle\right]\otimes|\downarrow\rangle \\ &= \left[\bigotimes_j \exp\left(\mathrm{i}\phi_{j,\uparrow}\right)|i_j\rangle\right]\otimes\left[|\uparrow\rangle + \prod_j \exp\left[-\mathrm{i}\left(\phi_{j,\uparrow}-\phi_{j,\downarrow}\right)\right]|\downarrow\rangle\right]/\sqrt{2} \\ &= \frac{e^{4\mathrm{i}\phi_0}}{\sqrt{2}}\left[\bigotimes_j \exp\left(\mathrm{i}\tilde{\phi}\delta_{i_jL}\right)|i_j\rangle\right]\otimes\left[|\uparrow\rangle + \prod_j \exp\left[-\mathrm{i}\left(\phi_{j,\uparrow}-\phi_{j,\downarrow}\right)\right]|\downarrow\rangle\right],\end{aligned} \tag{5.7}$$

where $|i_j\rangle \in \{|L\rangle, |R\rangle\}$, j indexes the photonic qubits belonging to the star or plaquette set, δ_{i_jL} is the Kronecker delta with $\delta_{i_jL} = [i_j = L]$, and $\phi_{j,*}$ is the phase shift resulting from the interaction between photon $|i_j\rangle$ and spin $|*\rangle \in \{|\uparrow\rangle, |\downarrow\rangle\}$. Given that the frequency detuning, δ, is set so that $\tilde{\phi} = \pm\pi/2$, we obtain $(\phi_{j,\uparrow} - \phi_{j,\downarrow}) = \pm\pi/2$ $(\mp\pi/2)$ for a left(right)-handed circularly polarised photon. We see from Eq. (5.7) that this relative phase shift between the two spins accumulates with each photon interaction: the total phase shift imparted in the case of two identically polarised photons is $\pm\pi$ whilst in the case of two photons of orthogonal polarisation, the relative phase shift is effectively zero. Given the nature of the eigenstates defined in Eq. (5.2), the spin state then must evolve to either $|+_S\rangle$ or $|-_S\rangle$, depending on whether the parity of the photonic state is even or odd, respectively, which then maps to the eigenvalue of the measurement operator. Therefore, by performing a quantum non-demolition measurement by means of a spin read-out in the X-basis, we can reveal the syndrome of the photonic data qubits.

In a surface code, the data qubits may be initialised by performing one cycle of all stabilizer operators in order to project the code to a simultaneous eigenstate of the star and plaquette operators, also referred to as the quiescent state [168]. The set of states that satisfy this condition grows exponentially with the number of data qubits, and the quiescent state that is generated by the concurrent measurement of all stabilizers is randomly selected from this space. In order to preserve the quiescent state post-measurement, including any errors that the syndrome extraction is meant to detect, we need to resolve any of the

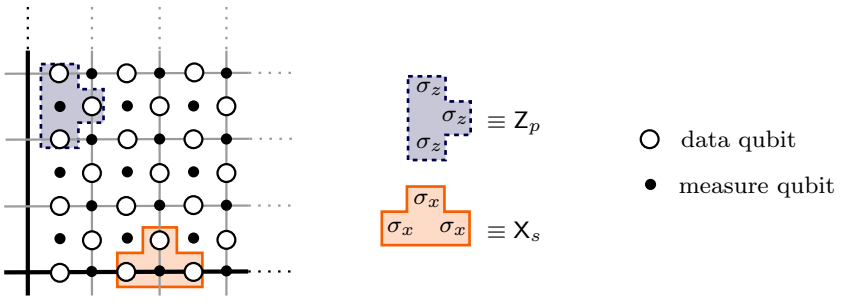

Figure 5.4: A schematic of the boundaries, indicated by bold lines, of a two-dimensional surface code. The plaquette, Z_p, and star, X_s, operators of weight three acting on the boundaries are shown in blue (dotted outline) and orange (solid outline), respectively.

differences in the phase shifts imparted on the photonic eigenstates by the spin–photon interaction. The phase shift acquired by the photonic states is seen clearly in the last line of Eq. (5.7), and has two contributions. First, there is the factor of $\exp(4\mathrm{i}\phi_0)$ that occurs for all syndrome measurements, regardless of the type of eigenstate. This renders it a global phase of the quiescent state and can therefore be ignored. The second contribution is of the form $\prod_j \exp\left(\mathrm{i}\tilde{\phi}\delta_{i_j L}\right)$, which introduces possible errors to the surface code in the form of phase-flips on some of the eigenstates. This is easily rectified by applying a polarisation-dependent phase shift acting solely on the right-hand circularly polarised photon, such that $|R\rangle \to \exp\left(\mathrm{i}\tilde{\phi}\right)|R\rangle$. By performing this rotation, we revert the state back to its original pre-measurement state.

Surface codes may vary in terms of their boundary conditions, resulting in modifications to the operators that would be applied to the data qubits at these boundaries. We consider here boundaries that call for operators comprised of a tensor product of three Pauli matrices, as shown in Fig. 5.4. We can make use of the same setup and the same frequency detuning δ as in the case of weight four operators, with the photonic and spin states evolving now as

$$\begin{aligned}\left[\bigotimes_j |i_j\rangle\right] \otimes |+\rangle_S \\ \to \frac{e^{3\mathrm{i}\phi_0}}{\sqrt{2}}\left[\bigotimes_j \exp\left(\mathrm{i}\tilde{\phi}\delta_{i_j L}\right)|i_j\rangle\right] \otimes \left[|\uparrow\rangle + \prod_j \exp\left[-\mathrm{i}\left(\phi_{j,\uparrow} - \phi_{j,\downarrow}\right)\right]|\downarrow\rangle\right],\end{aligned} \tag{5.8}$$

where j indexes over the three qubits in the star or plaquette set, and all other variables are as previously defined. Here, the spin state evolves to either $|L\rangle_S = \left(|\uparrow\rangle + \mathrm{i}\,|\downarrow\rangle\right)/\sqrt{2}$ or $|R\rangle_S = \left(|\uparrow\rangle - \mathrm{i}\,|\downarrow\rangle\right)/\sqrt{2}$, mapping to an eigenstate of $+1$ and -1, respectively. We therefore extract the syndrome by adjusting the spin read-out to measure the state in the Y-basis. Finally, any corrections that need to be made to phases imparted on the photonic state are performed in the same way as before.

5.5 Inherent symmetry in the interaction

The spin–photon interaction is inherently symmetric, as can be seen from the transformation in Eq. (5.5). Therefore, it is also possible to implement the scheme by swapping around the assignment of the data and measure qubits: the physical qubit is encoded in the spin of the quantum dot, with $|0\rangle \to |\uparrow\rangle$ and $|1\rangle \to |\downarrow\rangle$, and the photonic state "initialised" with horizontal polarisation, $|H\rangle = (|L\rangle + |R\rangle)/\sqrt{2}$. The photon, serving as the measure qubit, is allowed to interact consecutively with each data (spin) qubit, and the total system evolves as

$$\begin{aligned}&\left[\bigotimes_j |i_j\rangle\right] \otimes |H\rangle \\ &\qquad \to \frac{e^{4\mathrm{i}\phi_0}}{\sqrt{2}} \left[\bigotimes_j \exp\left(\mathrm{i}\tilde{\phi}\delta_{i_j\uparrow}\right)|i_j\rangle\right] \otimes \left[|L\rangle + \prod_j \exp\left[-\mathrm{i}\left(\phi_{j,L} - \phi_{j,R}\right)\right]|R\rangle\right],\end{aligned} \tag{5.9}$$

where now $|i_j\rangle \in \{|\uparrow\rangle, |\downarrow\rangle\}$. Given the symmetry of the interaction, the relative phase between the two photon polarisations accumulates in the same manner as for the spins, and the photon either remains in the horizontal polarisation or evolves to the vertical one, with $|V\rangle = -\mathrm{i}\left(|L\rangle - |R\rangle\right)/\sqrt{2}$. Therefore, the syndrome can be extracted by performing a photon measurement in the linear polarisation basis.

We see from Eq. (5.9) that we get possible phase-flip errors on the data qubits due to the arising spin-dependent phase shifts, similar to what occurs in the photonic implementation. Correcting these errors can be done by simply allowing a single $|R\rangle$ photon to interact with each data qubit. Taking the post-measurement spin state in Eq. (5.9), the interaction yields

$$\begin{aligned}&e^{4\mathrm{i}\phi_0}\left[\bigotimes_j \exp\left(\mathrm{i}\tilde{\phi}\delta_{i_j\uparrow}\right)|i_j\rangle\right] \otimes |R\rangle \\ &\to e^{4\mathrm{i}\phi_0}\left\{\bigotimes_j \exp\left[\mathrm{i}\left(\tilde{\phi}\delta_{i_j\uparrow} + \phi_0\delta_{i_j\uparrow} + \phi_h\delta_{i_j\downarrow}\right)\right]|i_j\rangle\right\} \otimes |R\rangle = e^{4\mathrm{i}(\phi_0+\phi_h)}\left[\bigotimes_j |i_j\rangle\right] \otimes |R\rangle,\end{aligned} \tag{5.10}$$

since $\tilde{\phi} + \phi_0 = \phi_h$ and the phase resulting from a hot cavity, ϕ_h, is the same for either spin state. The interaction results in an overall phase that is independent of the spin states, rendering an overall global phase that can be ignored.

5.6 Confidence

We will now study how robust the proposed scheme is against possible variations in the frequency detuning δ from the optimal. The difference in the phase shifts resulting from the hot and cold cavity interaction, $\tilde{\phi}$, is equal to $\pm\pi/2$ only at specific values of δ. Therefore, deviations in the detuning of the system from these values could impact the protocol by affecting the reliability of the spin measurement as an indicator of the syndrome. Let us

assume that $\tilde{\phi}$ is not necessarily equal to $\pm\pi/2$. Therefore, the relative phase between the two spins in Eq. (5.7), given by $\prod_j \exp\left[-\mathrm{i}\left(\phi_{j,\uparrow}-\phi_{j,\downarrow}\right)\right]$, may deviate from $0, \pm\pi$ post-interaction. The state of the spin subsystem post-interaction and pre-measurement is given by

$$\begin{aligned}&\frac{1}{\sqrt{2}}\left[\left|\uparrow\right\rangle+\prod_j \exp\left[-\mathrm{i}\left(\phi_{j,\uparrow}-\phi_{j,\downarrow}\right)\right]\left|\downarrow\right\rangle\right]\\&\quad=\frac{1}{2}\left[1+\prod_j \exp\left[-\mathrm{i}\left(\phi_{j,\uparrow}-\phi_{j,\downarrow}\right)\right]\right]\left|+\right\rangle_S+\frac{1}{2}\left[1-\prod_j \exp\left[-\mathrm{i}\left(\phi_{j,\uparrow}-\phi_{j,\downarrow}\right)\right]\right]\left|-\right\rangle_S,\end{aligned} \tag{5.11}$$

where both $\left|+\right\rangle_S$ and $\left|-\right\rangle_S$ may now have a non-zero probability amplitude associated to them. In this case, one can clearly see that there is a non-zero probability that the spin measurement in the X-basis does not correspond to the actual value of the syndrome. We will use the confidence [181] in the spin read-out as our figure of merit, giving us a measure for how well the extracted syndrome corresponds to the true value.

We start from the surface code which, for our work, we consider to be the ground state of the planar code. This is defined to be [17]

$$\left|\Psi_0\right\rangle \propto \prod_s \left(\mathbb{1}+\mathsf{X}_s\right)\left|0\right\rangle^{\otimes n}, \tag{5.12}$$

where $\mathbb{1}$ is the identity operator acting on the data qubits, n is the number of physical data qubits in the code encoding a single logical qubit and the matrix multiplication is performed over all star sets, s. The latter ensures that the resulting ground state is a simultaneous eigenstate of all possible star and plaquette operators. The code is assumed to be susceptible to coherent errors that can be described by means of a Pauli channel, given by

$$\mathcal{E}\left(\rho\right)=\left(1-p\right)\rho+x\sigma_x\rho\sigma_x+y\sigma_y\rho\sigma_y+z\sigma_z\rho\sigma_z, \tag{5.13}$$

acting on each individual data qubit. Here, ρ is the density matrix of the physical qubit; σ_i is the Pauli i matrix corresponding to the type of error, with $i=x,y,z$ and $\mathrm{i}\sigma_y=\sigma_z\sigma_x=-\sigma_x\sigma_z$; x,y,z are the respective probabilities of each type of error per single physical qubit; and $p=x+y+z$ is the total physical qubit error rate.

We first analyse plaquette operators, which detect bit-flip, or X-type, errors. We note at this point that it is not possible to detect phase-flip, or Z-type, errors when performing plaquette measurements using the spin–photon interface. In fact, let us assume that data qubit k belonging to the measured plaquette set has undergone an erroneous phase-flip such that

$$\bigotimes_{j\in\mathrm{plaq}(p)}\left|i_j\right\rangle \xrightarrow{\text{phase-flip on qubit } k} \sigma_{z,k}\bigotimes_j\left|i_j\right\rangle=\bigotimes_j\left(-1\right)^{\delta_{i_k1}}\left|i_j\right\rangle, \tag{5.14}$$

where $\delta_{i_k1}=[i_k=1]$ is the Kronecker delta denoting the phase-flip. It can then be seen that the plaquette measurement procedure in Eq. (5.7) is agnostic to any Z-type errors, as no information about the presence of the phase-flip is imparted onto the spin state.

In the ideal case where the condition $\tilde{\phi} = \pm\pi/2$ is satisfied, the spin–photon interaction followed by the syndrome measurement of a plaquette set with possible errors yields the following:

$$\left[\bigotimes_{j\in\text{plaq}} \mathcal{E}(\rho_j)\right] \otimes |+\rangle_S \langle +| \xrightarrow{\text{interaction}} p_+\rho_+ \otimes |+\rangle_S \langle +| + p_-\rho_- \otimes |-\rangle_S \langle -|, \tag{5.15}$$

where ρ_+, ρ_- are the density matrices of the data qubits in the absence and presence of X-type errors, respectively,[1] and p_+, p_- are the corresponding probabilities. Therefore, a measurement of the spin in the X-basis projects the state of the qubits onto the density matrix that corresponds to the obtained syndrome value. The post-measurement state is obtained by means of the POVM corresponding to the spin read-out, where we define the POVMs to be

$$\Pi_\pm = \mathbb{1} \otimes |\pm\rangle_S \langle \pm|, \tag{5.16}$$

and the post-measurement state given by

$$\rho_\pm = \frac{\text{Tr}_S\left[\Pi_\pm \rho_{\text{post-int.}}\right]}{\text{Tr}\left[\Pi_\pm \rho_{\text{post-int.}}\right]}. \tag{5.17}$$

Here, $\text{Tr}_S[.]$ denotes the partial trace over the spin subsystem.

When the condition of $\tilde{\phi} = \pm\pi/2$ is not perfectly satisfied, the state of the qubits may evolve such that there is a non-zero probability for a spin read-out to not match the projected qubit state, as shown in Eq. (5.11). We formally define the confidence in a spin measurement of $|\pm_S\rangle$ to be

$$\text{Confidence}_\pm = \frac{\text{Tr}\left[(\mathbb{P}_\pm \otimes |\pm\rangle_S \langle \pm|)\left(U\ \mathcal{E}(\rho) \otimes |+\rangle_S \langle +|\ U^\dagger\right)\right]}{\text{Tr}\left[\Pi_\pm\left(U\ \mathcal{E}(\rho) \otimes |+\rangle_S \langle +|\ U^\dagger\right)\right]}, \tag{5.18}$$

where $\mathcal{E}(\rho) \equiv \otimes_j \mathcal{E}(\rho_j)$, which we have contracted for notational convenience; U is the transformation arising from the spin–photon interaction as given in Eq. (5.5); and $\mathbb{P}_\pm$ is the projection operator for the ±1-eigenstates, with

$$\begin{aligned}\mathbb{P}_+ &= |0000\rangle\langle 0000| + |0011\rangle\langle 0011| + |0110\rangle\langle 0110| + \ldots + |1111\rangle\langle 1111|, \\ \mathbb{P}_- &= |0001\rangle\langle 0001| + |0010\rangle\langle 0010| + |0100\rangle\langle 0100| + \ldots + |1110\rangle\langle 1110|.\end{aligned} \tag{5.19}$$

The numerator in Eq. (5.18) gives the probability of measuring a given spin and, consequently, projecting the data qubits onto the subspace that corresponds to its syndrome. The confidence is then normalised by dividing by the total probability of measuring the same spin, without accounting for data qubits whose syndrome might not be in agreement to the spin readout. Therefore, we obtain the probability that the spin measurement heralds the correct syndrome value of the projected qubits. The same analysis applies to star operators, given their equivalence to plaquette operators up to a Hadamard gate before and after interaction.

[1] Strictly speaking, this is not fully accurate since theoretically there are certain X-type errors that cannot be detected by one subset of the operators but may be discerned by another subset belonging to the same family. However, we use this simplification in our notation as it has no bearing on our analysis.

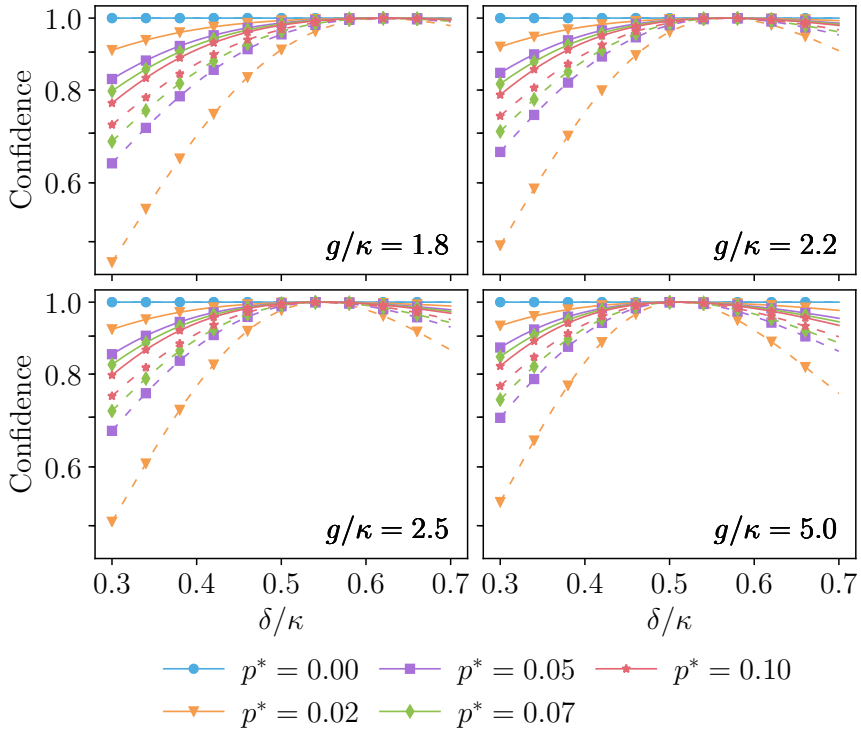

Figure 5.5: Confidence in the $|+_S\rangle$ (solid) and $|-_S\rangle$ (dashed) spin read-outs as a function of the frequency detuning $\delta = \omega_c - \omega = \omega_{X^-} - \omega$ for different coupling strengths, g. The single physical qubit error probability for either the X- or Z-type is denoted by p^*. The normalised linewidth, γ/κ, is set to 0.1.

In Fig. 5.5, we show the confidence in the spin measurements as a function of the frequency detuning, δ, for different coupling strengths, g, and single physical qubit error probabilities of either X- or Z- type, denoted by p^*. Here, we take $p^* = x + y$ ($p^* = y + z$) for $X(Z)$-type errors. Furthermore, we consider the strong coupling regime, the feasibility of which is substantiated by experimental values for g/κ reaching up to ~ 2.7 [182, 183]. First, we note that the distance of the code, which relates to the number of physical qubits in an array used to encode a logical qubit, has no effect on the confidence value, and that the plaquette and star operators show identical behaviour due to their equivalence up to a Hadamard gate.

5.7 Entanglement

The setup proposed in Fig. 5.2 may be modified to optimise for the type of physical resources required, as well as to accommodate for potential spectral inhomogeneity amongst the physical data qubits. Given the linear nature of the transformation, with the total phase shift imparted on a spin state after a sequence of interactions being equal to the sum of the phase shifts due to the individual interactions, we can choose to employ two or four measure qubits for a syndrome measurement.

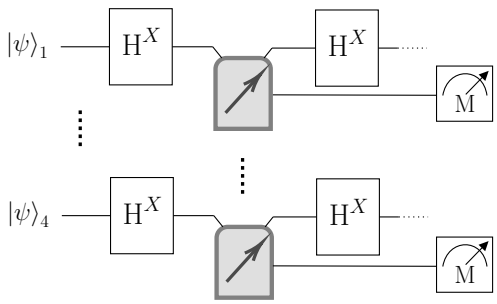

Figure 5.6: Schematic of the modified setup making use of multiple entangled quantum dots, with the optical states interacting with the spin states in parallel and Hadamard gate, H^X, applied pre- and post-interaction in the case of a star measurement, X_s. A spin measurement, M, in the X-basis is performed on each spin state.

The modified setup is shown in Fig. 5.6 and is made up of measure qubits that are entangled in a general GHZ-state [184] up to any Pauli operation, where

$$|\mathrm{GHZ}\rangle = \frac{|\uparrow\rangle^{\otimes M} + |\downarrow\rangle^{\otimes M}}{\sqrt{2}}, \tag{5.20}$$

and M is the size of the register. The data qubits interact in parallel with the spin states, with each photon interacting with only one spin (or two photons interacting with each spin in the case of a two-qubit register). Let us assume, without loss of generality, a four-qubit register with the spins initialised in the state given by Eq. (5.20). The total system will then transform in a manner similar to Eq. (5.7), with the spin sub-system evolving instead to

$$\begin{aligned}
&\xrightarrow{\text{interaction}} \frac{1}{\sqrt{2}}\left(|\uparrow\rangle^{\otimes 4} + e^{\mathrm{i}\Phi}\,|\downarrow\rangle^{\otimes 4}\right) \\
&\quad\propto \left(|+\rangle_S + |-\rangle_S\right)^{\otimes 4} + e^{\mathrm{i}\Phi}\left(|+\rangle_S - |-\rangle_S\right)^{\otimes 4} \\
&\quad= |++++\rangle_S + |+++-\rangle_S + |++-+\rangle_S + \ldots + |----\rangle_S \\
&\qquad + e^{\mathrm{i}\Phi}\left(|++++\rangle_S - |+++-\rangle_S - |++-+\rangle_S + \ldots + |----\rangle_S\right) \\
&\quad\propto \begin{cases} |++++\rangle_S + |++--\rangle_S + |+-+-\rangle_S + \ldots + |----\rangle_S & \text{if } \Phi = 0, 2\pi \\ |+++-\rangle_S + |++-+\rangle_S + |+-++\rangle_S + \ldots + |---+\rangle_S & \text{if } \Phi = \pm\pi \end{cases}.
\end{aligned} \tag{5.21}$$

Here we define $e^{\mathrm{i}\Phi} = \prod_j \exp\left[-\mathrm{i}\left(\phi_{j,\uparrow} - \phi_{j,\downarrow}\right)\right]$ for notational convenience. Therefore, the syndrome of the data qubits can be obtained by measuring the spin states in the X-basis, with the value determined by the parity of spin measurement. In the example given here, a syndrome of $+1$ (-1) is associated with $\Phi = 0, 2\pi$ ($\Phi = \pm\pi$) and, therefore, an even (odd) parity spin read-out.

The modification of the setup as outlined above calls for the generation of entanglement between the data qubits. One way of entangling the spin states of two quantum dots located

in single-sided cavities is by means of a linearly polarised photon interacting sequentially with each quantum dot [154, 170]. Let us first consider the ideal case with two identical quantum dots, with the spin states set to $(|\uparrow\rangle + |\downarrow\rangle)/\sqrt{2}$, and, say, a horizontally polarised photon. Then the initial state of the system is given by

$$\begin{aligned} |\Psi\rangle &= \frac{1}{2}|H\rangle \otimes (|\uparrow\rangle + |\downarrow\rangle) \otimes (|\uparrow\rangle + |\downarrow\rangle) \\ &= \frac{1}{\sqrt{2}^3}(|L\rangle + |R\rangle) \otimes (|\uparrow\rangle + |\downarrow\rangle) \otimes (|\uparrow\rangle + |\downarrow\rangle). \end{aligned} \tag{5.22}$$

The interaction then evolves the state to

$$\begin{aligned} |\Psi\rangle = \frac{e^{\mathrm{i}\phi_0}}{\sqrt{2}^3}\Big[&|L\rangle \otimes \left(e^{2\mathrm{i}\tilde{\phi}}|\uparrow\uparrow\rangle + e^{\mathrm{i}\tilde{\phi}}|\uparrow\downarrow\rangle + e^{\mathrm{i}\tilde{\phi}}|\downarrow\uparrow\rangle + |\downarrow\downarrow\rangle\right) \\ &+ |R\rangle \otimes \left(|\uparrow\uparrow\rangle + e^{\mathrm{i}\tilde{\phi}}|\uparrow\downarrow\rangle + e^{\mathrm{i}\tilde{\phi}}|\downarrow\uparrow\rangle + e^{2\mathrm{i}\tilde{\phi}}|\downarrow\downarrow\rangle\right)\Big] \\ = \frac{e^{\mathrm{i}\phi_0}}{2}\Big[&\pm\mathrm{i}|H\rangle \otimes (|\uparrow\downarrow\rangle + |\downarrow\uparrow\rangle) - \mathrm{i}|V\rangle \otimes (|\uparrow\uparrow\rangle - |\downarrow\downarrow\rangle)\Big], \end{aligned} \tag{5.23}$$

where $|H\rangle = (|L\rangle + |R\rangle)/\sqrt{2}$ and $|V\rangle = -\mathrm{i}(|L\rangle - |R\rangle)/\sqrt{2}$, and we assume $\tilde{\phi} = \pm\pi/2$. Here, we see clearly how the cavity-based interaction results in the so-called Faraday rotation, whereby the plane of polarisation undergoes a rotation, conditioned on the spin states. The spins are then entangled by means of a polarisation measurement of the photon, which projects the former onto a maximally entangled state.

We will now consider the case of entangling spectrally different spins, in order to accommodate for potentially distinct photonic qubits whilst satisfying the condition of $\tilde{\phi} = \pm\pi/2$ necessary for syndrome extraction. In this case, we may still make use of the entangling procedure outlined above, albeit with a possible reduction in the efficiency and fidelity. In non-identical systems, the amount of Faraday rotation may not be sufficient to result in perfect destructive interference, which is the underlying mechanism of this entanglement generation protocol.

We may generalise the expression in Eq. (5.23) for any two non-identical quantum dots, yielding the post-interaction state

$$\begin{aligned} |\Psi\rangle = &|H\rangle \otimes \Big[(r_{h_1}r_{h_2} + r_{0_1}r_{0_2})(|\uparrow\uparrow\rangle + |\downarrow\downarrow\rangle) + (r_{h_1}r_{0_2} + r_{0_1}r_{h_2})(|\uparrow\downarrow\rangle + |\downarrow\uparrow\rangle)\Big]/4 \\ &+ \mathrm{i}|V\rangle \otimes \Big[(r_{h_1}r_{h_2} - r_{0_1}r_{0_2})(|\uparrow\uparrow\rangle - |\downarrow\downarrow\rangle) + (r_{h_1}r_{0_2} - r_{0_1}r_{h_2})(|\uparrow\downarrow\rangle - |\downarrow\uparrow\rangle)\Big]/4, \end{aligned} \tag{5.24}$$

where r_{h_i} and r_{0_i} are the reflection coefficients for the hot and cold cavity interactions for system i, respectively. Let us consider the use of a photon with frequency ω such that $\tilde{\phi}_1 = -\tilde{\phi}_2$, where $\tilde{\phi}_i = \arg(r_{h_i}/r_{0_i})$ is the difference in the phase shifts for spin system i, and assume $|r_{h_i}| = |r_{0_i}| = 1$ for now. Therefore, we see that the detection of an orthogonally polarised photon, in this case $|V\rangle$, would maximally entangle the spins by projecting them onto the state $(|\uparrow\downarrow\rangle - |\downarrow\uparrow\rangle)/\sqrt{2}$. Similarly, one may choose to tune the

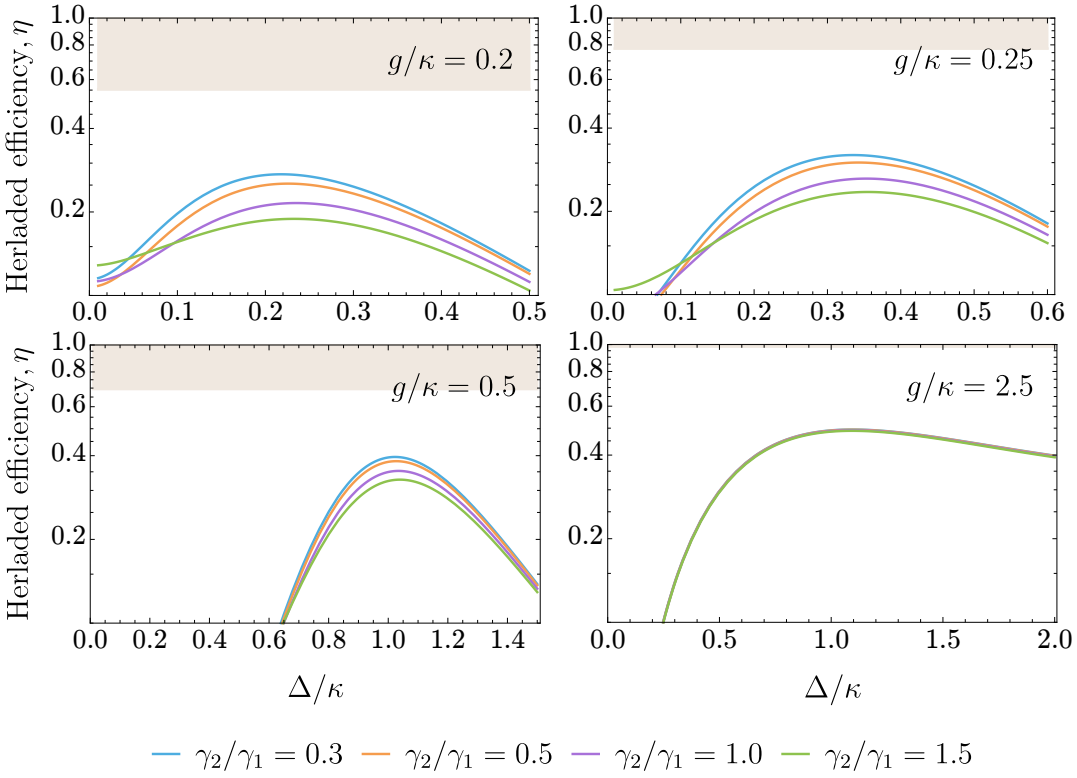

Figure 5.7: The heralded efficiency, η, of the entanglement generation scheme as a function of Δ/κ, where $\Delta = \omega_{X_1^-} - \omega_{X_2^-}$ is the characteristic energy detuning. We consider here different linewidth ratios, γ_2/γ_1, as well as various coupling strengths, g/κ, with $\gamma_1/\kappa = 0.1$ throughout. The shaded region indicates the maximum possible efficiency in the ideal case, i.e., when considering spectrally identical emitters.

photonic frequency such that $\tilde{\phi}_1 = \tilde{\phi}_2$, in order to probabilistically generate the entangled state $(|\uparrow\uparrow\rangle - |\downarrow\downarrow\rangle)/\sqrt{2}$.

Given that the success of this protocol is now probabilistic, we define the efficiency η of this entangling procedure to be the probability of measuring an orthogonally polarised photon, which consequently heralds the entanglement between the spin systems. We will limit our analysis to the case of $\tilde{\phi}_1 = -\tilde{\phi}_2$. This is because for quantum dot systems exhibiting typical spectral variations, this condition would result in $\tilde{\phi}_i$ approaching more closely $\pm\pi/2$, resulting in a stronger Faraday rotation and therefore maximising the probability of measuring an orthogonally polarised photon. The expression for the efficiency is then given by

$$\eta = \mathrm{Tr}\left[\left(|V\rangle\langle V| \otimes \mathbb{1}\right)\rho\right] = \frac{|r_{h_1}r_{h_2} - r_{0_1}r_{0_2}|^2 + |r_{h_1}r_{0_2} - r_{0_1}r_{h_2}|^2}{2^3}, \tag{5.25}$$

where ρ is the post-interaction state as defined in Eq. (5.24) and $\mathbb{1}$ is the identity operator acting on the two-spin sub-system.

We note at this point that we no longer make the assumption that $|r_{h_i}| \to 1$ in our calculations: we are now considering ranges for the detuning of the photonic frequency,

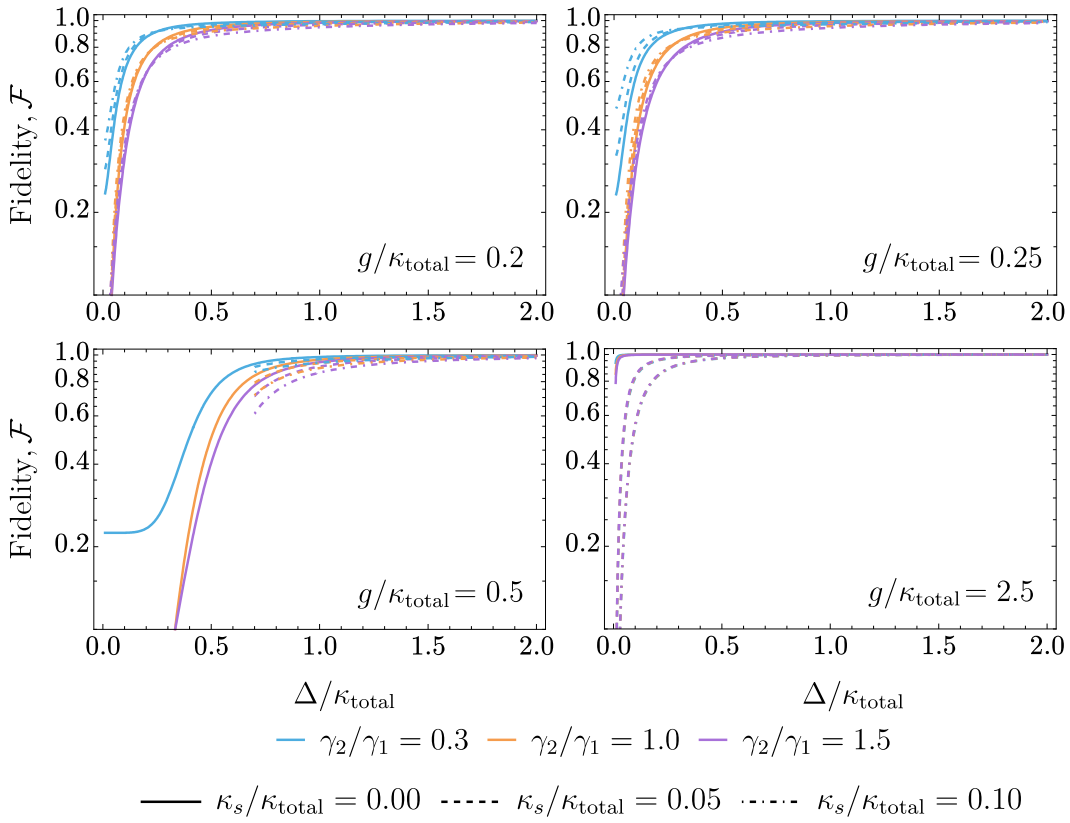

Figure 5.8: The fidelity, $\mathcal{F}$, of the entanglement generation scheme as a function of $\Delta/\kappa_{\text{total}}$, where $\Delta = \omega_{X_1^-} - \omega_{X_2^-}$ is the central energy detuning and $\kappa_{\text{total}} = \kappa + \kappa_s$. The linewidth ratio, γ_2/γ_1, is set to 0.3 (blue), 1.0 (orange) and 1.5 (purple); the cavity loss rate, κ_s/κ is set to 0.0 (solid), 0.2 (dashed) and 0.5 (dash-dotted); $\gamma_1/\kappa_{\text{total}} = 0.1$ throughout.

δ, where reflection off the hot cavity is no longer necessarily perfect due to potentially destructive interference effects and $|r_{h_i}| < 1$ for $\delta \approx g$. We must therefore also consider the effect of these losses, together with potential leakage losses κ_s, on the fidelity of the heralded entangled state. We define the fidelity to be

$$\mathcal{F} = |\langle\psi_{\text{ideal}}|\psi\rangle|^2 = \frac{|r_{h_1}r_{0_2} - r_{0_1}r_{h_2}|^2}{|r_{h_1}r_{h_2} - r_{0_1}r_{0_2}|^2 + |r_{h_1}r_{0_2} - r_{0_1}r_{h_2}|^2}, \tag{5.26}$$

where $|\psi_{\text{ideal}}\rangle = (|\uparrow\downarrow\rangle - |\downarrow\uparrow\rangle)/\sqrt{2}$ is the maximally entangled state that we wish to prepare, whilst $|\psi\rangle$ is the actual state heralded by the detection of photon $|V\rangle$.

In Figs 5.7 and 5.8 we show the efficiency η and fidelity $\mathcal{F}$, respectively, of the entangling procedure as a function of the characteristic energy detuning, $\Delta = \omega_{X_1^-} - \omega_{X_2^-}$. We consider here various coupling strengths g, and show that the adapted scheme may be employed both in the weak and the strong coupling regime. The efficiency η increases with increasing Δ until peaking at around 40–50% of the efficiency in the ideal case. Indeed, in the non-ideal case, $\tilde{\phi}$ approaches close to $\pm\pi/2$ once the two spin systems are sufficiently dissimilar, maximising the probability of heralding an entangled spin system. We also consider the

effect of variations in the linewidths between the two quantum dots, which may marginally enhance the efficiency for small enough values of g. The fidelity of the resulting state goes to unity for large Δ. This is because, for sufficiently detuned systems, we find that $|r_{h_i}| \approx |r_{0_i}|$ both in the lossless and lossy cases. This effectively cancels out the contributions of the $|\uparrow\uparrow\rangle$ and $|\downarrow\downarrow\rangle$ states and results in a high fidelity projected state.

We add a final comment on the decoherence time of the spin, T_2, as a source of limitation when it comes to the physical implementation of the syndrome extraction protocol. The coherent superposition of the spin states decays over time primarily due to nuclear spin interactions, with current experimental values for T_2 ranging from several ns [185–187] to around 100 ns [188]. The probability of measuring the spin state in its initial state decays by a factor of $\exp(-t/T_2)$, resulting in a reduction in the fidelity by a factor of $(1 + \exp[-t/T_2])/2$. In the case of a scheme making use of a single quantum dot, t would be the total time for the four photons to interact with the spin system. Current experimental demonstrations of exciton photons in micropillars show lifetime values of a few hundred ps [189–191], depending on the emitter–cavity detuning. Increasing the qubit register to n spin systems results in a reduction in fidelity by a factor of $(1 + \exp[-nt/T_2])/2$. Therefore, the reduction in fidelity remains the same as the register size is changed as n is inversely proportional to the total interaction time t.

5.8 Summary

In conclusion, we have shown that the spin–photon interface can be employed in quantum error correction to perform syndrome extraction and works well when considering less-than-ideal conditions. We consider a physical setup consisting of a micropillar cavity coupled to a quantum dot, and make use of the resulting optical circular birefringence and Faraday rotation in order to perform stabilizer measurement on the photonic data qubits. Working on the edge of the strong-coupling regime, we also show viability of the scheme by demonstrating the robustness over the detuning δ for coupling strengths g routinely reached experimentally. This gives evidence to the scheme working well even when accounting for possible imperfections, which are likely to occur during the physical implementation.

Furthermore, we consider the possibility of utilising entangled spin qubits, since increasing the register of the measure qubits might prove to be more useful in terms of resources, accommodates for spectral differences amongst data qubits, and allows for flexibility in the connectivity of the code [192, 193]. This setup may also prove to be more resource efficient when it comes to physical implementation of surface codes tailored for biased noise [194–196]: here, Hadamard transformations are applied to some of the Pauli matrices constituting the stabilizer operators. Finally, we show how entanglement generation is possible for spin systems with different characteristic energies both in the weak- and strong-coupling regimes, with high fidelity levels albeit with lower generation efficiency.

CHAPTER

6

TUNING THE PHOTONIC OUTPUT FROM A NANOCAVITY DEVICE

In this chapter, we will be studying the photon transmission and statistics resulting from the interaction of the field with a two-level system, or quantum emitter, embedded in a waveguide-based structure. The quantum emitter is positioned within a cavity that supports two orthogonal modes that in turn couple to waveguides. We will apply the input-output formalism to derive the single- and two-photon scattering matrices. This allows us to study the transport properties of the photons due to the light–matter interaction and the nonlinearity that arises from two-photon scattering. Furthermore, we will be considering its potential as a single-photon source by studying the photon statistics as a function of the frequency detuning for a weak coherent state.

6.1 Background and motivation

The objective behind the development of photonic-based nanostructures is to integrate these individual components within more extensive quantum optical networks. Elements necessary for the physical implementation of nanophotonic quantum technologies include chiral spin–photon interfaces, single-photon sources and optical nonlinearities to mediate photon–photon interactions. Waveguide-based architectures are advantageous in their scalability, robustness and capability to support tunable light-matter interaction. The device we study in this chapter is designed with the intent of serving as a chiral[1] interface, whereby the field transmission is unidirectional, whilst enhancing the interaction with an embedded quantum emitter [197]. This enhancement may be expressed in terms of the Purcell factor [36], which is defined to be the factor increase (or decrease) in the quantum

[1] We remind the reader that the use of the word "chiral" in this context is not meant to imply any true chirality within the physical structure of the setup, as discussed in Sec. 3.6.2. Here, the unidirectional behaviour stems purely from interference effects.

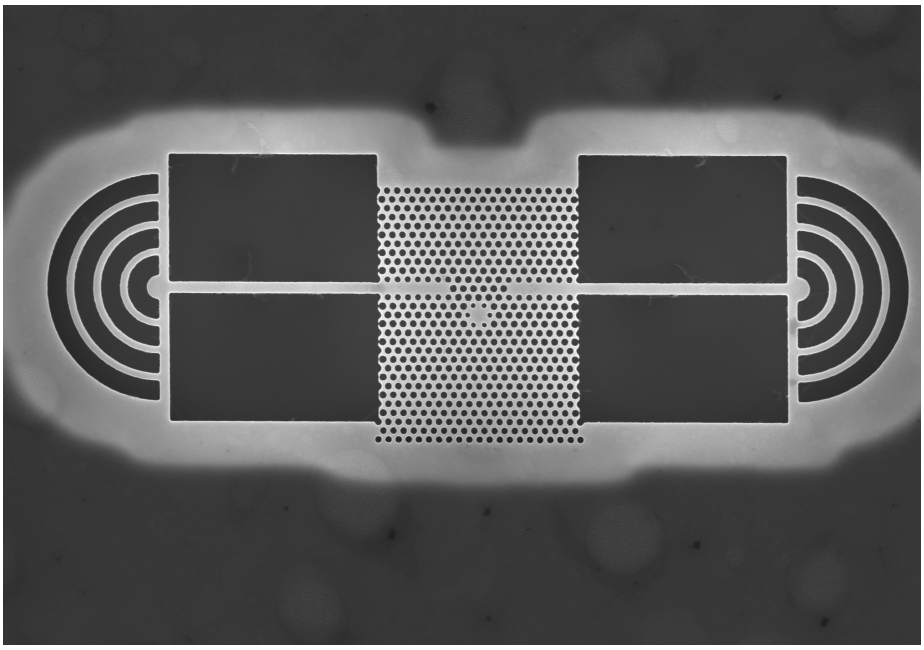

Figure 6.1: A SEM image of the device being modelled, comprising of an H1 photonic crystal cavity adjacent to two W1 waveguides. Image courtesy of Low Dimensional Structures and Devices, University of Sheffield.

system's spontaneous emission rate due to modifications in its environment. This may be improved by increasing the local density of states [61] via, e.g., engineering slow-light photonic modes [198, 199]. High Purcell factors are also desirable due to the resulting improvement in coupling efficiency [200]. Furthermore, this setup may serve as a switch, comparable to a transistor, with the transmission of a photon modulated by the presence, or absence, of a suitable control photon.

The physical system we shall be studying is comprised of a two-level system (TLS), physically realised by a quantum emitter, positioned within a photonic crystal cavity, with the latter coupled to two semi-infinite waveguides, as shown schematically in Fig. 3.3. We also show an SEM image of the fabricated device in Fig. 6.1. Advantages of using photonic crystal cavities include the possibility of achieving high Purcell factors, as demonstrated experimentally [201, 202], and efficient coupling to waveguides [203–205]. The cavity supports two orthogonal modes [206], χ and ψ, and the degeneracy is slightly lifted by the presence of the waveguides,[2] retaining some overlap between the linewidths of the two cavity modes. Furthermore, each cavity mode couples independently to the waveguides. We first consider the individual excitation of the cavity modes, in the absence of a quantum emitter. In this case, the x and y components of the two fields away from the cavity center will be either symmetric or anti-symmetric, as shown in Fig. 6.2. This results in fields that are in antiphase and would destructively interfere in one of the waveguides; the cavity, therefore,

[2] In practice, the fabricated cavity possesses some imperfections and asymmetries that lead to non-degeneracy between the modes even in the absence of the waveguides.

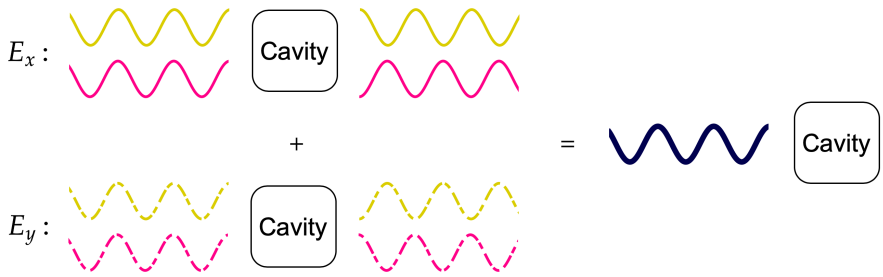

Figure 6.2: On the left, we show the decomposition of the χ (yellow) and ψ (pink) cavity modes in the absence of a quantum emitter. We denote the x and y components of the electric field by E_x (solid curves) and E_y (dotted curves), respectively. Here, the fields are all in phase in the left waveguide and in antiphase in the right waveguide. On the right, the cavity effectively transmits in one direction only due to the arising interference effects.

would effectively transmit in only one direction, as is required from a component within a chiral optical setup.

Next, suppose we wish to make use of the quantum emitter's optical transition in order to excite the two resonant modes concurrently. Making use of the dipole approximation, we may assume that the quantum emitter can be modelled as a superposition of dipoles with varying orientations [206]. Here we assume a circularly polarised dipole transition which can be described by a superposition of two orthogonally oriented dipoles with a relative phase of $\pm\pi/2$, depending on the handedness. Furthermore, each dipole excites only one of the cavity modes upon emission. In this case, emission from a circularly polarised dipole would lead to a phase difference of $\pm\pi/2$ between the field components of the χ and ψ modes within the waveguides. Therefore, the presence of an emitter hinders perfect destructive interference. However, we can make use of additional phase differences resulting from the interaction between the emitter and the non-degenerate cavity modes in order to re-establish unidirectional transmission [197].

6.2 Physical system

We start by defining the Hamiltonian for the system: specifically, we consider first the terms relating to the two semi-infinite waveguides. Setting $\hbar = 1$ and assuming a single cavity mode, the Hamiltonian for a cavity directly coupled to two semi-infinite waveguides may be expressed in the real-space basis by [66]

$$\begin{aligned} H = &\int \mathrm{d}x \left[a^\dagger(x)\left(-\mathrm{i}v_g\partial_x\right)a(x) + b^\dagger(x)\left(\mathrm{i}v_g\partial_x\right)b(x)\right] \\ &+ \int \mathrm{d}x\, \delta(x)\left[\tilde{V}_a a(x) + \tilde{V}_b b(x)\right] c^\dagger e^{\mathrm{i}\phi\theta(x)} + \mathrm{H.c.} \\ &+ H_{\mathrm{cavity}}. \end{aligned} \tag{6.1}$$

Here, v_g is the group velocity, assuming a linear dispersion relation around the central wavenumber;[3] c is the cavity mode operator; $\tilde{V}_i$ is the coupling strength between the cavity and waveguide mode i ($i = a, b$); and H_{cavity} is the Hamiltonian of the cavity system. In the case of a single infinite waveguide, the operator $a(x)$ [$a^\dagger(x)$] annihilates (creates) a right-moving photon at position x, and the operator $b(x)$ corresponds similarly to a left-moving photon [207]. Here, the waveguiding paths have been "folded over" as a result of modifying the operators by means of a canonical transformation such that $a(x)$ [$b(x)$] annihilates a photon in the left (right) waveguide, with $x < 0$ for an incoming photon and $x > 0$ for an outgoing one. The phase shift gained by the photon upon reflection off the cavity is given by ϕ and $\theta(x)$ is the switch-on function, such that $\lim_{x\to-\infty}\theta(x) = 0$ and $\lim_{x\to+\infty}\theta(x) = 1$ within a short spatial range. We will adopt the Heaviside step function, but the specific form of the function has no bearing on the derivation.

We wish to study the transport properties of the system in frequency space, and we therefore need to transform the Hamiltonian in Eq. (6.1). We first apply the following Fourier transforms on the bosonic operators

$$a(x) = \frac{1}{\sqrt{2\pi}}\int_{-\infty}^{+\infty} \mathrm{d}k\, a(k)\, e^{\mathrm{i}kx} \qquad \text{and} \qquad a^\dagger(x) = \frac{1}{\sqrt{2\pi}}\int_{-\infty}^{+\infty} \mathrm{d}k\, a^\dagger(k)\, e^{-\mathrm{i}kx}, \tag{6.2}$$

and similarly for $b(x)$ and $b^\dagger(x)$. We then change from a momentum basis to a frequency basis by assuming a linear dispersion relation with $\omega = v_g k$ ($\omega = -v_g k$) for the left (right) waveguides and defining the mode operators by $a(\omega) = a(k)/\sqrt{v_g}$ and $b(\omega) = b(k)/\sqrt{v_g}$ [81].

The above can be easily generalised to two cavity modes. Furthermore, we do not need to consider the Hamiltonian of the cavity system in real space as it would not be affected by the transformation of the bosonic mode operators. The total Hamiltonian of the system in frequency space may therefore be expressed as

$$\begin{aligned} H = &\int \mathrm{d}\omega\, \omega \left[a^\dagger(\omega)\, a(\omega) + b^\dagger(\omega)\, b(\omega)\right] + \frac{\omega_e \sigma_z}{2} + \sum_j \omega_j c_j^\dagger c_j \\ &+ \sum_j \left\{ g_j c_j \sigma_+ + \int \mathrm{d}\omega \left[V_{a,j} a(\omega) + V_{b,j} b(\omega) \right] c_j^\dagger \right\} + \text{H.c.}, \end{aligned} \tag{6.3}$$

where $a(\omega)$ and $b(\omega)$ are the mode operators for the left and right waveguides with frequency ω, respectively; ω_e is the transition frequency of the TLS with raising operator $\sigma_+ = |e\rangle\langle g| = \sigma_-^\dagger$ and $\sigma_z = 2\sigma_+\sigma_- - \mathbb{1}$; and c_j is the cavity mode operator with resonance frequency ω_j ($j = \chi, \psi$). The second line of the equation describes the interaction part of the Hamiltonian, with the TLS coupling to cavity mode j with strength g_j, and waveguide modes a and b coupling to cavity mode j with rates $V_{a,j}$ and $V_{b,j}$, respectively. Note that we have absorbed the phase factor resulting from the reflection off the cavity in the real space description into the coupling strength, such that $V_j e^{\mathrm{i}\phi/2} \to V_j$. The actual value of ϕ has no effect on the photon transport properties.

[3] This is valid for photons with sufficiently narrow bandwidths.

Parameter	Value	Notes
Mode resonant wavelength	$\lambda_\chi = 922.9\,\mathrm{nm}$ $\lambda_\psi = 921.9\,\mathrm{nm}$	$\omega = 2\pi c/\lambda$
Quantum emitter wavelength	$\lambda_e = 924.5\,\mathrm{nm}$	
Quality factor	$Q_\chi = 1600$ $Q_\psi = 700$	$V = \sqrt{\kappa/2\pi} = \sqrt{\frac{\omega/2Q}{2\pi}}$
Coupling strength	$g_\chi = 2\pi \cdot 10\,\mathrm{GHz}$ $g_\psi = 2\pi\mathrm{i} \cdot 10\,\mathrm{GHz}$	Within the typical range of values found in the literature, e.g. [208]

Table 6.1: Parameters used in Fig. 6.3. The cavity mode resonances and the quality factors have been obtained from FDTD (finite-difference time-domain) simulations [197].

6.3 Single-photon scattering

We start off by considering the scattering matrix elements for the scattering of a single photon. We derive this by making use of the Heisenberg equations of motion and the input-output formalism, as discussed in Sec. 3.4. This gives us the following set of input-output relations:

$$\begin{aligned} a_{\mathrm{out}}(t) &= a_{\mathrm{in}}(t) - \sqrt{2\pi}\mathrm{i}\sum_j V_{a,j}^* c_j(t)\,, \\ b_{\mathrm{out}}(t) &= b_{\mathrm{in}}(t) - \sqrt{2\pi}\mathrm{i}\sum_j V_{b,j}^* c_j(t)\,, \end{aligned} \tag{6.4}$$

where $\left[\mu_{\mathrm{in}}(t), \nu_{\mathrm{in}}^\dagger(t')\right] = \delta_{\mu\nu}\delta(t-t')$ for $\mu,\nu = a,b$. We also obtain the following system of coupled partial differential equations:

$$\begin{aligned} \partial_t c_j(t) &= -\mathrm{i}\omega_j c_j(t) - \mathrm{i}g_j^*\sigma_-(t) - \mathrm{i}\sum_{\mu=a,b} V_{\mu,j}\left[\sqrt{2\pi}\mu_{\mathrm{in}}(t) - \pi\mathrm{i}\sum_{k=\chi,\psi} V_{\mu,k}^* c_k(t)\right], \\ \partial_t \sigma_-(t) &= -\mathrm{i}\omega_e\sigma_-(t) + \mathrm{i}\sum_j g_j c_j \sigma_z(t)\,. \end{aligned} \tag{6.5}$$

The single-photon scattering matrix $S_{\mu,\nu}(p,k) = \langle p_\mu^- | k_\nu^+\rangle$ is the probability amplitude associated with a single incoming photon with frequency k in waveguide $\nu \in \{a,b\}$ scattering into waveguide $\mu \in \{a,b\}$ and obtaining the frequency p [81]. By making use of the input-output relations and solving the system of differential equations defined above by means of Fourier transformations, we obtain the expression

$$\begin{aligned} \langle p_\mu^- | k_\nu^+\rangle &\equiv \langle 0|\mu_{\mathrm{out}}(p)\,\nu_{\mathrm{in}}^\dagger(k)\,|0\rangle \\ &= \left\{\delta_{\mu\nu} - \sum_{\substack{i,j=\chi,\psi \\ i\neq j}} \frac{V_{\mu,i}^*}{A_i(p)\,A_j(p) - B_i(p)\,B_j(p)}\left[V_{\nu,i}A_j(p) + V_{\nu,j}B_j(p)\right]\right\}\delta(p-k) \\ &\equiv t_{\mu,\nu}(p)\,\delta(p-k)\,, \end{aligned} \tag{6.6}$$

where p, k are the frequencies of the outgoing and incoming photons, respectively, and where we define

$$A_j(p) = -\mathrm{i}(p - \omega_j) + \frac{\mathrm{i}|g_j|^2}{p - \omega_e} + \pi\left(|V_{a,j}|^2 + |V_{b,j}|^2\right) \tag{6.7a}$$

and

$$B_j(p) = \frac{-\mathrm{i}g_i^* g_j}{p - \omega_e} - \pi\left(V_{a,i}V_{a,j}^* + V_{b,i}V_{b,j}^*\right) \quad \text{with} \quad i \neq j. \tag{6.7b}$$

The expression obtained in Eq. (6.6) consists of two parts. The first term comprises the Kronecker delta $\delta_{\mu\nu}$ and represents the contribution to the scattering due to reflection off the cavity, whilst neglecting any coupling to the cavity modes. The second term represents the contribution to the final state $|p_\mu^-\rangle$ from the coupling of the input photon in the initial waveguide to the cavity modes as well as the two-level system. The scattering amplitude also contains a Dirac delta function which imposes conservation of energy such that the frequencies of the incoming and outgoing photons are equal.

In Fig. 6.3 we show the transmission for a single photon incoming from the left waveguide and exiting through the right, making use of the parameters defined in Table 6.1. The theoretical result is in very strong agreement with numerical simulations obtained by means of FDTD simulations, with the former being advantageous due to its convenient analytical form and offering deeper insight into the interference mechanism. We note here that a phase of π is added to the value of $V_{a,\chi}$ in order to model the relative phases observed in the field as it couples from the cavity to either waveguide. Similarly, the relative phase of $\pi/2$ between the two values of the coupling strength, g_χ and g_ψ, is attributed to the manner in which a circularly polarised dipole couples to a phase delayed superposition of the two cavity modes.

6.4 Two-photon scattering

In this section we will be considering the resulting scattering event for two co-propagating photons as they are transmitted through this setup. The TLS induces optical non-linearities at the few photon level due to its rapid saturation at very low incident powers [78,209]. By extending the analysis in the previous section to two photons, we can observe the emergence of this behaviour.

We start by considering the corresponding scattering matrix, given by

$$\begin{aligned} &S_{\mu_1,\mu_2,\nu_1,\nu_2}(p_1, p_2, k_1, k_2) \\ &\quad = \langle p_{1,\mu_1} p_{2,\mu_2}^- | k_{1,\nu_1} k_{2,\nu_2}^+ \rangle \\ &\quad = \langle p_{1,\mu_1}^- | \mu_{2,\mathrm{in}}(p_2) | k_{1,\nu_1} k_{2,\nu_2}^+ \rangle - \sqrt{2\pi}\mathrm{i} \sum_{j=\chi,\psi} V_{\mu_2,j}^* \langle p_{1,\mu_1}^- | c_j(p_2) | k_{1,\nu_1} k_{2,\nu_2}^+ \rangle, \end{aligned} \tag{6.8}$$

with $|k_{i,\nu_i}^+\rangle = \nu_{i,\mathrm{in}}^\dagger(k_i)|0\rangle$, with $i = 1, 2$, and $|p_{1,\mu_1}^-\rangle = \mu_{1,\mathrm{out}}^\dagger(p_1)|0\rangle$, as was similarly defined in the single-photon case. We can solve the expression by considering the single-photon

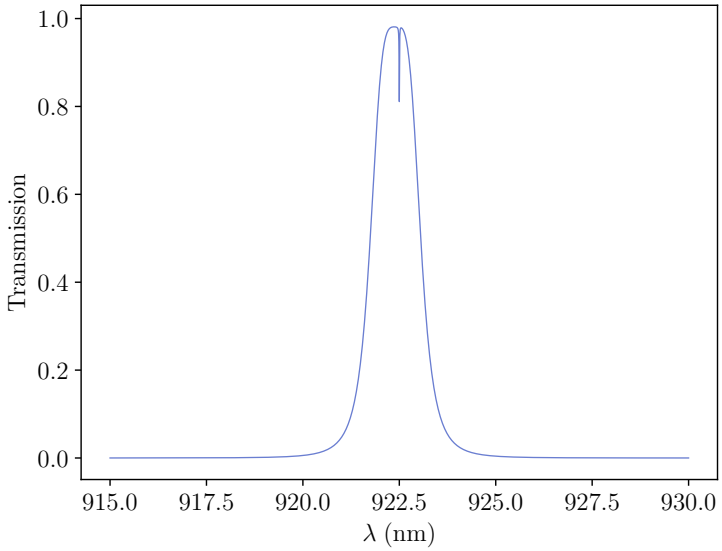

Figure 6.3: Single-photon transmission through the waveguide-cavity system as a function of the photonic wavelength, λ, with the field incoming from the left and outgoing to the right. We make use of the parameters defined in Table 6.1.

scattering matrix and the set of coupled differential equations, giving us the following:

$$\begin{aligned} &S_{\mu_1,\mu_2,\nu_1,\nu_2}\left(p_1,p_2,k_1,k_2\right) \\ &\quad = S_{\mu_1,\nu_1}\left(p_1,k_1\right) S_{\mu_2,\nu_2}\left(p_2,k_2\right) + S_{\mu_1,\nu_2}\left(p_1,k_2\right) S_{\mu_2,\nu_1}\left(p_2,k_1\right) \\ &\quad\quad + B_{\mu_1,\mu_2,\nu_1,\nu_2}\left(p_1,p_2,k_1,k_2\right) \delta\left(p_1+p_2-k_1-k_2\right). \end{aligned} \tag{6.9}$$

The first two terms on the right-hand side of the equation represent the linear contribution of the interaction, whereby the individual frequencies of either photon is maintained post-scattering, and are simply the product of two single-photon scattering events. The last term is the so-called bound state term[4] [210–212]: this describes the non-linear part of the interaction as well as spectral and directional correlations between the two photons. The nature of these correlations depends on the initial spectral wavepacket of the photonic input state.

We assume an initial optical state with two photons co-propagating in the left waveguide towards the right, given by

$$|\Psi\rangle = \frac{1}{\sqrt{2}} \int \mathrm{d}k_1\, \mathrm{d}k_2\, \xi_{\mathrm{Gaus}}\left(k_1\right) \xi_{\mathrm{Gaus}}\left(k_2\right) a_{\mathrm{in}}^{\dagger}\left(k_1\right) a_{\mathrm{in}}^{\dagger}\left(k_2\right) |0\rangle\,, \tag{6.10}$$

with the wavepacket normalised such that $\int \mathrm{d}k_1\, \mathrm{d}k_2\, |\xi_{\mathrm{Gaus}}\left(k_1\right) \xi_{\mathrm{Gaus}}\left(k_2\right)|^2 = 1$ and with a Gaussian distribution given by

$$\xi_{\mathrm{Gaus}}\left(k\right) = \frac{1}{\left(\pi\sigma'^2\right)^{1/4}} \exp\left[\frac{-\left(k-k_0\right)^2}{2\sigma'^2}\right], \tag{6.11}$$

[4]Here we omit the explicit expression for the bound state term due to its convoluted form for this particular system. We give a more detailed explanation for this in App. B.

where k_0 is the central frequency of the wavepacket, $\sigma' = \sigma/\left(2\sqrt{\ln 2}\right)$ where σ is the spectral full width at half maximum, and the two photons have identical central frequencies and spectral widths, such that $\xi(k_1, k_2) = \xi(k_2, k_1)$. The two photons are assumed to be uncorrelated as their wavepacket factorizes into the product of two single photons. However, this need not necessarily be the case. For example, one could consider a biphoton state produced by parametric down conversion, resulting in two photons that are correlated in their frequencies and wavevectors [213].

Given the definition of the scattering matrix and the symmetric wavefunction, the optical state post-scattering is given by

$$|\Psi\rangle = \frac{1}{2\sqrt{2}} \sum_{\mu_1,\mu_2=a,b} \int \mathrm{d}k_1\, \mathrm{d}k_2\, \tilde{\xi}_{\mu_1,\mu_2}(k_1, k_2)\, \mu_{1,\mathrm{out}}(k_1)\, \mu_{2,\mathrm{out}}(k_2)\, |0\rangle\,, \tag{6.12}$$

where $\tilde{\xi}_{\mu_1,\mu_2}(k_1, k_2)$ is the post-scattering wavefunction given by

$$\begin{aligned} \tilde{\xi}_{\mu_1,\mu_2}(k_1, k_2) = {} & 2\, t_{\mu_1,a}(k_1)\, t_{\mu_2,a}(k_2)\, \xi(k_1, k_2) \\ & + \int \mathrm{d}p\, B_{\mu_1,\mu_2,\nu_1,\nu_2}(k_1, k_2, p, k_1 + k_2 - p)\, \xi(p, k_1 + k_2 - p)\,. \end{aligned} \tag{6.13}$$

We can therefore determine the directional probability densities of the scattered photons as a function of the photonic frequencies from the resulting wavefunctions.

Here, the probability density for two photons scattering into the same waveguide is $|\tilde{\xi}_{\mu,\mu}(k_1, k_2)|^2/4$, with $\mu = (a, b)$, and that for each photon scattering into a different waveguide is $|\tilde{\xi}_{a,b}(k_1, k_2)|^2/2$. In Fig. 6.4 we show the spectra of the outgoing field for an initial Gaussian wavefunction with various linewidths. Here, we show the probability distribution for the transmission of both photons into the left or right waveguide as well as the probability of just one photon being scattered in the forwards direction. Moreover, we also show the effect of the non-linear term of the scattering interaction by setting the term to zero and then calculating the resulting probability densities for the counter-propagating output. We see that the linewidth of the incoming photonic wavefunction has an effect on the strength of the bound state term. This allows us to tune the amount of, say, directional entanglement of the scattered photons where mere linear effects would not be sufficient. Additionally, the cavity mode frequencies may be moderately tuned and, hence, provide additional degrees of freedom.

6.5 Second-order correlation function

The implementation of optics-based quantum technologies relies on the sourcing of non-classical light [214–216], including single-photon states [217, 218]. This has generated keen interest in the development of such sources, with particular focus on the use of classical coherent light as the input followed by some form of modification of its statistics. Methods of manipulation rely on interference effects, such as photon blockade [219–222] and the Fano effect [223]. Hence, we will now describe the photon statistics for the transmitted field in this device.

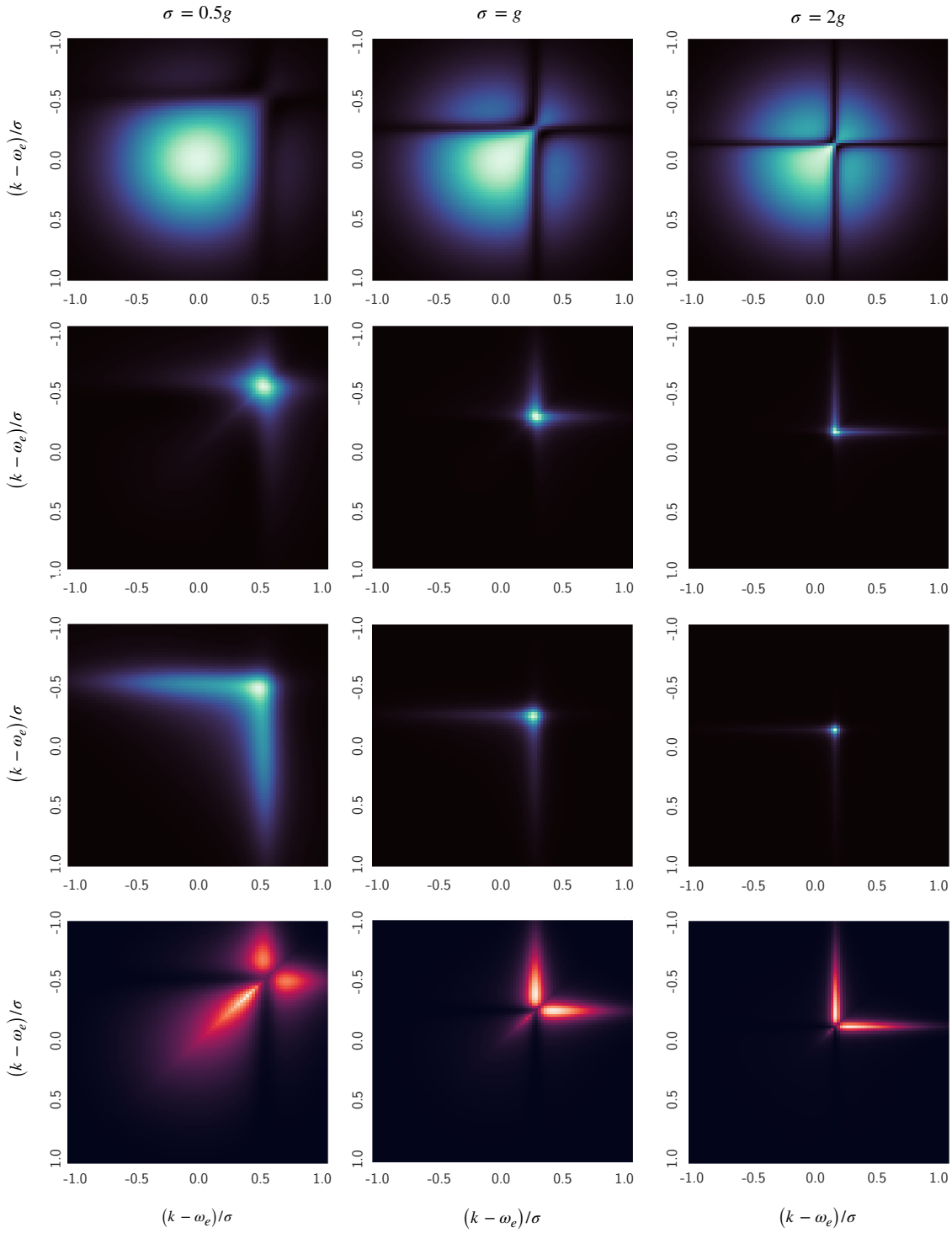

Figure 6.4: Probability densities for both photons exiting into the left waveguide (top row), counter-propagating photons (second row) and both photons exiting into the right waveguide (third row) as a function of frequency detuning for an initial Gaussian two-photon input state. We also show the effect of the bound state term on the transmission statistics of the counter-propagating photons by setting this to zero for the scattering interaction (bottom row). We vary the linewidth of the initial wavefunction, σ, across the columns (as labelled). We make use of the parameters defined in Table 6.1.

We use the normalised second-order correlation function to analyse the field transmitted into the right waveguide. This is an intensity correlation function showing the normalised probability of detecting a photon at time $(t+\tau)$ given a photon detected at time t, and is given by [224]

$$g^{(2)}(\tau) = \lim_{t\to\infty} \frac{\langle b^{\dagger}_{\text{out}}(t)\, b^{\dagger}_{\text{out}}(t+\tau)\, b_{\text{out}}(t+\tau)\, b_{\text{out}}(t)\rangle}{\langle b^{\dagger}_{\text{out}}(t)\, b_{\text{out}}(t)\rangle \langle b^{\dagger}_{\text{out}}(t+\tau)\, b_{\text{out}}(t+\tau)\rangle}, \tag{6.14}$$

where $t \to \infty$ indicates that the operators are taken to act in the asymptotic limit with the optical field having reached the steady state post-interaction. We take the expectation values to be those for a coherent state input in the left waveguide with

$$|\alpha_k^{+}\rangle = e^{-|\alpha_k|^2/2} \sum_{n=0}^{\infty} \frac{\left[\alpha_k a^{\dagger}_{\text{in}}(k)\right]^n}{n!} |0\rangle, \tag{6.15}$$

where $|\alpha_k|^2$ is the mean photon number and k is the frequency.

There exist a few methods to calculate the expression for $g^{(2)}$, including use of the quantum regression theorem [80, 225] and establishing coupled differential equations in terms of various expectation classes for the excitation operator [223, 226]. However, due to the indirect coupling between the waveguides and the TLS, the calculations are not tractable with these methods. Instead, we make the assumption of a weak coherent state [221, 227], with $\alpha_k \to 0$, which can be experimentally realised by a highly attenuated laser. From Eq. (6.14) we obtain

$$\lim_{\alpha_k\to 0} g^{(2)}(\tau) = \frac{\langle k_a k_a^{+}| b^{\dagger}_{\text{out}}(t)\, b^{\dagger}_{\text{out}}(t+\tau)\, b_{\text{out}}(t+\tau)\, b_{\text{out}}(t)\, |k_a k_a^{+}\rangle}{4\,\langle k_a^{+}| b^{\dagger}_{\text{out}}(t)\, b_{\text{out}}(t)\, |k_a^{+}\rangle \langle k_a^{+}| b^{\dagger}_{\text{out}}(t+\tau)\, b_{\text{out}}(t+\tau)\, |k_a^{+}\rangle}, \tag{6.16}$$

where $|k_a^{+}\rangle = a^{\dagger}_{\text{in}}(k)\,|0\rangle$ and $|k_a k_a^{+}\rangle = [a^{\dagger}_{\text{in}}(k)]^2\,|0\rangle$.

We can simplify further by taking the Fourier transform of the output operators and obtaining an expression in terms of the single- and two-photon scattering matrices:

$$\begin{aligned}
\lim_{\alpha_k\to 0} g^{(2)}(\tau) &= \frac{|\int \mathrm{d}p_1\, \mathrm{d}p_2\, S_{b,b,a,a}(p_1,p_2,k,k)\, e^{-\mathrm{i}p_2\tau}|^2}{4|t_{b,a}(k)|^4} \\
&= \frac{|2\, t^2_{b,a}(k)\, e^{-\mathrm{i}k\tau} + \int \mathrm{d}p\, B_{b,b,a,a}(p,2k-p,k,k)\, e^{-\mathrm{i}(2k-p)\tau}|^2}{4|t_{b,a}(k)|^4} \\
&= 1 + \frac{|\int \mathrm{d}p\, B_{b,b,a,a}(p,2k-p,k,k)\, e^{-\mathrm{i}(2k-p)\tau}|^2}{4|t_{b,a}(k)|^4} \\
&\quad + 2\,\mathrm{Re}\left(\frac{\int \mathrm{d}p\, B_{b,b,a,a}(p,2k-p,k,k)\, e^{-\mathrm{i}(k-p)\tau}}{t^2_{b,a}(k)}\right).
\end{aligned} \tag{6.17}$$

Setting the time delay to zero, $\tau = 0$, we can determine the degree of bunching ($g^{(2)}(0) > 1$) or antibunching ($g^{(2)}(0) < 1$) experienced by the outgoing field. Furthermore, given the form of Eq. (6.17), we can discern between the contributions to the correlation function from the bound state of the light–matter interaction and the interference effects

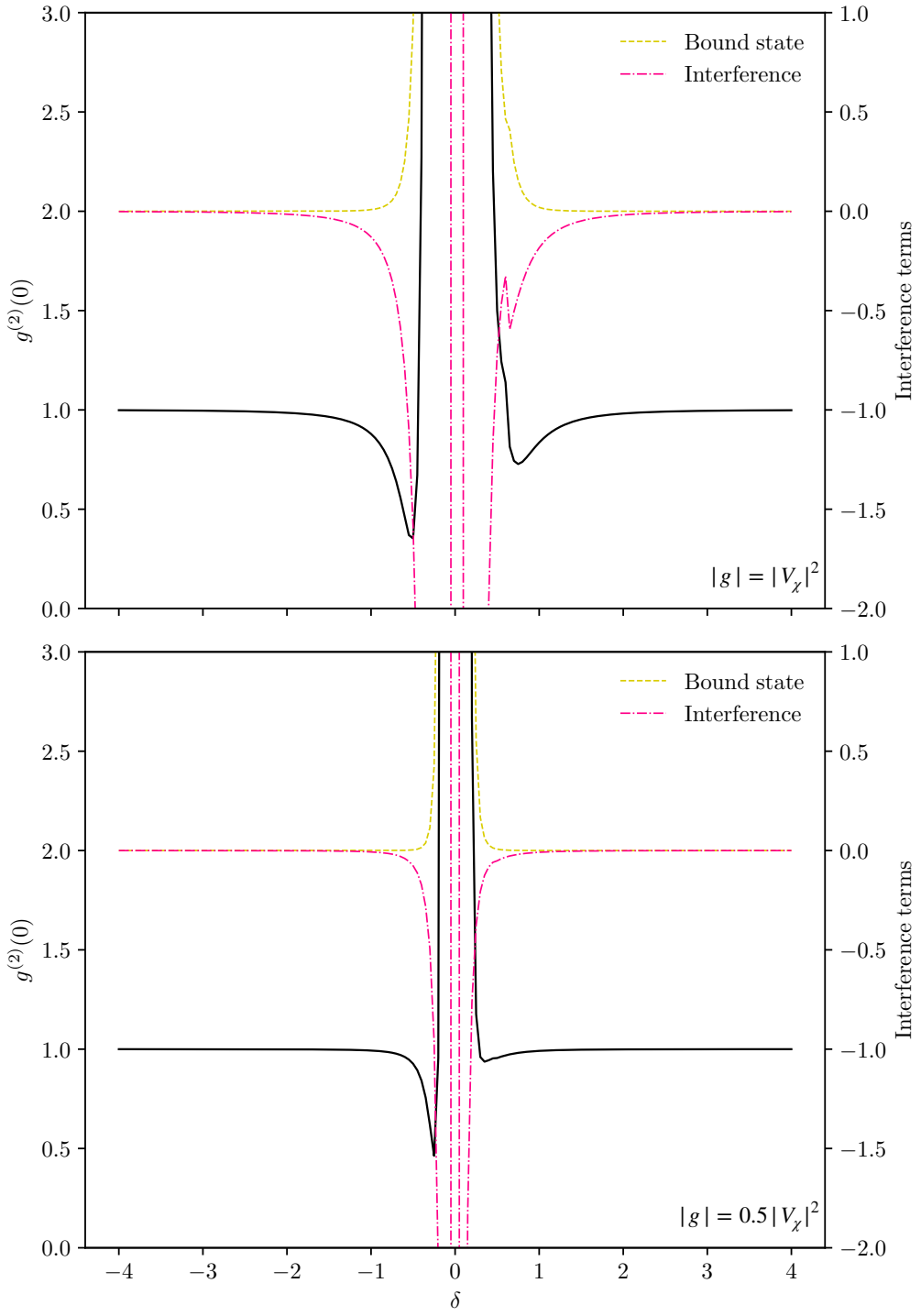

Figure 6.5: On the left axis, we show the second-order correlation function, $g^{(2)}(0)$, as a function of the normalised detuning, δ. Here, $\delta = (k - \omega_e)/|g|$, where $|g|$ is the absolute value of the coupling strength between the cavity modes and TLS. On the right axis, we show how the contributions from the bound state and interference terms affect the magnitude of the $g^{(2)}(0)$ and how antibunching is a result of the interference effects arising from the coupling within the device. We make use of the parameters defined in Table 6.1, and set (a) $|g| = |V_\chi|^2$ and (b) $|g| = 0.5|V_\chi|^2$.

that arise due to the relative phase between the various coupling terms [223]. These are given by the last two terms of the equation, respectively.

In Fig. 6.5 we show the correlation function at zero time delay, together with the contributions from the two effects, as a function of the normalised frequency detuning, δ, between the coherent source and the TLS transition frequency. Here, we set $\delta = (k - \omega_e)/|g|$, with $|g|$ being the absolute value of the coupling strength between either cavity mode and the TLS, and use the values specified in Table 6.1. We see that by tuning the detuning we may modify the statistics of the output field to vary between antibunched and bunched. Give that the bound state term is always positive, due to its form in Eq. (6.14), we can see how the effect of antibunching requires the destructive two-photon interference contribution. From the figures, one can observe how antibunching occurs at the points where the bound state term is small whilst the interference values are greater in magnitude and opposite in sign. These destructive effect in turn suppresses two-photon state transmission to the output in relation to the single-photon state, resulting in sub-Poissonian statistics of the outgoing optical state.

6.6 Summary

In conclusion, we have characterised the proposed setup by considering the scattering interaction at the few-photon level. Specifically, we first expressed the Hamiltonian for the system by considering the waveguide mode operators in the position basis. We also explained how the mechanism underlying the idea of chiral transport translates to the coupling terms within the Hamiltonian. Next, we derived the scattering matrix elements for a single- and two-photon input state by making use of the input-output formalism, which allows us to express the asymptotic output states resulting from the interaction. We showed the spectra of the scattered two-photon states that would result in this setup, and considered also the effect of the non-linear part of the interaction. In particular, we showed how the linewidth of initial photons determines the strength of this type of interaction. Finally, we considered the photon statistics for the transmitted field in the context of possible single-photon sources. By taking into account a weak coherent state, we expressed the second-order correlation function and showed how the relative detuning between the field and the emitter may be adjusted so as to cause antibunching effects at the output.

CHAPTER

7

CONCLUSION AND FUTURE WORK

7.1 Conclusion

This thesis has centred around the study and application of light–matter interactions in the context of quantum information processes. We particularly focus on systems consisting of photonic nanostructures and semiconductor quantum dots. This is motivated by the fact that the structures are well-suited as integral components in different types of photonic quantum technologies, as evidenced by the research and development in these fields. We will now summarise the work and results presented in this thesis.

We start by presenting an introduction to this thesis and providing context for how this work fits within the wider research field in Chapter 1. Next, in Chapter 2, we present the foundations of quantum mechanics, which underpins the theory used throughout, and discuss the mathematical description of the quantised electromagnetic field and some emergent photonic states. Finally, we discuss the concept of entanglement and how it is a resource in quantum technology, as well as quantum error correction in surface codes.

In Chapter 3, we give a detailed account of the theory of quantum optics and light–matter interaction that is used in our work. We start from the fundamentals by deriving the rudimentary Hamiltonian describing the interaction between an optical field and the charge of a two-level system, widely known as the Jaynes–Cummings model, and apply the rotating-wave approximation to allow for easier solutions. We generalise this Hamiltonian to a continuum of modes, as would be the case in a photonic waveguide, and consider its form in different bases and the inclusion of loss. We then present different approaches to the study of photon interaction: a wavefunction approach for a single photon and the scattering matrix technique, based on the input–output formalism, to describe the post-interaction state of multi-photon scattering.

We start by presenting original work and research in Chapter 4, where we study how

spectrally distinct solid-state emitters, specifically quantum dots, can be fully entangled by means of photon scattering. Fabricated quantum dots naturally show variations in their central energies and linewidths, making the process of deterministic entanglement a difficult one. However, we show how we can do this for two non-identical quantum dots by repeatedly scattering off photons at an optimal frequency. This builds up the amount of entanglement between them and is heralded by the measurement of the photons. We also consider how the scheme performs when introducing losses and deviation in the frequency away from the optimal. Most of the work assumes a single biphoton state as the input, and we hence account for the possibility of higher order photon states and show how the scheme remains successful when using photon-number resolving detectors.

In Chapter 5 we study how the spin–photon interface can be used to perform syndrome extraction for quantum error correction in surface codes. Specifically, we consider a quantum dot coupled to a micropillar cavity and use the arising property of birefringence to extract the syndrome of a set of qubits, which would give information about the location of possible errors. We consider a photonic implementation of the scheme and study how robust the confidence in the spin readout is to deviations of the relative frequency detuning from the optimal. The scheme may also be performed using entangled spin states in order to optimise for resource requirements. We therefore also study the generation of entanglement between spectrally dissimilar spin systems, providing the efficiency and fidelity as figures of merit.

Finally, in Chapter 6, we present work done on characterising and modelling an experimental device designed to be a component integrated within a wider quantum optical network, serving as a unidirectional emitter of light. We first start by describing the model and the derivation of its Hamiltonian, before making use of the input–output formalism and scattering matrix theory to describe the single- and two-photon scattering events. We study the strength of the arising non-linearity and its effects on the directionality of the photonic transmission. Finally, we consider the photon statistics for the proposed device. Assuming a weak coherent state in the form of a strongly attenuated laser, we show how the setup may induce anti-bunching of the transmitted photon at certain frequency detunings and approximates a possible single-photon source.

In conclusion, we have presented theoretical work that fits within the overarching theme of quantum information theory and light–matter interactions. We have considered physical systems (semiconductor quantum dots, photonic waveguides and cavities) that are actively researched by the experimental community and demonstrated their potential applications in quantum technology.

7.2 Future work

Naturally, the work we have studied and presented here is not fully exhaustive and there are several directions in which to take the work further. In this section we will outline a few possible ways of building on the research presented in the three work chapters.

For Chapter 4, it would be interesting to investigate further the entanglement of dissimilar quantum dots by considering, say, three or more such emitters embedded within

a generalised Mach-Zehnder interferometer. One may consider an optical input state that undergoes some unitary transformation before and after scattering, all of which can be physically implemented using only a combination of linear optical elements [228]. An obvious starting point is the quantum Fourier transform, which would give a photon distribution that is equal in magnitude across all output modes. The increase in the dimension of the spin Hilbert space allows for the generation of more useful and exotic entangled states, such as GHZ states. Given that the concurrence is applicable only for mixed states of two qubits, one would need to make use of alternative entanglement measures, e.g., concentratable entanglement [229, 230].

With regards to the work done in Chapter 5, one possible direction for future work is to consider the application of the micropillar cavity system to perform other families of measurements used in quantum error correction. These include, for example, lattice surgery used for the entangling of logical qubits [231,232] as well as the generation and measurement of cluster states for one-way, or measurement-based, quantum computing [233–235]. The physical setup considered in this work has also been proposed for Bell state analysis [158], and it would be interesting to see whether or not this could be generalised to measure amongst a broader class of two-qubit states and how well state teleportation could be performed starting with a less entangled state. Finally, another possible avenue is the study of its potential application in quantum entanglement purification schemes [53], especially for physical systems that differ in their spectral properties.

A clear direction for the work in Chapter 6 is to experimentally realise the variation in the photon number statistics of the transmitted field. The sufficiency of the theoretical model can be evaluated from the comparison to the experimental results, and any sources of error could be incorporated into the model. These might include short dephasing times, spectral wandering and broadening of the emitter linewidth. One could also study its potential application as a controlled-phase gate, where the phase shift induced by the interaction can be measured by means of homodyne detection. Finally, it would be interesting to consider how entanglement between various degrees of freedom may be generated using this device [236, 237]. One might consider using optical states at the input that are easily sourced in the lab or else expand the Hilbert space of the total system by increasing the number of emitters and cavity modes.

APPENDIX

A

CONCURRENCE TRAJECTORIES

Here, we present the Python code used to generate the concurrence trajectories of the two-spin state, generalised to account for the possibility of obtaining a mixed state.

```
from qutip import *
import numpy as np
import pylab as plt
import matplotlib.pyplot as plt
import math

a = basis(2, 0)
b = basis(2, 1)
c = basis(2, 0).dag()
d = basis(2, 1).dag()

# defining variables
Ea = 1.0
Eb = 4.0
Gammaa = 1.0  # typical range (0,2.5)\nu eV
ddelta = 2.0  # detuning between the two linewidths, Gammab=Gammaa+
    ddelta
Gammab = Gammaa + ddelta
# hw=((Eb*Gammaa)-(Ea*Gammab))/(Gammaa-Gammab)
hw = 0.5 * (Ea + Eb - math.sqrt((Ea - Eb) ** 2 - (Gammaa * Gammab)))
Delta1 = hw - Ea  # Delta1=(hbar*w1)-Ea in \nu eV
Delta2 = hw - Eb  # Delta2=(hbar*w2)-Eb in \nu eV
delta = Delta2 - Delta1
# to get equal frequencies, Delta1-Delta2+delta=0
beta = 1.0
gammaa=(Gammaa*(1.0-beta))/beta
```

```
gammab=(Gammab*(1.0-beta))/beta

# defining transmission coefficients
ta1 = (Delta1 - (1j * 0.5 * (Gammaa - gammaa))) / (Delta1 + (1j * (
    Gammaa + gammaa) * 0.5))
ta2 = (Delta2 - delta - (1j * 0.5 * (Gammaa - gammaa))) / (Delta2 -
    delta + (1j * (Gammaa + gammaa) * 0.5))
tb1 = (Delta1 + delta - (1j * 0.5 * (Gammab - gammab))) / (Delta1 +
    delta + (1j * 0.5 * (Gammab + gammab)))
tb2 = (Delta2 - (1j * 0.5 * (Gammab - gammab))) / (Delta2 + (1j *
    0.5 * (Gammab + gammab)))

# def tar(eea):
tar = (-1j * (Gammaa * gammaa) ** 0.5) / (Delta1 + (1j * 0.5 * (
    Gammaa + gammaa) ** 0.5))
#       return tar

# def tbr(eeb):
tbr = (-1j * (Gammab * gammab) ** 0.5) / (Delta2 + (1j * 0.5 * (
    Gammab + gammab) ** 0.5))
#       return tbr

# defining probability amplitudes post first interaction
# P20
a1 = (ta1 * ta2) + (ta2 * tb1) - (ta1 * tb2) - (tb1 * tb2)
a2 = (ta1 * ta2) + ta2 - ta1 - 1
a3 = 1 + tb1 - tb2 - (tb1 * tb2)
a4 = 0

# P02
a5 = (ta1 * ta2) - (ta2 * tb1) + (ta1 * tb2) - (tb1 * tb2)
a6 = (ta1 * ta2) - ta2 + ta1 - 1
a7 = 1 - tb1 + tb2 - (tb1 * tb2)
a8 = 0

# P11
a9 = (ta1 * ta2) - (ta2 * tb1) - (ta1 * tb2) + (tb1 * tb2)
a10 = (ta1 * ta2) - ta2 - ta1 + 1
a11 = 1 - tb1 - tb2 + (tb1 * tb2)
a12 = 0
a13 = (ta1 * ta2) + (ta2 * tb1) + (ta1 * tb2) + (tb1 * tb2)
a14 = (ta1 * ta2) + ta2 + ta1 + 1
a15 = 1 + tb1 + tb2 + (tb1 * tb2)
a16 = 4

#P10 & P01
a17 = ta1 * tar
a18 = tb1 * tbr
```

```
#P00
a19 = tar ** 2
a20 = tbr ** 2

# counters
x = 0
y = 0
i = 0
k = 0

plt.clf()

for x in range(40):  # no of trajectories
    # setting up initial density matrix
    phi = 0.5 * tensor(a + b, a + b)
    rhoq = phi * phi.dag()
    rho = rhoq.full()  # converting from Qobj() to array
    concurrences = np.array([])
    outcomes = np.array([])
    probabilities = np.array([])
    for y in range(30):  # no of iterations for a single trajectory
        # defining probabilities of 3 different detection events
        P20 = (rho[0, 0] * abs(a1) ** 2) + (rho[1, 1] * abs(a2) **
           2) + (rho[2, 2] * abs(a3) ** 2)
        P02 = (rho[0, 0] * abs(a5) ** 2) + (rho[1, 1] * abs(a6) **
           2) + (rho[2, 2] * abs(a7) ** 2)
        P11 = (rho[0, 0] * abs(a9 + a13) ** 2) + (rho[1, 1] * abs(
           a10 + a14) ** 2) + (
                rho[2, 2] * abs(a11 + a15) ** 2) + (rho[3, 3] * abs(
                   a12 + a16) ** 2)
        P10 = 8 * ((rho[0, 0] * abs(a17) ** 2) + (rho[1, 1] * abs(
           a17) ** 2) + (rho[0, 0] * abs(a18) ** 2) + (
                    rho[2, 2] * abs(a18) ** 2))
        P01 = 8 * ((rho[0, 0] * abs(a17) ** 2) + (rho[1, 1] * abs(
           a17) ** 2) + (rho[0, 0] * abs(a18) ** 2) + (
                rho[2, 2] * abs(a18) ** 2))
        P00 = 8 * ((rho[0, 0] * abs(a19) ** 2) + (rho[1, 1] * abs(
           a19) ** 2) + (rho[0, 0] * abs(a20) ** 2) + (
                rho[2, 2] * abs(a20) ** 2))
        # probabilities, normalized probabilities set as array
        # prob=np.array([P20,P02,P11,P10,P01,P00])
        # prob=np.array([P20+P10,P02+P01,P11,P00])
        prob = np.array([P20 + P10, P02 + P01, P11, P00,
                         (P20 + P10 + P02 + P01 + P11 + P00) * 0.05
                            / 0.95])  # for 2,2 detection events
        probn = np.array([((P20 + P10) / sum(prob)).real, ((P02 +
           P01) / sum(prob)).real, (P11 / sum(prob)).real,
                          (P00 / sum(prob)).real,
```

```
                    (((P20 + P10 + P02 + P01 + P11 + P00) *
                       0.05 / 0.95) / sum(prob)).real])
# probn=np.array([0,0,1,0,0])
# weighted random choice of outcome
outcomes = np.append(outcomes, np.random.choice(5, 1, p=
    probn))  # 0=P20+P10 1=P02+P01 2=P11 4=P00
if y == 50:  # to test effect of multiphoton state
    j = 10
else:
    j = int(outcomes[-1])  # set j as last outcome
    probabilities = np.append(probabilities, probn[j])
# obtain new density matrix
if j == 4:
    rho10 = (((rho[0, 0] * (b3) * (b3).conjugate() * tensor(
        a, a) * tensor(c, c)) + (rho[0, 1] * (b3) * (b4).
        conjugate() * tensor(a, a) * tensor(c, d)) + (rho[0,
        2] * (b3) * (b5).conjugate() * tensor(a, a) * tensor(
        d, c)) + (rho[0, 3] * (b3) * (b6).conjugate() *
        tensor(a, a) * tensor(d, d)) + (rho[1, 0] * (b4) * (
        b3).conjugate() * tensor(a, b) * tensor(c, c)) + (rho
        [1, 1] * (b4) * (b4).conjugate() * tensor(a, b) *
        tensor(c, d)) + (rho[1, 2] * (b4) * (b5).conjugate()
        * tensor(a, b) * tensor(d, c)) + (rho[1, 3] * (b4) *
        (b6).conjugate() * tensor(a, b) * tensor(d, d)) + (
        rho[2, 0] * (b5) * (b3).conjugate() * tensor(b, a) *
        tensor(c, c)) + (rho[2, 1] * (b5) * (b4).conjugate()
        * tensor(b, a) * tensor(c, d)) + (rho[2, 2] * (b5) *
        (b5).conjugate() * tensor(b, a) * tensor(d, c)) + (
        rho[2, 3] * (b5) * (b6).conjugate() * tensor(b, a) *
        tensor(d, d)) + (rho[3, 0] * (b6) * (b3).conjugate()
        * tensor(b, b) * tensor(c, c)) + (rho[3, 1] * (b6) *
        (b4).conjugate() * tensor(b, b) * tensor(c, d)) + (
        rho[3, 2] * (b6) * (b5).conjugate() * tensor(b, b) *
        tensor(d, c)) + (rho[3, 3] * (b6) * (b6).conjugate()
        * tensor(b, b) * tensor(d, d)))) + (2 * (((rho[1, 1]
        * (b1) * (b1).conjugate() * tensor(a, b) * tensor(c,
        d)) + (rho[1, 2] * (b1) * (b2).conjugate() * tensor(a
        , b) * tensor(d, c)) + (rho[2, 1] * (b2) * (b1).
        conjugate() * tensor(b, a) * tensor(c, d)) + (rho[2,
        2] * (b2) * (b2).conjugate() * tensor(b, a) * tensor(
        d, c)))))
    rhoq = rho10.unit()
    rho = rhoq.full()
    del rho10
if j == 0:
    rho1 = (1 / (P20 + P10)) * ((P20 * ((rho[0, 0] * a1 * a1
        .conjugate() * tensor(a, a) * tensor(c, c)) + (rho[0,
         1] * a1 * a2.conjugate() * tensor(a, a) * tensor(c,
```

```
            d)) + (rho[0, 2] * a1 * a3.conjugate() * tensor(a, a)
             * tensor(d, c)) + (rho[0, 3] * a1 * a4.conjugate() *
             tensor(a, a) * tensor(d, d)) + (rho[1, 0] * a2 * a1.
            conjugate() * tensor(a, b) * tensor(c, c)) + (rho[1,
            1] * a2 * a2.conjugate() * tensor(a, b) * tensor(c, d
            )) + (rho[1, 2] * a2 * a3.conjugate() * tensor(a, b)
            * tensor(d, c)) + (rho[1, 3] * a2 * a4.conjugate() *
            tensor(a, b) * tensor(d, d)) + (rho[2, 0] * a3 * a1.
            conjugate() * tensor(b, a) * tensor(c, c)) + (rho[2,
            1] * a3 * a2.conjugate() * tensor(b, a) * tensor(c, d
            )) + (rho[2, 2] * a3 * a3.conjugate() * tensor(b, a)
            * tensor(d, c)) + (rho[2, 3] * a3 * a4.conjugate() *
            tensor(b, a) * tensor(d, d)) + (rho[3, 0] * a4 * a1.
            conjugate() * tensor(b, b) * tensor(c, c)) + (rho[3,
            1] * a4 * a2.conjugate() * tensor(b, b) * tensor(c, d
            )) + (rho[3, 2] * a4 * a3.conjugate() * tensor(b, b)
            * tensor(d, c)) + (rho[3, 3] * a4 * a4.conjugate() *
            tensor(b, b) * tensor(d, d)))) + (P10 * ((rho[0, 0] *
             ((a17 * a17.conjugate()) + (a18 * a18.conjugate()))
            * tensor(a, a) * tensor(c, c)) + (rho[0, 1] * a17 *
            a17.conjugate() * tensor(a, a) * tensor(c, d)) + (rho
            [0, 2] * a18 * a18.conjugate() * tensor(a, a) *
            tensor(d, c)) + (rho[1, 0] * a17 * a17.conjugate() *
            tensor(a, b) * tensor(c, c)) + (rho[1, 1] * a17 * a17
            .conjugate() * tensor(a, b) * tensor(c, d)) + (rho[2,
             0] * a18 * a18.conjugate() * tensor(b, a) * tensor(c
            , c)) + (rho[2, 2] * a18 * a18.conjugate() * tensor(b
            , a) * tensor(d, c)))))
        rhoq = rho1.unit()
        rhoq = tensor(sigmax(), sigmax()) * rhoq * tensor(sigmax
            (), sigmax())
        rho = rhoq.full()
        del rho1
    if j == 1:
        rho2 = (1 / (P02 + P01)) * ((P02 * ((rho[0, 0] * a5 * a5
            .conjugate() * tensor(a, a) * tensor(c, c)) + (rho[0,
             1] * a5 * a6.conjugate() * tensor(a, a) * tensor(c,
            d)) + (rho[0, 2] * a5 * a7.conjugate() * tensor(a, a)
             * tensor(d, c)) + (rho[0, 3] * a5 * a8.conjugate() *
             tensor(a, a) * tensor(d, d)) + (rho[1, 0] * a6 * a5.
            conjugate() * tensor(a, b) * tensor(c, c)) + (rho[1,
            1] * a6 * a6.conjugate() * tensor(a, b) * tensor(c, d
            )) + (rho[1, 2] * a6 * a7.conjugate() * tensor(a, b)
            * tensor(d, c)) + (rho[1, 3] * a6 * a8.conjugate() *
            tensor(a, b) * tensor(d, d)) + (rho[2, 0] * a7 * a5.
            conjugate() * tensor(b, a) * tensor(c, c)) + (rho[2,
            1] * a7 * a6.conjugate() * tensor(b, a) * tensor(c, d
            )) + (rho[2, 2] * a7 * a7.conjugate() * tensor(b, a)
```

```
            * tensor(d, c)) + (rho[2, 3] * a7 * a8.conjugate() *
            tensor(b, a) * tensor(d, d)) + (rho[3, 0] * a8 * a5.
            conjugate() * tensor(b, b) * tensor(c, c)) + (rho[3,
            1] * a8 * a6.conjugate() * tensor(b, b) * tensor(c, d
            )) + (rho[3, 2] * a8 * a7.conjugate() * tensor(b, b)
            * tensor(d, c)) + (rho[3, 3] * a8 * a8.conjugate() *
            tensor(b, b) * tensor(d, d)))) + (P01 * ((rho[0, 0] *
             ((a17 * a17.conjugate()) + (a18 * a18.conjugate()))
            * tensor(a, a) * tensor(c, c)) + (rho[0, 1] * a17 *
            a17.conjugate() * tensor(a, a) * tensor(c, d)) + (rho
            [0, 2] * a18 * a18.conjugate() * tensor(a, a) *
            tensor(d, c)) + (rho[1, 0] * a17 * a17.conjugate() *
            tensor(a, b) * tensor(c, c)) + (rho[1, 1] * a17 * a17
            .conjugate() * tensor(a, b) * tensor(c, d)) + (rho[2,
             0] * a18 * a18.conjugate() * tensor(b, a) * tensor(c
            , c)) + (rho[2, 2] * a18 * a18.conjugate() * tensor(b
            , a) * tensor(d, c)))))
        rhoq = rho2.unit()
        rhoq = tensor(sigmax(), sigmax()) * rhoq * tensor(sigmax
            (), sigmax())
        rho = rhoq.full()
        del rho2
    if j == 2:
        rho3 = (1 / prob[j]) * (((rho[0, 0] * (a9 + a13) * (a9 +
             a13).conjugate() * tensor(a, a) * tensor(c, c)) + (
            rho[0, 1] * (a9 + a13) * (a10 + a14).conjugate() *
            tensor(a, a) * tensor(c, d)) + (rho[0, 2] * (a9 + a13
            ) * (a11 + a15).conjugate() * tensor(a, a) * tensor(d
            ,c)) + (rho[0, 3] * (a9 + a13) * (a12 + a16).
            conjugate() * tensor(a, a) * tensor(d,d)) + (rho[1,
            0] * (a10 + a14) * (a9 + a13).conjugate() * tensor(a,
             b) * tensor(c,c)) + (rho[1, 1] * (a10 + a14) * (a10
            + a14).conjugate() * tensor(a, b) * tensor(c,d)) + (
            rho[1, 2] * (a10 + a14) * (a11 + a15).conjugate() *
            tensor(a, b) * tensor(d,c)) + (rho[1, 3] * (a10 + a14
            ) * (a12 + a16).conjugate() * tensor(a, b) * tensor(d
            ,d)) + (rho[2, 0] * (a11 + a15) * (a9 + a13).
            conjugate() * tensor(b, a) * tensor(c,c)) + (rho[2,
            1] * (a11 + a15) * (a10 + a14).conjugate() * tensor(b
            , a) * tensor(c,d)) + (rho[2, 2] * (a11 + a15) * (a11
             + a15).conjugate() * tensor(b, a) * tensor(d,c)) + (
            rho[2, 3] * (a11 + a15) * (a12 + a16).conjugate() *
            tensor(b, a) * tensor(d,d)) + (rho[3, 0] * (a12 + a16
            ) * (a9 + a13).conjugate() * tensor(b, b) * tensor(c,
            c)) + (rho[3, 1] * (a12 + a16) * (a10 + a14).
            conjugate() * tensor(b, b) * tensor(c,d)) + (rho[3,
            2] * (a12 + a16) * (a11 + a15).conjugate() * tensor(b
            , b) * tensor(d,c)) + (rho[3, 3] * (a12 + a16) * (a12
```

```
            + a16).conjugate() * tensor(b, b) * tensor(d,d))))
        rhoq = rho3.unit()
        rhoq = tensor(sigmax(), sigmax()) * rhoq * tensor(sigmax
           (), sigmax())
        rho = rhoq.full()
        del rho3
    if j == 5:
        rho4 = (1 / prob[j]) * ((rho[0, 0] * abs(a19) ** 2 *
           tensor(a, a) * tensor(c, c)) + (rho[0, 1] * abs(a19)
           ** 2 * tensor(a, a) * tensor(c, d)) + (rho[1, 0] *
           abs(a19) ** 2 * tensor(a, b) * tensor(c, c)) + (rho
           [1, 1] * abs(a19) ** 2 * tensor(a, b) * tensor(c, d))
            + (rho[0, 0] * abs(a20) ** 2 * tensor(a, a) * tensor
           (c, c)) + (rho[0, 2] * abs(a20) ** 2 * tensor(a, a) *
            tensor(d, c)) + (rho[2, 0] * abs(a20) ** 2 * tensor(
           b, a) * tensor(c, c)) + (rho[2, 2] * abs(a20) ** 2 *
           tensor(b, a) * tensor(d, c)))
        rhoq = rho4.unit()
        rhoq=tensor(sigmax(),sigmax())*rhoq*tensor(sigmax(),
           sigmax())
        rho = rhoq.full()
        del rho4
    del j, P20, P02, P11, P10, P01, P00
    concurrences = np.append(concurrences, concurrence(rhoq))
```

APPENDIX

B

TWO-PHOTON SCATTERING MATRIX

In this appendix we give the solution to the two-photon scattering matrix elements for the setup proposed in Chapter 6, following a similar treatment to that described in Refs [227, 238]. We start from the formal definition of the two-photon scattering matrix element as given in Eq. (6.8):

$$\begin{aligned} &S_{\mu_1,\mu_2,\nu_1,\nu_2}\left(p_1,p_2,k_1,k_2\right) \\ &\qquad = \langle p_{1,\mu_1} p_{2,\mu_2}^{-} | k_{1,\nu_1} k_{2,\nu_2}^{+} \rangle \\ &\qquad = \langle p_{1,\mu_1}^{-} | \mu_{2,\text{in}}\left(p_2\right) | k_{1,\nu_1} k_{2,\nu_2}^{+} \rangle - \sqrt{2\pi}\mathrm{i} \sum_{j=\chi,\psi} V_{\mu_2,j}^{*} \langle p_{1,\mu_1}^{-} | c_j\left(p_2\right) | k_{1,\nu_1} k_{2,\nu_2}^{+} \rangle , \end{aligned} \tag{B.1}$$

where $|k_{i,\nu_i}^{+}\rangle = \nu_{i,\text{in}}^{\dagger}\left(k_i\right)|0\rangle$ with $i \in \{1,2\}$, and $|p_{1,\mu_1}^{-}\rangle = \mu_{1,\text{out}}^{\dagger}\left(p_1\right)|0\rangle$. The first term in the last line can be evaluated by using the commutation relations of the field operators, $[\mu_{\text{in}}(k), \nu_{\text{in}}^{\dagger}(p)] = \delta_{\mu\nu}\delta(k-p)$. This gives

$$\langle p_{1,\mu_1}^{-} | \mu_{2,\text{in}}\left(p_2\right) | k_{1,\nu_1} k_{2,\nu_2}^{+} \rangle = S_{\mu_1,\nu_1}\left(p_1,k_1\right) S_{\mu_2,\nu_2}\left(p_2,k_2\right) + S_{\mu_1,\nu_2}\left(p_1,k_2\right) S_{\mu_2,\nu_1}\left(p_2,k_1\right) . \tag{B.2}$$

In order to solve the second term, we make use of the Heisenberg equations of motion for the operators $c_j\left(t\right)$ and $\sigma_{-}\left(t\right)$, which results in a set of coupled differential equations. Pre- and post-multiplying by $\langle p_{1,\mu_1}^{-}|$ and $|k_{1,\nu_1} k_{2,\nu_2}^{+}\rangle$, respectively, and taking the Fourier transform, we obtain

$$\begin{aligned} -\mathrm{i}p \langle p_{1,\mu_1}^{-} | c_j\left(p\right) | k_{1,\nu_1} k_{2,\nu_2}^{+} \rangle = &-\mathrm{i}\omega_j \langle p_{1,\mu_1}^{-} | c_j\left(p\right) | k_{1,\nu_1} k_{2,\nu_2}^{+} \rangle - \mathrm{i} g_j^{*} \langle p_{1,\mu_1}^{-} | \sigma_{-}\left(p\right) | k_{1,\nu_1} k_{2,\nu_2}^{+} \rangle \\ &- \mathrm{i} \sum_{\mu} V_{\mu,j} \sqrt{2\pi} \langle p_{1,\mu_1}^{-} | \mu_{\text{in}}\left(p\right) | k_{1,\nu_1} k_{2,\nu_2}^{+} \rangle \\ &- \pi \sum_{\mu,k} V_{\mu,j} V_{\mu,k}^{*} \langle p_{1,\mu_1}^{-} | c_k\left(p\right) | k_{1,\nu_1} k_{2,\nu_2}^{+} \rangle , \end{aligned} \tag{B.3a}$$

$$
\begin{aligned}
-\mathrm{i}p\left\langle p_{1,\mu_1}^{-}\right|\sigma_{-}\left(p\right)\left|k_{1,\nu_1}k_{2,\nu_2}^{+}\right\rangle &= -\mathrm{i}\omega_e\left\langle p_{1,\mu_1}^{-}\right|\sigma_{-}\left(p\right)\left|k_{1,\nu_1}k_{2,\nu_2}^{+}\right\rangle + \mathrm{i}\sum_j g_j\left\langle p_{1,\mu_1}^{-}\right|c_j\sigma_z\left(p\right)\left|k_{1,\nu_1}k_{2,\nu_2}^{+}\right\rangle \\
&= -\mathrm{i}\omega_e\left\langle p_{1,\mu_1}^{-}\right|\sigma_{-}\left(p\right)\left|k_{1,\nu_1}k_{2,\nu_2}^{+}\right\rangle \\
&\quad + 2\mathrm{i}\sum_j \frac{g_j}{\sqrt{2\pi}}\int \mathrm{d}p'\ \left\langle p_{1,\mu_1}^{-}\right|\sigma_{+}\left(p'\right)\sigma_{-}c_j\left(p+p'\right)\left|k_{1,\nu_1}k_{2,\nu_2}^{+}\right\rangle \\
&\quad - \mathrm{i}\sum_j g_j\left\langle p_{1,\mu_1}^{-}\right|c_j\left(p\right)\left|k_{1,\nu_1}k_{2,\nu_2}^{+}\right\rangle,
\end{aligned}
\tag{B.3b}
$$

where $\mu \in \{a, b\}$ and $k \in \{\chi, \psi\}$, and where we have made use of the convolution property of the Fourier transform. In order to solve the above set of equations, we need to obtain an expression for

$$
\left\langle p_{1,\mu_1}^{-}\right|\sigma_{+}\left(p'\right)\sigma_{-}c_j\left(p+p'\right)\left|k_{1,\nu_1}k_{2,\nu_2}^{+}\right\rangle = \left\langle p_{1,\mu_1}^{-}\right|\sigma_{+}\left(p'\right)\left|0\right\rangle\left\langle 0\right|\sigma_{-}c_j\left(p+p'\right)\left|k_{1,\nu_1}k_{2,\nu_2}^{+}\right\rangle,
\tag{B.4}
$$

where multiplying by the identity gives a non-zero contribution only for the zero excitation outer product. The first inner product in Eq. (B.4) can be solved by

$$
\begin{aligned}
\left\langle p_{1,\mu_1}^{-}\right|\sigma_{+}\left(p'\right)\left|0\right\rangle &= \sum_{\mu'}\int \mathrm{d}k\ \left\langle p_{1,\mu_1}^{-}\right|k_{\mu'}^{+}\right\rangle\left\langle k_{\mu'}^{+}\right|\sigma_{+}\left(p'\right)\left|0\right\rangle \\
&= \sum_{\mu'} S_{\mu_1,\mu'}\left(p_1,p'\right)\sum_{j\neq k}\frac{g_k^*}{\left(\omega_e - p'\right)}\left[\frac{-_{\mu',j}^{*}\sqrt{2\pi}B_j^*\left(p'\right) -_{\mu',k}^{*}\sqrt{2\pi}A_j^*\left(p'\right)}{A_j^*\left(p'\right)A_k^*\left(p'\right) - B_j^*\left(p'\right)B_k^*\left(p'\right)}\right],
\end{aligned}
\tag{B.5}
$$

where $A_j^*\left(p'\right)$ and $B_j^*\left(p'\right)$ are the complex conjugate of the functions defined in Eq. (6.7).

In order to solve the second inner product in Eq. (B.4), we need to find $\partial_t\sigma_{-}c_j\left(t\right)$ and $\partial_t c_j c_k\left(t\right)$ using the Heisenberg equation of motion. Similarly, we pre- and post-multiply by $\left\langle 0\right|$ and $\left|k_{1,\nu_1}k_{2,\nu_2}^{+}\right\rangle$ and take the Fourier transform to obtain

$$
\begin{aligned}
&-\mathrm{i}p\left\langle 0\right|\sigma_{-}c_j\left(p\right)\left|k_{1,\nu_1}k_{2,\nu_2}^{+}\right\rangle \\
&= -\mathrm{i}\left(\omega_e+\omega_j\right)\left\langle 0\right|\sigma_{-}c_j\left(p\right)\left|k_{1,\nu_1}k_{2,\nu_2}^{+}\right\rangle - \mathrm{i}\sum_k g_k\left\langle 0\right|c_j c_k\left(p\right)\left|k_{1,\nu_1}k_{2,\nu_2}^{+}\right\rangle \\
&\quad - \mathrm{i}\sum_\mu V_{\mu,j}\sqrt{2\pi}\left\langle 0\right|\mu_{\mathrm{in}}\sigma_{-}\left(p\right)\left|k_{1,\nu_1}k_{2,\nu_2}^{+}\right\rangle - \pi\sum_{\mu,k}V_{\mu,j}V_{\mu,k}^*\left\langle 0\right|\sigma_{-}c_k\left(p\right)\left|k_{1,\nu_1}k_{2,\nu_2}^{+}\right\rangle
\end{aligned}
\tag{B.6a}
$$

$$
\begin{aligned}
\text{and}\qquad &-\mathrm{i}p\left\langle 0\right|c_j c_k\left(p\right)\left|k_{1,\nu_1}k_{2,\nu_2}^{+}\right\rangle \\
&= -\mathrm{i}\left(\omega_j+\omega_k\right)\left\langle 0\right|c_j c_k\left(p\right)\left|k_{1,\nu_1}k_{2,\nu_2}^{+}\right\rangle \\
&\quad - \mathrm{i}\sum_\mu \sqrt{2\pi}\left\langle 0\right|\left[V_{\mu,k}\,\mu_{\mathrm{in}}c_j\left(p\right) + V_{\mu,j}\,\mu_{\mathrm{in}}c_k\left(p\right)\right]\left|k_{1,\nu_1}k_{2,\nu_2}^{+}\right\rangle \\
&\quad - \pi\sum_{\mu,l}\left\langle 0\right|\left[V_{\mu,j}V_{\mu,l}^*\,c_k c_l\left(p\right) + V_{\mu,k}V_{\mu,l}^*\,c_j c_l\left(p\right)\right]\left|k_{1,\nu_1}k_{2,\nu_2}^{+}\right\rangle \\
&\quad - \mathrm{i}\left\langle 0\right|\left[g_j^*\,c_k\sigma_{-}\left(p\right) + g_k^*\,c_j\sigma_{-}\left(p\right)\right]\left|k_{1,\nu_1}k_{2,\nu_2}^{+}\right\rangle.
\end{aligned}
\tag{B.6b}
$$

We solve this by setting the above equations into matrix form, with $-\mathrm{i}p\mathbf{x} = \mathbf{A}\mathbf{x} + \mathbf{B}$, and solving $\mathbf{x} = -\left(\mathrm{i}p\mathbb{1} + \mathbf{A}\right)^{-1}\mathbf{B}$, where we define

$$\mathbf{x} = \langle 0| \begin{bmatrix} \sigma_- c_\chi(p) \\ \sigma_- c_\psi(p) \\ c_\chi c_\chi(p) \\ c_\chi c_\psi(p) \\ c_\psi c_\psi(p) \end{bmatrix} |k_{1,\nu_1} k_{2,\nu_2}^{+}\rangle, \tag{B.7a}$$

$$\mathbf{A} = \begin{bmatrix} -\mathrm{i}(\omega_e + \omega_\chi) - \pi\sum_\mu |V_{\mu,\chi}|^2 & -\pi\sum_\mu V_{\mu,\chi}V_{\mu,\psi}^* & -\mathrm{i}g_\chi \\ -\pi\sum_\mu V_{\mu,\psi}V_{\mu,\chi}^* & -\mathrm{i}(\omega_e + \omega_\psi) - \pi\sum_\mu |V_{\mu,\psi}|^2 & 0 \\ -2\mathrm{i}g_\chi^* & 0 & -2\mathrm{i}\omega_\chi - 2\pi\sum_\mu |V_{\mu,\chi}|^2 \\ -\mathrm{i}g_\psi^* & -\mathrm{i}g_\chi^* & -\pi\sum_{\mu,\chi}^* V_{\mu,\psi} \\ 0 & -2\mathrm{i}g_\psi^* & 0 \end{bmatrix}$$
$$\begin{bmatrix} -\mathrm{i}g_\psi & 0 \\ -\mathrm{i}g_\chi & -\mathrm{i}g_\psi \\ 2\pi\sum_\mu V_{\mu,\chi}V_{\mu,\psi}^* & 0 \\ -\mathrm{i}(\omega_\chi + \omega_\psi) - \pi\sum_\mu \left(|V_{\mu,\chi}|^2 + |V_{\mu,\psi}|^2\right) & -\pi\sum_{\mu,\psi}^* V_{\mu,\chi} \\ -2\pi\sum_\mu V_{\mu,\chi}^* V_{\mu,\psi} & -2\mathrm{i}\omega_\psi - 2\pi\sum_\mu |V_{\mu,\psi}|^2 \end{bmatrix}, \tag{B.7b}$$

$$\mathbf{B} = -\sqrt{2\pi}\mathrm{i}\langle 0| \begin{bmatrix} \sum_\mu V_{\mu,\chi}\,\mu_{\mathrm{in}}\sigma_-(p) \\ \sum_\mu V_{\mu,\psi}\,\mu_{\mathrm{in}}\sigma_-(p) \\ 2\sum_\mu V_{\mu,\chi}\,\mu_{\mathrm{in}}c_\chi(p) \\ \sum_\mu \left[V_{\mu,\psi}\,\mu_{\mathrm{in}}c_\chi(p) + V_{\mu,\chi}\,\mu_{\mathrm{in}}c_\psi(p)\right] \\ 2\sum_\mu V_{\mu,\psi}\,\mu_{\mathrm{in}}c_\psi(p) \end{bmatrix} |k_{1,\nu_1} k_{2,\nu_2}^{+}\rangle, \tag{B.7c}$$

where $[c_\chi(p), c_\psi(p)] = 0$.

BIBLIOGRAPHY

[1] A. Einstein, "Über einen die erzeugung und verwandlung des lichtes betreffenden heuristischen gesichtspunkt," *Annalen der Physik*, vol. 322, no. 6, pp. 132–148, 1905.

[2] P. Ehrenfest, "Welche züge der lichtquantenhypothese spielen in der theorie der wärmestrahlung eine wesentliche rolle?," *Annalen der Physik*, vol. 341, no. 11, pp. 91–118, 1911.

[3] E. N. Sgourou, A. Daskalopulu, L. H. Tsoukalas, G. Stamoulis, R. V. Vovk, and A. Chroneos, "Seventy-five years since the point-contact transistor: Germanium revisited," *Applied Sciences*, vol. 12, p. 11993, Nov. 2022.

[4] J. P. Dowling and G. J. Milburn, "Quantum technology: the second quantum revolution," *Philosophical Transactions of the Royal Society of London. Series A: Mathematical, Physical and Engineering Sciences*, vol. 361, pp. 1655–1674, June 2003.

[5] D. Deutsch, "Quantum theory, the church–turing principle and the universal quantum computer," *Proceedings of the Royal Society of London. A. Mathematical and Physical Sciences*, vol. 400, pp. 97–117, July 1985.

[6] P. Shor, "Algorithms for quantum computation: discrete logarithms and factoring," in *Proceedings 35th Annual Symposium on Foundations of Computer Science*, pp. 124–134, IEEE Comput. Soc. Press, 1994.

[7] N. S. Blunt, J. Camps, O. Crawford, R. Izsák, S. Leontica, A. Mirani, A. E. Moylett, S. A. Scivier, C. Sünderhauf, P. Schopf, J. M. Taylor, and N. Holzmann, "Perspective on the current state-of-the-art of quantum computing for drug discovery applications," *Journal of Chemical Theory and Computation*, vol. 18, pp. 7001–7023, Nov. 2022.

[8] M. Motta, G. O. Jones, J. E. Rice, T. P. Gujarati, R. Sakuma, I. Liepuoniute, J. M. Garcia, and Y. ya Ohnishi, "Quantum chemistry simulation of ground- and excited-

state properties of the sulfonium cation on a superconducting quantum processor," *Chemical Science*, vol. 14, no. 11, pp. 2915–2927, 2023.

[9] X. Yuan, S. Endo, Q. Zhao, Y. Li, and S. C. Benjamin, "Theory of variational quantum simulation," *Quantum*, vol. 3, p. 191, Oct. 2019.

[10] D. P. DiVincenzo, "The physical implementation of quantum computation," *Fortschritte der Physik*, vol. 48, pp. 771–783, Sept. 2000.

[11] C. A. Pérez-Delgado and P. Kok, "Quantum computers: Definition and implementations," *Physical Review A*, vol. 83, p. 012303, Jan. 2011.

[12] S. Takeda and A. Furusawa, "Toward large-scale fault-tolerant universal photonic quantum computing," *APL Photonics*, vol. 4, p. 060902, June 2019.

[13] D. Loss and D. P. DiVincenzo, "Quantum computation with quantum dots," *Physical Review A*, vol. 57, pp. 120–126, Jan. 1998.

[14] V. Acosta and P. Hemmer, "Nitrogen-vacancy centers: Physics and applications," *MRS Bulletin*, vol. 38, pp. 127–130, Feb. 2013.

[15] M. H. Devoret and R. J. Schoelkopf, "Superconducting circuits for quantum information: An outlook," *Science*, vol. 339, pp. 1169–1174, Mar. 2013.

[16] D. Kielpinski, C. Monroe, and D. J. Wineland, "Architecture for a large-scale ion-trap quantum computer," *Nature*, vol. 417, pp. 709–711, June 2002.

[17] M. A. Nielsen and I. L. Chuang, *Quantum Computation and Quantum Information*. Cambridge University Press, June 2012.

[18] S. Slussarenko and G. J. Pryde, "Photonic quantum information processing: A concise review," *Applied Physics Reviews*, vol. 6, p. 041303, Dec. 2019.

[19] E. Knill, R. Laflamme, and G. J. Milburn, "A scheme for efficient quantum computation with linear optics," *Nature*, vol. 409, pp. 46–52, Jan. 2001.

[20] S. Sun, H. Kim, Z. Luo, G. S. Solomon, and E. Waks, "Nanophotonic spin-photon quantum transistor," in *Frontiers in Optics 2017*, p. LM3F.3, OSA, 2017.

[21] A. Javadi, D. Ding, M. H. Appel, S. Mahmoodian, M. C. Löbl, I. Söllner, R. Schott, C. Papon, T. Pregnolato, S. Stobbe, L. Midolo, T. Schröder, A. D. Wieck, A. Ludwig, R. J. Warburton, and P. Lodahl, "Spin–photon interface and spin-controlled photon switching in a nanobeam waveguide," *Nature Nanotechnology*, vol. 13, pp. 398–403, Mar. 2018.

[22] C. P. Michaels, J. A. Martínez, R. Debroux, R. A. Parker, A. M. Stramma, L. I. Huber, C. M. Purser, M. Atatüre, and D. A. Gangloff, "Multidimensional cluster states using a single spin-photon interface coupled strongly to an intrinsic nuclear register," *Quantum*, vol. 5, p. 565, Oct. 2021.

[23] J. Borregaard, A. S. Sørensen, and P. Lodahl, "Quantum networks with deterministic spin–photon interfaces," *Advanced Quantum Technologies*, vol. 2, p. 1800091, Apr. 2019.

[24] J. C. F. Matthews, A. Politi, A. Stefanov, and J. L. O'Brien, "Manipulation of multiphoton entanglement in waveguide quantum circuits," *Nature Photonics*, vol. 3, pp. 346–350, May 2009.

[25] N. C. Harris, D. Bunandar, M. Pant, G. R. Steinbrecher, J. Mower, M. Prabhu, T. Baehr-Jones, M. Hochberg, and D. Englund, "Large-scale quantum photonic circuits in silicon," *Nanophotonics*, vol. 5, pp. 456–468, Aug. 2016.

[26] N. Prtljaga, C. Bentham, J. O'Hara, B. Royall, E. Clarke, L. R. Wilson, M. S. Skolnick, and A. M. Fox, "On-chip interference of single photons from an embedded quantum dot and an external laser," *Applied Physics Letters*, vol. 108, p. 251101, June 2016.

[27] G. Moody, V. J. Sorger, D. J. Blumenthal, P. W. Juodawlkis, W. Loh, C. Sorace-Agaskar, A. E. Jones, K. C. Balram, J. C. F. Matthews, A. Laing, M. Davanco, L. Chang, J. E. Bowers, N. Quack, C. Galland, I. Aharonovich, M. A. Wolff, C. Schuck, N. Sinclair, M. Lončar, T. Komljenovic, D. Weld, S. Mookherjea, S. Buckley, M. Radulaski, S. Reitzenstein, B. Pingault, B. Machielse, D. Mukhopadhyay, A. Akimov, A. Zheltikov, G. S. Agarwal, K. Srinivasan, J. Lu, H. X. Tang, W. Jiang, T. P. McKenna, A. H. Safavi-Naeini, S. Steinhauer, A. W. Elshaari, V. Zwiller, P. S. Davids, N. Martinez, M. Gehl, J. Chiaverini, K. K. Mehta, J. Romero, N. B. Lingaraju, A. M. Weiner, D. Peace, R. Cernansky, M. Lobino, E. Diamanti, L. T. Vidarte, and R. M. Camacho, "2022 roadmap on integrated quantum photonics," *Journal of Physics: Photonics*, vol. 4, p. 012501, Jan. 2022.

[28] A. Chanana, H. Larocque, R. Moreira, J. Carolan, B. Guha, E. G. Melo, V. Anant, J. Song, D. Englund, D. J. Blumenthal, K. Srinivasan, and M. Davanco, "Ultra-low loss quantum photonic circuits integrated with single quantum emitters," *Nature Communications*, vol. 13, p. 7693, Dec. 2022.

[29] J. L. O'Brien, A. Furusawa, and J. Vučković, "Photonic quantum technologies," *Nature Photonics*, vol. 3, pp. 687–695, Dec. 2009.

[30] I. Aharonovich, D. Englund, and M. Toth, "Solid-state single-photon emitters," *Nature Photonics*, vol. 10, pp. 631–641, Sept. 2016.

[31] N. Somaschi, V. Giesz, L. D. Santis, J. C. Loredo, M. P. Almeida, G. Hornecker, S. L. Portalupi, T. Grange, C. Antón, J. Demory, C. Gómez, I. Sagnes, N. D. Lanzillotti-Kimura, A. Lemaítre, A. Auffeves, A. G. White, L. Lanco, and P. Senellart, "Near-optimal single-photon sources in the solid state," *Nature Photonics*, vol. 10, pp. 340–345, Mar. 2016.

[32] M. Chen, L. Lu, H. Yu, C. Li, and N. Zhao, "Integration of colloidal quantum dots with photonic structures for optoelectronic and optical devices," *Advanced Science*, vol. 8, p. 2101560, July 2021.

[33] M. Sartison, O. C. Ibarra, I. Caltzidis, D. Reuter, and K. D. Jöns, "Scalable integration of quantum emitters into photonic integrated circuits," *Materials for Quantum Technology*, vol. 2, p. 023002, June 2022.

[34] S. M. Thon, M. T. Rakher, H. Kim, J. Gudat, W. T. M. Irvine, P. M. Petroff, and D. Bouwmeester, "Strong coupling through optical positioning of a quantum dot in a photonic crystal cavity," *Applied Physics Letters*, vol. 94, p. 111115, Mar. 2009.

[35] S. Reitzenstein and A. Forchel, "Quantum dot micropillars," *Journal of Physics D: Applied Physics*, vol. 43, p. 033001, Jan. 2010.

[36] E. M. Purcell, "Proceedings of the american physical society," *Physical Review*, vol. 69, p. 681, June 1946.

[37] W. Gerlach and O. Stern, "Der experimentelle nachweis der richtungsquantelung im magnetfeld," *Zeitschrift für Physik*, vol. 9, pp. 349–352, Dec. 1922.

[38] H. J. Kimble, M. Dagenais, and L. Mandel, "Photon antibunching in resonance fluorescence," *Physical Review Letters*, vol. 39, pp. 691–695, Sept. 1977.

[39] H. Goldstein, C. P. Poole, and J. L. Safko, *Classical Mechanics*. Upper Saddle River, NJ: Pearson, 3 ed., June 2001.

[40] J. V. Neumann, *Mathematical Foundations of Quantum Mechanics*. Princeton university press, 2018.

[41] H.-P. Breuer and F. Petruccione, *The theory of Open Quantum Systems*. Clarendon, 2010.

[42] L. V. Prokhorov, "Quantization of the electromagnetic field," *Soviet Physics Uspekhi*, vol. 31, pp. 151–162, Feb. 1988.

[43] C. G. Gerry and P. L. Knight, *Introductory Quantum Optics*. Cambridge University Press, 2012.

[44] R. Bennett, T. M. Barlow, and A. Beige, "A physically motivated quantization of the electromagnetic field," *European Journal of Physics*, vol. 37, p. 014001, Oct. 2015.

[45] S. M. Dutra, *Cavity Quantum Electrodynamics: The Strange Theory of Light in a Box*. John Wiley & Sons, Nov. 2004.

[46] J. D. Jackson, *Classical Electrodynamics*. New York: John Wiley & Sons, 1999.

[47] M. O. Scully and M. S. Zubairy, *Quantum Optics*. Cambridge University Press, Sept. 1997.

[48] J. D. Bjorken and S. D. Drell, *Relativistic Quantum Fields*. Pure & Applied Physics S., New York, NY: McGraw-Hill, Jan. 1965.

[49] R. J. Glauber, "Coherent and incoherent states of the radiation field," *Physical Review*, vol. 131, pp. 2766–2788, Sept. 1963.

[50] C. H. Bennett, G. Brassard, Crépeau, R. Jozsa, A. Peres, and W. K. Wootters, "Teleporting an unknown quantum state via dual classical and einstein-podolsky-rosen channels," *Physical Review Letters*, vol. 70, no. 13, pp. 1895–1899, 1993.

[51] W. K. Wootters and W. H. Zurek, "A single quantum cannot be cloned," *Nature*, vol. 299, pp. 802–803, Oct. 1982.

[52] C. H. Bennett, H. J. Bernstein, S. Popescu, and B. Schumacher, "Concentrating partial entanglement by local operations," *Physical Review A*, vol. 53, pp. 2046–2052, Apr. 1996.

[53] C. H. Bennett, D. P. DiVincenzo, J. A. Smolin, and W. K. Wootters, "Mixed-state entanglement and quantum error correction," *Physical Review A*, vol. 54, pp. 3824–3851, Nov. 1996.

[54] S. Hill and W. K. Wootters, "Entanglement of a pair of quantum bits," *Physical Review Letters*, vol. 78, pp. 5022–5025, June 1997.

[55] W. K. Wootters, "Entanglement of Formation of an Arbitrary State of Two Qubits," *Physical Review Letters*, vol. 80, no. 10, pp. 2245–2248, 1998.

[56] P. W. Shor, "Scheme for reducing decoherence in quantum computer memory," *Physical Review A*, vol. 52, pp. R2493–R2496, Oct. 1995.

[57] S. M. Barnett, *Quantum Information*. Oxford Master Series in Physics, London, England: Oxford University Press, May 2009.

[58] A. M. Steane, "Error correcting codes in quantum theory," *Physical Review Letters*, vol. 77, pp. 793–797, July 1996.

[59] D. Gottesman, *Stabilizer Codes and Quantum Error Correction*. PhD thesis, California Institute of Technology, 1997.

[60] G. S. Agarwal, *Quantum Optics*. Cambridge University Press, Nov. 2012.

[61] M. Fox, *Quantum Optics: An Introduction*. Oxford University Press, 2006.

[62] E. Jaynes and F. Cummings, "Comparison of quantum and semiclassical radiation theories with application to the beam maser," *Proceedings of the IEEE*, vol. 51, no. 1, pp. 89–109, 1963.

[63] J. Braumüller, M. Marthaler, A. Schneider, A. Stehli, H. Rotzinger, M. Weides, and A. V. Ustinov, "Analog quantum simulation of the Rabi model in the ultra-strong coupling regime," *Nature Communications*, vol. 8, p. 779, Oct. 2017.

[64] K. J. Blow, R. Loudon, S. J. D. Phoenix, and T. J. Shepherd, "Continuum fields in quantum optics," *Physical Review A*, vol. 42, pp. 4102–4114, Oct. 1990.

[65] R. Loudon, *The quantum theory of light*. London, England: Oxford University Press, 3 ed., Sept. 2000.

[66] J.-T. Shen and S. Fan, "Theory of single-photon transport in a single-mode waveguide. I. coupling to a cavity containing a two-level atom," *Physical Review A*, vol. 79, p. 023837, Feb. 2009.

[67] H. Zheng, *Interacting Photons in Waveguide-QED and Applications in Quantum Information Processing*. PhD thesis, Duke University, 2013.

[68] J. Southall, D. Hodgson, R. Purdy, and A. Beige, "Locally acting mirror Hamiltonians," *Journal of Modern Optics*, vol. 68, pp. 647–660, June 2021.

[69] B. Dawson, N. Furtak-Wells, T. Mann, G. Jose, and A. Beige, "The quantum optics of asymmetric mirrors with coherent light absorption," *Frontiers in Photonics*, vol. 2, p. 700737, July 2021.

[70] D. Hodgson, J. Southall, R. Purdy, and A. Beige, "Local photons," *Frontiers in Photonics*, vol. 3, p. 978855, Sept. 2022.

[71] E. Rephaeli and S. Fan, "Dissipation in few-photon waveguide transport [Invited]," *Photonics Research*, vol. 1, no. 3, p. 110, 2013.

[72] K. Mølmer, Y. Castin, and J. Dalibard, "Monte Carlo wave-function method in quantum optics," *Journal of the Optical Society of America B*, vol. 10, p. 524, Mar. 1993.

[73] H. J. Carmichael, "Quantum trajectory theory for cascaded open systems," *Physical Review Letters*, vol. 70, pp. 2273–2276, Apr. 1993.

[74] Y. Chen, M. Wubs, J. Mørk, and A. F. Koenderink, "Coherent single-photon absorption by single emitters coupled to one-dimensional nanophotonic waveguides," *New Journal of Physics*, vol. 13, p. 103010, Oct. 2011.

[75] A. Nysteen, *Few-photon Non-linearities in Nanophotonic Devices for Quantum Information Technology*. PhD thesis, Technical University of Denmark, 2015.

[76] V. Weisskopf and E. Wigner, "Berechnung der natürlichen linienbreite auf grund der diracschen lichttheorie," *Zeitschrift für Physik*, vol. 63, pp. 54–73, Jan. 1930.

[77] M. Duda. Private Communications, Aug 2022.

[78] A. Nysteen, D. P. S. McCutcheon, and J. Mørk, "Strong nonlinearity-induced correlations for counterpropagating photons scattering on a two-level emitter," *Physical Review A*, vol. 91, p. 063823, June 2015.

[79] C. W. Gardiner and M. J. Collett, "Input and output in damped quantum systems: Quantum stochastic differential equations and the master equation," *Physical Review A*, vol. 31, pp. 3761–3774, June 1985.

[80] D. F. Walls and G. J. Milburn, *Quantum Optics*. Heidelberg: Springer Berlin, 2008.

[81] S. Fan, Ş. E. Kocabaş, and J.-T. Shen, "Input-output formalism for few-photon transport in one-dimensional nanophotonic waveguides coupled to a qubit," *Physical Review A*, vol. 82, no. 6, p. 063821, 2010.

[82] J. H. Davies, *The Physics of Low-dimensional Semiconductors*. Cambridge University Press, Dec. 1997.

[83] Y. Toda, S. Shinomori, K. Suzuki, and Y. Arakawa, "Near-field magneto-optical spectroscopy of single self-assembled InAs quantum dots," *Applied Physics Letters*, vol. 73, pp. 517–519, July 1998.

[84] A. Kuther, M. Bayer, A. Forchel, A. Gorbunov, V. B. Timofeev, F. Schäfer, and J. P. Reithmaier, "Zeeman splitting of excitons and biexcitons in single $In_{0.60}Ga_{0.40}As$/GaAs self-assembled quantum dots," *Physical Review B*, vol. 58, pp. R7508–R7511, Sept. 1998.

[85] P. Lodahl, S. Mahmoodian, S. Stobbe, A. Rauschenbeutel, P. Schneeweiss, J. Volz, H. Pichler, and P. Zoller, "Chiral quantum optics," *Nature*, vol. 541, no. 7638, pp. 473–480, 2017.

[86] M. J. Mehrabad, A. P. Foster, R. Dost, E. Clarke, P. K. Patil, A. M. Fox, M. S. Skolnick, and L. R. Wilson, "Chiral topological photonics with an embedded quantum emitter," *Optica*, vol. 7, p. 1690, Nov. 2020.

[87] R. J. Coles, D. M. Price, J. E. Dixon, B. Royall, E. Clarke, P. Kok, M. S. Skolnick, A. M. Fox, and M. N. Makhonin, "Chirality of nanophotonic waveguide with embedded quantum emitter for unidirectional spin transfer," *Nature Communications*, vol. 7, no. 1, p. 11183, 2016.

[88] E. Callus and P. Kok, "Cumulative generation of maximal entanglement between spectrally distinct qubits using squeezed light," *Physical Review A*, vol. 104, p. 052407, Nov. 2021.

[89] C. Bennett and P. Shor, "Quantum information theory," *IEEE Transactions on Information Theory*, vol. 44, no. 6, pp. 2724–2742, 1998.

[90] C. H. Bennett and D. P. DiVincenzo, "Quantum information and computation," *Nature*, vol. 404, pp. 247–255, Mar. 2000.

[91] R. Jozsa, "Entanglement and quantum computation," *arXiv preprint*, 1997. arXiv:quant-ph/9707034.

[92] R. Jozsa and N. Linden, "On the role of entanglement in quantum-computational speed-up," *Proceedings of the Royal Society of London. Series A: Mathematical, Physical and Engineering Sciences*, vol. 459, no. 2036, pp. 2011–2032, 2003.

[93] U. Vazirani and T. Vidick, "Robust device independent quantum key distribution," in *Proceedings of the 5th conference on Innovations in theoretical computer science - ITCS '14*, pp. 35–36, ACM Press, 2014.

[94] C. H. Bennett, P. W. Shor, J. A. Smolin, and A. V. Thapliyal, "Entanglement-assisted classical capacity of noisy quantum channels," *Physical Review Letters*, vol. 83, no. 15, pp. 3081–3084, 1999.

[95] J. M. Gambetta, J. M. Chow, and M. Steffen, "Building logical qubits in a superconducting quantum computing system," *npj Quantum Information*, vol. 3, p. 2, Jan. 2017.

[96] P. Krantz, M. Kjaergaard, F. Yan, T. P. Orlando, S. Gustavsson, and W. D. Oliver, "A quantum engineer's guide to superconducting qubits," *Applied Physics Reviews*, vol. 6, p. 021318, June 2019.

[97] M. Kjaergaard, M. E. Schwartz, J. Braumüller, P. Krantz, J. I.-J. Wang, S. Gustavsson, and W. D. Oliver, "Superconducting qubits: Current state of play," *Annual Review of Condensed Matter Physics*, vol. 11, pp. 369–395, Mar. 2020.

[98] J. I. Cirac and P. Zoller, "Quantum computations with cold trapped ions," *Physical Review Letters*, vol. 74, pp. 4091–4094, May 1995.

[99] C. D. Bruzewicz, J. Chiaverini, R. McConnell, and J. M. Sage, "Trapped-ion quantum computing: Progress and challenges," *Applied Physics Reviews*, vol. 6, p. 021314, June 2019.

[100] L.-M. Duan and H. J. Kimble, "Scalable photonic quantum computation through cavity-assisted interactions," *Physical Review Letters*, vol. 92, p. 127902, Mar. 2004.

[101] P. Kok, W. J. Munro, K. Nemoto, T. C. Ralph, J. P. Dowling, and G. J. Milburn, "Linear optical quantum computing with photonic qubits," *Reviews of Modern Physics*, vol. 79, pp. 135–174, Jan. 2007.

[102] K. V. Kavokin, "Fine structure of the quantum-dot trion," *physica status solidi (a)*, vol. 195, pp. 592–595, Feb. 2003.

[103] A. Ramsay, S. Boyle, T. Godden, R. Kolodka, A. Khatab, J. Oliveira, J. Skiba-Szymanska, H.-Y. Liu, M. Hopkinson, A. Fox, and M. Skolnick, "Towards coherent optical control of a single hole spin: Rabi rotation of a trion conditional on the spin state of the hole," *Solid State Communications*, vol. 149, pp. 1458–1465, Sept. 2009.

[104] C. Cabrillo, J. I. Cirac, P. García-Fernández, and P. Zoller, "Creation of entangled states of distant atoms by interference," *Physical Review A*, vol. 59, no. 2, pp. 1025–1033, 1999.

[105] M. B. Plenio, S. F. Huelga, A. Beige, and P. L. Knight, "Cavity-loss-induced generation of entangled atoms," *Physical Review A*, vol. 59, pp. 2468–2475, Mar. 1999.

[106] D. E. Browne, M. B. Plenio, and S. F. Huelga, "Robust creation of entanglement between ions in spatially separate cavities," *Physical Review Letters*, vol. 91, p. 067901, Aug. 2003.

[107] L.-M. Duan and H. J. Kimble, "Efficient engineering of multiatom entanglement through single-photon detections," *Physical Review Letters*, vol. 90, no. 25, p. 253601, 2003.

[108] C. Simon and W. T. M. Irvine, "Robust long-distance entanglement and a loophole-free Bell test with ions and photons," *Physical Review Letters*, vol. 91, p. 110405, Sept. 2003.

[109] X.-L. Feng, Z.-M. Zhang, X.-D. Li, S.-Q. Gong, and Z.-Z. Xu, "Entangling distant atoms by interference of polarized photons," *Physical Review Letters*, vol. 90, p. 217902, May 2003.

[110] S. D. Barrett and P. Kok, "Efficient high-fidelity quantum computation using matter qubits and linear optics," *Physical Review A*, vol. 71, no. 6, p. 060310, 2005.

[111] D. L. Moehring, P. Maunz, S. Olmschenk, K. C. Younge, D. N. Matsukevich, L.-M. Duan, and C. Monroe, "Entanglement of single-atom quantum bits at a distance," *Nature*, vol. 449, pp. 68–71, Sept. 2007.

[112] J. Metz and S. D. Barrett, "Effect of frequency-mismatched photons in quantum-information processing," *Physical Review A*, vol. 77, p. 042323, Apr. 2008.

[113] J. Yang, G. W. Lin, Y. P. Niu, and S. Q. Gong, "Quantum entangling gates using the strong coupling between two optical emitters and nanowire surface plasmons," *Optics Express*, vol. 21, p. 15618, June 2013.

[114] T. Li and F.-G. Deng, "Error-rejecting quantum computing with solid-state spins assisted by low-q optical microcavities," *Phys. Rev. A*, vol. 94, p. 062310, Dec 2016.

[115] Y. Arakawa and M. J. Holmes, "Progress in quantum-dot single photon sources for quantum information technologies: A broad spectrum overview," *Applied Physics Reviews*, vol. 7, no. 2, p. 021309, 2020.

[116] T. Heuser, J. Große, A. Kaganskiy, D. Brunner, and S. Reitzenstein, "Fabrication of dense diameter-tuned quantum dot micropillar arrays for applications in photonic information processing," *APL Photonics*, vol. 3, no. 11, p. 116103, 2018.

[117] L. Zhai, M. C. Löbl, J.-P. Jahn, Y. Huo, P. Treutlein, O. G. Schmidt, A. Rastelli, and R. J. Warburton, "Large-range frequency tuning of a narrow-linewidth quantum emitter," *Applied Physics Letters*, vol. 117, no. 8, p. 083106, 2020.

[118] A. Sipahigil, R. E. Evans, D. D. Sukachev, M. J. Burek, J. Borregaard, M. K. Bhaskar, C. T. Nguyen, J. L. Pacheco, H. A. Atikian, C. Meuwly, R. M. Camacho, F. Jelezko, E. Bielejec, H. Park, M. Lončar, and M. D. Lukin, "An integrated diamond nanophotonics platform for quantum-optical networks," *Science*, vol. 354, pp. 847–850, Oct. 2016.

[119] D. L. Hurst, K. B. Joanesarson, J. Iles-Smith, J. Mork, and P. Kok, "Generating Maximal Entanglement between Spectrally Distinct Solid-State Emitters," *Physical Review Letters*, vol. 123, no. 2, p. 023603, 2019.

[120] S. Mahmoodian, P. Lodahl, and A. S. Sørensen, "Quantum networks with chiral-light–matter interaction in waveguides," *Physical Review Letters*, vol. 117, p. 240501, Dec. 2016.

[121] J.-T. Shen and S. Fan, "Strongly correlated multiparticle transport in one dimension through a quantum impurity," *Physical Review A*, vol. 76, no. 6, p. 062709, 2007.

[122] D. N. Klyshko, *Photons and Nonlinear Optics*. New York: Gordon and Breach, 1988.

[123] C. Couteau, "Spontaneous parametric down-conversion," *Contemporary Physics*, vol. 59, no. 3, pp. 291–304, 2018.

[124] P. Kok and B. Lovett, *Introduction to Optical Quantum Information*. Cambridge University Press, 2010.

[125] J. Schneeloch, S. H. Knarr, D. F. Bogorin, M. L. Levangie, C. C. Tison, R. Frank, G. A. Howland, M. L. Fanto, and P. M. Alsing, "Introduction to the absolute brightness and number statistics in spontaneous parametric down-conversion," *Journal of Optics*, vol. 21, no. 4, p. 043501, 2019.

[126] C. K. Hong, Z. Y. Ou, and L. Mandel, "Measurement of subpicosecond time intervals between two photons by interference," *Physical Review Letters*, vol. 59, pp. 2044–2046, Nov. 1987.

[127] S. Xu, E. Rephaeli, and S. Fan, "Analytic properties of two-photon scattering matrix in integrated quantum systems determined by the cluster decomposition principle," *Physical Review Letters*, vol. 111, p. 223602, Nov. 2013.

[128] M. Arcari, I. Söllner, A. Javadi, S. L. Hansen, S. Mahmoodian, J. Liu, H. Thyrrestrup, E. H. Lee, J. D. Song, S. Stobbe, and P. Lodahl, "Near-Unity Coupling Efficiency of a Quantum Emitter to a Photonic Crystal Waveguide," *Physical Review Letters*, vol. 113, no. 9, p. 093603, 2014.

[129] A. Javadi, S. Mahmoodian, I. Söllner, and P. Lodahl, "Numerical modeling of the coupling efficiency of single quantum emitters in photonic-crystal waveguides," *Journal of the Optical Society of America B*, vol. 35, p. 514, Feb. 2018.

[130] L. Scarpelli, B. Lang, F. Masia, D. M. Beggs, E. A. Muljarov, A. B. Young, R. Oulton, M. Kamp, S. Höfling, C. Schneider, and W. Langbein, "99% beta factor and directional coupling of quantum dots to fast light in photonic crystal waveguides determined by spectral imaging," *Physical Review B*, vol. 100, no. 3, p. 035311, 2019.

[131] M. Jönsson and G. Björk, "Evaluating the performance of photon-number-resolving detectors," *Physical Review A*, vol. 99, p. 043822, Apr. 2019.

[132] J. Provazník, L. Lachman, R. Filip, and P. Marek, "Benchmarking photon number resolving detectors," *Optics Express*, vol. 28, p. 14839, May 2020.

[133] H. Wang, J. Guo, J. Miao, W. Luo, Y. Gu, R. Xie, F. Wang, L. Zhang, P. Wang, and W. Hu, "Emerging single-photon detectors based on low-dimensional materials," *Small*, vol. 18, p. 2103963, Oct. 2021.

[134] D. V. Reddy, R. R. Nerem, S. W. Nam, R. P. Mirin, and V. B. Verma, "Superconducting nanowire single-photon detectors with 98% system detection efficiency at 1550 nm," *Optica*, vol. 7, p. 1649, Nov. 2020.

[135] L. You, "Superconducting nanowire single-photon detectors for quantum information," *Nanophotonics*, vol. 9, pp. 2673–2692, June 2020.

[136] I. E. Zadeh, J. Chang, J. W. N. Los, S. Gyger, A. W. Elshaari, S. Steinhauer, S. N. Dorenbos, and V. Zwiller, "Superconducting nanowire single-photon detectors: A perspective on evolution, state-of-the-art, future developments, and applications," *Applied Physics Letters*, vol. 118, p. 190502, May 2021.

[137] J. Chang, J. W. N. Los, J. O. Tenorio-Pearl, N. Noordzij, R. Gourgues, A. Guardiani, J. R. Zichi, S. F. Pereira, H. P. Urbach, V. Zwiller, S. N. Dorenbos, and I. E. Zadeh, "Detecting telecom single photons with $99.5-2.07\pm0.5\%$ system detection efficiency and high time resolution," *APL Photonics*, vol. 6, p. 036114, Mar. 2021.

[138] J. Fischer, M. Trif, W. Coish, and D. Loss, "Spin interactions, relaxation and decoherence in quantum dots," *Solid State Communications*, vol. 149, no. 35-36, pp. 1443–1450, 2009.

[139] W. A. Coish and J. Baugh, "Nuclear spins in nanostructures," *physica status solidi (b)*, vol. 246, pp. 2203–2215, Aug. 2009.

[140] C. Kloeffel and D. Loss, "Prospects for spin-based quantum computing in quantum dots," *Annual Review of Condensed Matter Physics*, vol. 4, pp. 51–81, Apr. 2013.

[141] J. Houel, J. H. Prechtel, A. V. Kuhlmann, D. Brunner, C. E. Kuklewicz, B. D. Gerardot, N. G. Stoltz, P. M. Petroff, and R. J. Warburton, "High Resolution Coherent Population Trapping on a Single Hole Spin in a Semiconductor Quantum Dot," *Physical Review Letters*, vol. 112, no. 10, p. 107401, 2014.

[142] J. H. Prechtel, A. V. Kuhlmann, J. Houel, A. Ludwig, S. R. Valentin, A. D. Wieck, and R. J. Warburton, "Decoupling a hole spin qubit from the nuclear spins," *Nature Materials*, vol. 15, no. 9, pp. 981–986, 2016.

[143] J. Yoneda, K. Takeda, T. Otsuka, T. Nakajima, M. R. Delbecq, G. Allison, T. Honda, T. Kodera, S. Oda, Y. Hoshi, N. Usami, K. M. Itoh, and S. Tarucha, "A quantum-dot spin qubit with coherence limited by charge noise and fidelity higher than 99.9%," *Nature Nanotechnology*, vol. 13, no. 2, pp. 102–106, 2018.

[144] K. D. Jahnke, B. Naydenov, T. Teraji, S. Koizumi, T. Umeda, J. Isoya, and F. Jelezko, "Long coherence time of spin qubits in 12C enriched polycrystalline chemical vapor deposition diamond," *Applied Physics Letters*, vol. 101, no. 1, p. 012405, 2012.

[145] J. M. Zadrozny, J. Niklas, O. G. Poluektov, and D. E. Freedman, "Millisecond Coherence Time in a Tunable Molecular Electronic Spin Qubit," *ACS Central Science*, vol. 1, no. 9, pp. 488–492, 2015.

[146] E. D. Herbschleb, H. Kato, Y. Maruyama, T. Danjo, T. Makino, S. Yamasaki, I. Ohki, K. Hayashi, H. Morishita, M. Fujiwara, and N. Mizuochi, "Ultra-long coherence times amongst room-temperature solid-state spins," *Nature Communications*, vol. 10, no. 1, p. 3766, 2019.

[147] N. Bar-Gill, L. Pham, A. Jarmola, D. Budker, and R. Walsworth, "Solid-state electronic spin coherence time approaching one second," *Nature Communications*, vol. 4, no. 1, p. 1743, 2013.

[148] E. Callus and P. Kok, "Spin-augmented observables for efficient photonic quantum error correction," *arXiv preprint*, 2022. arXiv:2211.14123.

[149] H. J. Kimble, "The quantum internet," *Nature*, vol. 453, pp. 1023–1030, June 2008.

[150] M. Atatüre, D. Englund, N. Vamivakas, S.-Y. Lee, and J. Wrachtrup, "Material platforms for spin-based photonic quantum technologies," *Nature Reviews Materials*, vol. 3, pp. 38–51, Apr. 2018.

[151] B. Hacker, S. Welte, G. Rempe, and S. Ritter, "A photon–photon quantum gate based on a single atom in an optical resonator," *Nature*, vol. 536, pp. 193–196, July 2016.

[152] A. Javadi, I. Söllner, M. Arcari, S. L. Hansen, L. Midolo, S. Mahmoodian, G. Kiršanskė, T. Pregnolato, E. H. Lee, J. D. Song, S. Stobbe, and P. Lodahl, "Single-photon non-linear optics with a quantum dot in a waveguide," *Nature Communications*, vol. 6, p. 8655, Oct. 2015.

[153] J. I. Cirac, P. Zoller, H. J. Kimble, and H. Mabuchi, "Quantum state transfer and entanglement distribution among distant nodes in a quantum network," *Physical Review Letters*, vol. 78, pp. 3221–3224, Apr. 1997.

[154] A. B. Young, C. Y. Hu, and J. G. Rarity, "Generating entanglement with low-q-factor microcavities," *Physical Review A*, vol. 87, p. 012332, Jan. 2013.

[155] A. Delteil, Z. Sun, W. bo Gao, E. Togan, S. Faelt, and A. Imamoğlu, "Generation of heralded entanglement between distant hole spins," *Nature Physics*, vol. 12, pp. 218–223, Dec. 2015.

[156] C. Y. Hu, W. J. Munro, and J. G. Rarity, "Deterministic photon entangler using a charged quantum dot inside a microcavity," *Physical Review B*, vol. 78, p. 125318, Sept. 2008.

[157] S. E. Economou and P. Dev, "Spin-photon entanglement interfaces in silicon carbide defect centers," *Nanotechnology*, vol. 27, p. 504001, Nov. 2016.

[158] C. Y. Hu and J. G. Rarity, "Loss-resistant state teleportation and entanglement swapping using a quantum-dot spin in an optical microcavity," *Physical Review B*, vol. 83, p. 115303, Mar. 2011.

[159] C. Y. Hu, W. J. Munro, J. L. O'Brien, and J. G. Rarity, "Robust photon-spin entangling gate using a quantum-dot spin in a microcavity," *arXiv preprint*, Jan. 2009. arXiv:0901.3964.

[160] C. Y. Hu, W. J. Munro, J. L. O'Brien, and J. G. Rarity, "Proposed entanglement beam splitter using a quantum-dot spin in a double-sided optical microcavity," *Physical Review B*, vol. 80, p. 205326, Nov. 2009.

[161] C. Bonato, F. Haupt, S. S. R. Oemrawsingh, J. Gudat, D. Ding, M. P. van Exter, and D. Bouwmeester, "CNOT and Bell-state analysis in the weak-coupling cavity QED regime," *Physical Review Letters*, vol. 104, p. 160503, Apr. 2010.

[162] J. Calsamiglia and N. Lütkenhaus, "Maximum efficiency of a linear-optical Bell-state analyzer," *Applied Physics B*, vol. 72, pp. 67–71, Jan. 2001.

[163] J. Roffe, "Quantum error correction: an introductory guide," *Contemporary Physics*, vol. 60, pp. 226–245, July 2019.

[164] A. Y. Kitaev, "Quantum computations: algorithms and error correction," *Russian Mathematical Surveys*, vol. 52, pp. 1191–1249, Dec. 1997.

[165] A. Y. Kitaev, "Fault-tolerant quantum computation by anyons," *Ann. Phys. (N. Y.)*, vol. 303, pp. 2–30, Jan. 2003.

[166] S. B. Bravyi and A. Y. Kitaev, "Quantum codes on a lattice with boundary," *arXiv preprint*, Nov. 1998. arXiv:quant-ph/9811052.

[167] M. H. Freedman and D. A. Meyer, "Projective plane and planar quantum codes," *arXiv preprint*, Oct. 1998. arXiv:quant-ph/9810055.

[168] A. G. Fowler, M. Mariantoni, J. M. Martinis, and A. N. Cleland, "Surface codes: Towards practical large-scale quantum computation," *Physical Review A*, vol. 86, p. 032324, Sept. 2012.

[169] R. J. Warburton, "Single spins in self-assembled quantum dots," *Nature Materials*, vol. 12, pp. 483–493, May 2013.

[170] C. Y. Hu, A. Young, J. L. O'Brien, W. J. Munro, and J. G. Rarity, "Giant optical Faraday rotation induced by a single-electron spin in a quantum dot: Applications to entangling remote spins via a single photon," *Physical Review B*, vol. 78, p. 085307, Aug. 2008.

[171] C. Y. Hu and J. G. Rarity, "Extended linear regime of cavity-QED enhanced optical circular birefringence induced by a charged quantum dot," *Physical Review B*, vol. 91, p. 075304, Feb. 2015.

[172] H. F. Hofmann, K. Kojima, S. Takeuchi, and K. Sasaki, "Optimized phase switching using a single-atom nonlinearity," *Journal of Optics B: Quantum and Semiclassical Optics*, vol. 5, pp. 218–221, Apr. 2003.

[173] A. Auffèves-Garnier, C. Simon, J.-M. Gérard, and J.-P. Poizat, "Giant optical nonlinearity induced by a single two-level system interacting with a cavity in the purcell regime," *Physical Review A*, vol. 75, p. 053823, May 2007.

[174] G. Slavcheva, M. Koleva, and A. Rastelli, "Ultrafast pulse phase shifts in a charged-quantum-dot–micropillar system," *Physical Review B*, vol. 99, p. 115433, Mar. 2019.

[175] M. Atatüre, J. Dreiser, A. Badolato, and A. Imamoglu, "Observation of faraday rotation from a single confined spin," *Nature Physics*, vol. 3, pp. 101–106, Jan. 2007.

[176] M. H. Mikkelsen, J. Berezovsky, N. G. Stoltz, L. A. Coldren, and D. D. Awschalom, "Optically detected coherent spin dynamics of a single electron in a quantum dot," *Nature Physics*, vol. 3, pp. 770–773, Oct. 2007.

[177] P. Androvitsaneas, A. B. Young, C. Schneider, S. Maier, M. Kamp, S. Höfling, S. Knauer, E. Harbord, C. Y. Hu, J. G. Rarity, and R. Oulton, "Charged quantum dot micropillar system for deterministic light-matter interactions," *Physical Review B*, vol. 93, p. 241409(R), June 2016.

[178] S. Sun, H. Kim, G. S. Solomon, and E. Waks, "A quantum phase switch between a single solid-state spin and a photon," *Nature Nanotechnology*, vol. 11, pp. 539–544, Feb. 2016.

[179] L. Wells, S. Kalliakos, B. Villa, D. Ellis, R. Stevenson, A. Bennett, I. Farrer, D. Ritchie, and A. Shields, "Photon phase shift at the few-photon level and optical switching by a quantum dot in a microcavity," *Physical Review Applied*, vol. 11, p. 061001, June 2019.

[180] P. Androvitsaneas, A. B. Young, J. M. Lennon, C. Schneider, S. Maier, J. J. Hinchliff, G. S. Atkinson, E. Harbord, M. Kamp, S. Höfling, J. G. Rarity, and R. Oulton, "Efficient quantum photonic phase shift in a low q-factor regime," *ACS Photonics*, vol. 6, pp. 429–435, Jan. 2019.

[181] P. Kok and S. L. Braunstein, "Detection devices in entanglement-based optical state preparation," *Physical Review A*, vol. 63, p. 033812, Feb. 2001.

[182] T. Volz, A. Reinhard, M. Winger, A. Badolato, K. J. Hennessy, E. L. Hu, and A. Imamoğlu, "Ultrafast all-optical switching by single photons," *Nature Photonics*, vol. 6, pp. 605–609, Aug. 2012.

[183] S. Reitzenstein, C. Hofmann, A. Gorbunov, M. Strauß, S. H. Kwon, C. Schneider, A. Löffler, S. Höfling, M. Kamp, and A. Forchel, "AlAs/GaAs micropillar cavities with quality factors exceeding 150.000," *Applied Physics Letters*, vol. 90, p. 251109, June 2007.

[184] D. M. Greenberger, M. A. Horne, and A. Zeilinger, "Going beyond Bell's theorem," in *Bell's Theorem, Quantum Theory and Conceptions of the Universe*, pp. 69–72, Springer Netherlands, 1989.

[185] P. Androvitsaneas, A. B. Young, T. Nutz, J. M. Lennon, S. Mister, C. Schneider, M. Kamp, S. Höfling, D. P. S. McCutcheon, E. Harbord, J. G. Rarity, and R. Oulton, "Quantum modulation of a coherent state wavepacket with a single electron spin," *arXiv preprint*, July 2022. arXiv:2207.05596.

[186] K. X. Tran, A. S. Bracker, M. K. Yakes, J. Q. Grim, and S. G. Carter, "Enhanced spin coherence of a self-assembled quantum dot molecule at the optimal electrical bias," *Physical Review Letters*, vol. 129, p. 027403, July 2022.

[187] Y. Q. Huang, Y. Puttisong, I. A. Buyanova, X. J. Yang, A. Subagyo, K. Sueoka, A. Murayama, and W. M. Chen, "Size dependence of electron spin dephasing in InGaAs quantum dots," *Applied Physics Letters*, vol. 106, p. 093109, Mar. 2015.

[188] L. Zaporski, N. Shofer, J. H. Bodey, S. Manna, G. Gillard, M. H. Appel, C. Schimpf, S. F. C. da Silva, J. Jarman, G. Delamare, G. Park, U. Haeusler, E. A. Chekhovich, A. Rastelli, D. A. Gangloff, M. Atatüre, and C. L. Gall, "Ideal refocusing of an optically active spin qubit under strong hyperfine interactions," *Nature Nanotechnology*, vol. 18, pp. 257–263, Jan. 2023.

[189] L. Ginés, M. Moczała-Dusanowska, D. Dlaka, R. Hošák, J. R. Gonzales-Ureta, J. Lee, M. Ježek, E. Harbord, R. Oulton, S. Höfling, A. B. Young, C. Schneider, and A. Predojević, "High extraction efficiency source of photon pairs based on a quantum dot embedded in a broadband micropillar cavity," *Physical Review Letters*, vol. 129, p. 033601, July 2022.

[190] L. Ginés, M. Moczała-Dusanowska, R. Hošák, M. Ježek, S. Höfling, C. Schneider, and A. Predojevic, "Modification of emission rate in broadband deterministic micropillar cavities," in *Conference on Lasers and Electro-Optics*, p. JTh3A.18, Optica Publishing Group, 2021.

[191] T. Huber, M. Davanco, M. Müller, Y. Shuai, O. Gazzano, and G. S. Solomon, "Filter-free single-photon quantum dot resonance fluorescence in an integrated cavity-waveguide device," *Optica*, vol. 7, p. 380, Apr. 2020.

[192] C. Chamberland, G. Zhu, T. J. Yoder, J. B. Hertzberg, and A. W. Cross, "Topological and subsystem codes on low-degree graphs with flag qubits," *Physical Review X*, vol. 10, p. 011022, Jan. 2020.

[193] C. Chamberland, A. Kubica, T. J. Yoder, and G. Zhu, "Triangular color codes on trivalent graphs with flag qubits," *New Journal of Physics*, vol. 22, p. 023019, Feb. 2020.

[194] K. Tiurev, P.-J. H. S. Derks, J. Roffe, J. Eisert, and J.-M. Reiner, "Correcting non-independent and non-identically distributed errors with surface codes," *arXiv preprint*, 2022. arXiv:2208.02191.

[195] J. P. B. Ataides, D. K. Tuckett, S. D. Bartlett, S. T. Flammia, and B. J. Brown, "The XZZX surface code," *Nature Communications*, vol. 12, p. 2172, Apr. 2021.

[196] D. K. Tuckett, S. D. Bartlett, and S. T. Flammia, "Ultrahigh error threshold for surface codes with biased noise," *Physical Review Letters*, vol. 120, p. 050505, Jan. 2018.

[197] D. Hallett, A. P. Foster, D. Whittaker, M. S. Skolnick, and L. R. Wilson, "Engineering chiral light–matter interactions in a waveguide-coupled nanocavity," *ACS Photonics*, vol. 9, pp. 706–713, Jan. 2022.

[198] S. Mahmoodian, K. Prindal-Nielsen, I. Söllner, S. Stobbe, and P. Lodahl, "Engineering chiral light–matter interaction in photonic crystal waveguides with slow light," *Optical Materials Express*, vol. 7, p. 43, Dec. 2016.

[199] T. Lund-Hansen, S. Stobbe, B. Julsgaard, H. Thyrrestrup, T. Sünner, M. Kamp, A. Forchel, and P. Lodahl, "Experimental realization of highly efficient broadband coupling of single quantum dots to a photonic crystal waveguide," *Physical Review Letters*, vol. 101, p. 113903, Sept. 2008.

[200] V. S. C. M. Rao and S. Hughes, "Single quantum-dot purcell factor and β factor in a photonic crystal waveguide," *Physical Review B*, vol. 75, p. 205437, May 2007.

[201] F. Liu, A. J. Brash, J. O'Hara, L. M. P. P. Martins, C. L. Phillips, R. J. Coles, B. Royall, E. Clarke, C. Bentham, N. Prtljaga, I. E. Itskevich, L. R. Wilson, M. S. Skolnick, and A. M. Fox, "High purcell factor generation of indistinguishable on-chip single photons," *Nature Nanotechnology*, vol. 13, pp. 835–840, July 2018.

[202] R. E. Evans, M. K. Bhaskar, D. D. Sukachev, C. T. Nguyen, A. Sipahigil, M. J. Burek, B. Machielse, G. H. Zhang, A. S. Zibrov, E. Bielejec, H. Park, M. Lončar, and M. D. Lukin, "Photon-mediated interactions between quantum emitters in a diamond nanocavity," *Science*, vol. 362, pp. 662–665, Nov. 2018.

[203] C. Bentham, I. E. Itskevich, R. J. Coles, B. Royall, E. Clarke, J. O'Hara, N. Prtljaga, A. M. Fox, M. S. Skolnick, and L. R. Wilson, "On-chip electrically controlled routing of photons from a single quantum dot," *Applied Physics Letters*, vol. 106, p. 221101, June 2015.

[204] D. Englund, A. Faraon, B. Zhang, Y. Yamamoto, and J. Vučković, "Generation and transfer of single photons on a photonic crystal chip," *Optics Express*, vol. 15, no. 9, p. 5550, 2007.

[205] A. Faraon, E. Waks, D. Englund, I. Fushman, and J. Vučković, "Efficient photonic crystal cavity-waveguide couplers," *Applied Physics Letters*, vol. 90, p. 073102, Feb. 2007.

[206] A. C. T. Thijssen, M. J. Cryan, J. G. Rarity, and R. Oulton, "Transfer of arbitrary quantum emitter states to near-field photon superpositions in nanocavities," *Optics Express*, vol. 20, p. 22412, Sept. 2012.

[207] J.-T. Shen and S. Fan, "Coherent single photon transport in a one-dimensional waveguide coupled with superconducting quantum bits," *Physical Review Letters*, vol. 95, p. 213001, Nov. 2005.

[208] J. Vučković, "Quantum optics and cavity QED with quantum dots in photonic crystals," in *Quantum Optics and Nanophotonics*, pp. 365–406, Oxford University Press, May 2017.

[209] D. E. Chang, V. Vuletić, and M. D. Lukin, "Quantum nonlinear optics — photon by photon," *Nature Photonics*, vol. 8, pp. 685–694, Aug. 2014.

[210] E. Sanchez-Burillo, D. Zueco, J. J. Garcia-Ripoll, and L. Martin-Moreno, "Scattering in the ultrastrong regime: Nonlinear optics with one photon," *Physical Review Letters*, vol. 113, p. 263604, Dec. 2014.

[211] T. Shi, Y.-H. Wu, A. González-Tudela, and J. Cirac, "Bound states in boson impurity models," *Physical Review X*, vol. 6, p. 021027, May 2016.

[212] S. Mahmoodian, G. Calajó, D. E. Chang, K. Hammerer, and A. S. Sørensen, "Dynamics of many-body photon bound states in chiral waveguide QED," *Physical Review X*, vol. 10, p. 031011, July 2020.

[213] K. Wang, "Quantum theory of two-photon wavepacket interference in a beamsplitter," *Journal of Physics B: Atomic, Molecular and Optical Physics*, vol. 39, pp. R293–R324, Sept. 2006.

[214] I. A. Walmsley, "Quantum optics: Science and technology in a new light," *Science*, vol. 348, pp. 525–530, May 2015.

[215] D. Browne, S. Bose, F. Mintert, and M. Kim, "From quantum optics to quantum technologies," *Progress in Quantum Electronics*, vol. 54, pp. 2–18, Aug. 2017.

[216] S. M. Barnett, A. Beige, A. Ekert, B. M. Garraway, C. H. Keitel, V. Kendon, M. Lein, G. J. Milburn, H. M. Moya-Cessa, M. Murao, J. K. Pachos, G. M. Palma, E. Paspalakis, S. J. Phoenix, B. Piraux, M. B. Plenio, B. C. Sanders, J. Twamley, A. Vidiella-Barranco, and M. Kim, "Journeys from quantum optics to quantum technology," *Progress in Quantum Electronics*, vol. 54, pp. 19–45, Aug. 2017.

[217] S. Buckley, K. Rivoire, and J. Vučković, "Engineered quantum dot single-photon sources," *Reports on Progress in Physics*, vol. 75, p. 126503, Nov. 2012.

[218] P. Senellart, G. Solomon, and A. White, "High-performance semiconductor quantum-dot single-photon sources," *Nature Nanotechnology*, vol. 12, pp. 1026–1039, Nov. 2017.

[219] A. Faraon, I. Fushman, D. Englund, N. Stoltz, P. Petroff, and J. Vučković, "Coherent generation of non-classical light on a chip via photon-induced tunnelling and blockade," *Nature Physics*, vol. 4, pp. 859–863, Sept. 2008.

[220] M. Radulaski, K. A. Fischer, K. G. Lagoudakis, J. L. Zhang, and J. Vučković, "Photon blockade in two-emitter-cavity systems," *Physical Review A*, vol. 96, p. 011801, July 2017.

[221] R. Trivedi, M. Radulaski, K. A. Fischer, S. Fan, and J. Vučković, "Photon blockade in weakly driven cavity quantum electrodynamics systems with many emitters," *Physical Review Letters*, vol. 122, p. 243602, June 2019.

[222] E. Z. Casalengua, J. C. L. Carreño, F. P. Laussy, and E. del Valle, "Conventional and unconventional photon statistics," *Laser & Photonics Reviews*, vol. 14, p. 1900279, May 2020.

[223] A. Foster, D. Hallett, I. Iorsh, S. Sheldon, M. Godsland, B. Royall, E. Clarke, I. Shelykh, A. Fox, M. Skolnick, I. Itskevich, and L. Wilson, "Tunable photon statistics exploiting the Fano effect in a waveguide," *Physical Review Letters*, vol. 122, p. 173603, May 2019.

[224] L. Mandel and E. Wolf, *Optical Coherence and Quantum Optics*. Cambridge University Press, Sept. 1995.

[225] H. J. Carmichael, *Statistical Methods in Quantum Optics 1: Master Equations and Fokker-Planck Equations*. Theoretical and Mathematical Physics, Berlin, Germany: Springer, Dec. 2010.

[226] Ş. E. Kocabaş, E. Rephaeli, and S. Fan, "Resonance fluorescence in a waveguide geometry," *Physical Review A*, vol. 85, p. 023817, Feb. 2012.

[227] S. Xu and S. Fan, "Fano interference in two-photon transport," *Physical Review A*, vol. 94, p. 043826, Oct. 2016.

[228] M. Reck, A. Zeilinger, H. J. Bernstein, and P. Bertani, "Experimental realization of any discrete unitary operator," *Physical Review Letters*, vol. 73, pp. 58–61, July 1994.

[229] J. L. Beckey, N. Gigena, P. J. Coles, and M. Cerezo, "Computable and operationally meaningful multipartite entanglement measures," *Physical Review Letters*, vol. 127, p. 140501, Sept. 2021.

[230] A. R. Cullen and P. Kok, "Calculating concentratable entanglement in graph states," *Physical Review A*, vol. 106, p. 042411, Oct. 2022.

[231] D. Horsman, A. G. Fowler, S. Devitt, and R. V. Meter, "Surface code quantum computing by lattice surgery," *New Journal of Physics*, vol. 14, p. 123011, Dec. 2012.

[232] A. Erhard, H. P. Nautrup, M. Meth, L. Postler, R. Stricker, M. Stadler, V. Negnevitsky, M. Ringbauer, P. Schindler, H. J. Briegel, R. Blatt, N. Friis, and T. Monz, "Entangling logical qubits with lattice surgery," *Nature*, vol. 589, pp. 220–224, Jan. 2021.

[233] R. Raussendorf and H. J. Briegel, "A one-way quantum computer," *Physical Review Letters*, vol. 86, pp. 5188–5191, May 2001.

[234] R. Raussendorf, J. Harrington, and K. Goyal, "Topological fault-tolerance in cluster state quantum computation," *New Journal of Physics*, vol. 9, pp. 199–199, June 2007.

[235] R. Raussendorf and J. Harrington, "Fault-tolerant quantum computation with high threshold in two dimensions," *Physical Review Letters*, vol. 98, p. 190504, May 2007.

[236] M. H. Appel, A. Tiranov, S. Pabst, M. L. Chan, C. Starup, Y. Wang, L. Midolo, K. Tiurev, S. Scholz, A. D. Wieck, A. Ludwig, A. S. Sørensen, and P. Lodahl, "Entangling a hole spin with a time-bin photon: A waveguide approach for quantum dot sources of multiphoton entanglement," *Physical Review Letters*, vol. 128, p. 233602, June 2022.

[237] M. L. Chan, A. Tiranov, M. H. Appel, Y. Wang, L. Midolo, S. Scholz, A. D. Wieck, A. Ludwig, A. S. Sørensen, and P. Lodahl, "On-chip spin-photon entanglement based on photon-scattering of a quantum dot," *npj Quantum Information*, vol. 9, p. 49, May 2023.

[238] K. B. Joanesarson, J. Iles-Smith, M. Heuck, and J. Mørk, "Few-photon transport in Fano-resonance waveguide geometries," *Physical Review A*, vol. 101, p. 063809, June 2020.